PROPERTIES OF GRAIN BOUNDARIES AND Ag-CERAMIC INTERFACE IN BISMUTH BASED SUPERCONDUCTORS

by
MUSTAFA AKDOĞAN

THESIS SUBMITTED TO
THE GRADUATE SCHOOL OF NATURAL AND APPLIED SCIENCES
OF
THE ABANT İZZET BAYSAL UNIVERSITY
IN PARTIAL FULFILLMENT OF THE REQUIREMENTS FOR THE DEGREE OF
DOCTOR OF PHILOSOPHY
IN
THE DEPARTMENT OF PHYSICS

DECEMBER 2009

Approval of the Graduate School of Natural Sciences

Prof. Dr. Nihat Çelebi
Director

I certify that this thesis satisfies all the requirements as a thesis for the degree of Doctor of Philosophy.

Prof. Dr. Kıvılcım Kılıç
Head of Physics Department

This is to certify that we have read this thesis and that in our opinion it is fully adequate, in scope and quality as a thesis for the degree of Doctor of Philosophy.

Prof. Dr. İbrahim Belenli
Co-Supervisor

Assoc. Prof. Dr. Cabir Terzioğlu
Supervisor

Examining Committee Members

1. Prof. Dr. İbrahim Belenli .....
2. Assoc. Prof. Dr. Cabir Terzioğlu .....
3. Prof. Dr. Ahmet Varilci .....
4. Prof. Dr. Resul Eryiğit .....
5. Assist Prof. Dr. Erdal Bekiroğlu .....

ABSTRACT

PROPERTIES OF GRAIN BOUNDARIES AND Ag-CERAMIC INTERFACE IN BISMUTH BASED SUPERCONDUCTORS

Akdoğan, Mustafa
Doctor of Philosophy, Department of Physics
Supervisor: Assoc. Prof. Dr. Cabir Terzioğlu
Co-Supervisor: Prof. Dr. İbrahim Belenli

December 2009, 119 pages

The main objective of this thesis was the preparation of $Bi_{1.8}Pb_{0.4}Ca_{2.2}Sr_2Cu_3O_x$/Ag multilayered samples (2, 4 and 8 layers) and to investigation of the effect of multilayering with Ag on the superconducting and the microstructural properties of $Bi_{1.8}Pb_{0.4}Ca_{2.2}Sr_2Cu_3O_x$. Towards that end, we have done a three main investigations: 1) Studied the optimal annealing temperature for bettering superconducting properties, 2) Investigated the effect of diffusion doped Ag on the microstructure and superconducting properties of $Bi_{1.8}Pb_{0.4}Ca_{2.2}Sr_2Cu_3O_x$ and 3) Studied the effect of Ag layering on the superconducting and microstructural properties of $Bi_{1.8}Pb_{0.4}Ca_{2.2}Sr_2Cu_3O_x$.

First, we prepared $Bi_{1.8}Pb_{0.4}Ca_{2.2}Sr_2Cu_3O_x$ ceramic superconductors annealed at 830, 835, 840, 845, and 850 °C using the solid state reaction method to investigate the optimum annealing temperature. The investigations consist of XRD, SEM, dc resistivity and transport critical current density measurements. The highest T_c and J_c values were found to be 106 K and 124 A/cm^2 for the sample annealed at 840 °C for 48 hours (*B840*), respectively. Large grain size, denser surface and high volume fraction of the high-T_c phase were obtained for the sample *B840*.

Then, we prepared silver diffusion doped $Bi_{1.8}Pb_{0.4}Ca_{2.2}Sr_2Cu_3O_x$ to investigate the effect of the silver diffusion on the microstructural and superconducting properties and to calculate silver diffusion coefficient and activation energy in $Bi_{1.8}Pb_{0.4}Ca_{2.2}Sr_2Cu_3O_x$. The diffusion doping of $Bi_{1.8}Pb_{0.4}Ca_{2.2}Sr_2Cu_3O_x$ by silver increased the critical current density from 123 to 696 A/cm^2 and the transition critical temperature by about 3 K compared with the undoped sample. *Ag*-doping increased the amount of high-T_c phase and improved the surface morphology. It also causes an increase of the lattice parameter *c* by an amount of 0.15%. The temperature dependence of the silver diffusion coefficient in the range of 600-800°C is described by $D = 2.9\text{x}10^{-4}\, exp(-\, 1.05\ \text{eV}/k_BT)$.

Finally, $Bi_{1.8}Pb_{0.4}Ca_{2.2}Sr_2Cu_3O_x$/Ag multilayered samples (2, 4 and 8 layers) were fabricated by powder in tube (PIT) method. PIT technique consists of filling the powder into the silver tube, drawing, rolling, pressing and annealing procedure. The rolling process was not effective in obtaining further substantially increases of the powder density, but greatly improved the orientation of ceramic grains inside the silver sheath. XRD, SEM, dc electrical resistivity as a function of temperature and magnetic field, critical current density at 77 K as a function of magnetic field measurements were performed to investigate the effect of Ag layering on

microstructural and superconducting properties of multilayered samples. The sample is composed of a highly oriented Bi-2223 phase in the region near the Ag layer. The eight-layered sample exhibits a rather high I_c value of 126 A. T_c and J_c are enhanced from 107 K to 109 K and from 240 A/cm^2 to 600 A/cm^2 by increasing the number of Ag layers, respectively. The reason for improving J_c properties is that grain growth near the Ag region was progressed with extending layers. The formation of the dense oriented structure is near the interface between oxide and the Ag layer. This suggests that Ag plays an important role in the improvement of J_c. The enhancement of J_c is achieved by an increase in interface are between Ag and Bi-oxide.

Keywords: Bi-2223, Bi-2212, Ag-diffusion, Diffusion coefficient, Annealing temperature, Transition temperature, Critical current density, Grain boundary, Interface, High temperature superconductivity.

ÖZET

BİZMUT TABANLI SÜPERİLETKENLERDE TANECİK SINIRLARI VE Ag-SERAMİK ARAYÜZÜN ÖZELLİKLERİ

Akdoğan, Mustafa
Doktora, Fizik Bölümü
Tez Danışmanı: Doç. Dr. Cabir Terzioğlu
Yardımcı Tez Danışmanı: Prof. Dr. İbrahim Belenli

Aralık 2009, 119 sayfa

Bu tezin ana konusu $Bi_{1.8}Pb_{0.4}Ca_{2.2}Sr_2Cu_3O_x$/Ag stokiyometrisine sahip çok katlı (2, 4 ve 8 katlı) numunelerin üretimi ve Ag ile oluşturulan çok katın $Bi_{1.8}Pb_{0.4}Ca_{2.2}Sr_2Cu_3O_x$ stokiyometrisinin süperiletkenlik ve mikroyapı özelliklerine etkisini araştırmak idi. Bu amaçla, üç temel araştırma yaptık: 1) Süperiletkenlik özelliklerini iyileştirmek için en iyi tavlama sıcaklığını araştırdık, 2) $Bi_{1.8}Pb_{0.4}Ca_{2.2}Sr_2Cu_3O_x$ stokiyometrisinin mikroyapı ve süperiletkenlik özelliklerine Ag difüzyonunun etkisini gözlemledik ve 3) $Bi_{1.8}Pb_{0.4}Ca_{2.2}Sr_2Cu_3O_x$ stokiyometrisinin süperiletkenlik ve mikroyapı özelliklerine Ag katmanının etkisini araştırdık.

İlk olarak, en iyi tavlama sıcaklığını incelemek için katı hal tepkime yöntemi kullanılarak 830, 835, 840, 845 ve 850 °C de tavlanmış $Bi_{1.8}Pb_{0.4}Ca_{2.2}Sr_2Cu_3O_x$ seramik süperiletkenler hazırladık. İncelemeler XRD, SEM, dc özdirenç ve taşıyıcı kritik akım yoğunluğu ölçümlerini içermektedir. En yüksek T_c ve J_c değerleri 840 °C de 48 saat *(B840)* tavlanmış numune için sırasıyla 106 K ve 124 A/cm^2 olarak bulundu. *B840* numunesi için büyük tanecik boyutu, daha yoğun yüzey ve yüksek hacim oranına sahip yüksek-T_c fazı elde edildi.

Ardından, $Bi_{1.8}Pb_{0.4}Ca_{2.2}Sr_2Cu_3O_x$ stokiyometrisine gümüş difüzyonunun mikroyapısal ve süperiletkenlik özellikleri açısından etkisini araştırmak ve gümüş difüzyonu katsayısı ve aktivasyon enerjisini hesaplamak için gümüş difüzyonu ile katkılanmış $Bi_{1.8}Pb_{0.4}Ca_{2.2}Sr_2Cu_3O_x$ numunesi hazırladık. Katkılanmamış numune ile karşılaştırıldığında $Bi_{1.8}Pb_{0.4}Ca_{2.2}Sr_2Cu_3O_x$ stokiyometrisine gümüş difüzyonu katkılanması kritik akım yoğunluğunu 123 den 696 A/cm^2'ye yükseltti ve kritik geçiş sıcaklığını yaklaşık 3 K artırdı. *Ag*-katkılanması yüksek-T_c faz miktarını artırdı ve yüzey morfolojisini iyileştirdi. Aynı zamanda gümüş katkılanması *c* örgü parametresinin %0.15 civarı artmasına neden oldu. Bu çalışmada, 600-800 °C aralığında gümüş difüzyon katsayısının sıcaklığa bağımlılığı $D = 2.9\text{x}10^{-4}\ exp(-\ 1.05\ \text{eV}/k_BT)$ olarak tanımlanmıştır.

Son olarak, $Bi_{1.8}Pb_{0.4}Ca_{2.2}Sr_2Cu_3O_x$/Ag çok katlı numuneleri (2, 4 ve 8 katlı) boru içerisinde toz (PIT) metodu ile üretildi. PIT tekniği tozun gümüş boru içerisine doldurulması, borunun uzatılması, uzatılan borunun haddelenmesi, haddelenmiş borunun preslenmesi ve tavlanması işlem basamaklarından oluşmaktadır. Haddeleme işlemi artması beklenen gümüş içerisindeki toz yoğunluğunun artırılması konusunda etkili değildi fakat gümüş kılıf içerisindeki seramik taneciklerinin yönelimini büyük ölçüde iyileştirdi. Katlı numunelerin mikroyapısal ve süperiletkenlik üzerine Ag

katmanının etkisini araştırmak için XRD, SEM, sıcaklık ve manyetik alanın fonksiyonu olarak dc elektriksel özdirenç ve manyetik alanın fonksiyonu olarak 77 K de kritik akım yoğunluğu ölçümlerini gerçekleştirdik. Numune, Ag katmanına yakın bölgede yüksek ölçüde Bi-2223 fazına yönlenmiştir. Sekiz-katlı numune kabaca 126 A gibi yüksek I_c değeri sergilemektedir. Ag katman sayısının artması ile T_c ve J_c sırasıyla 107 K den 109 K'e ve 240 A/cm^2 den 600 A/cm^2'ye artırıldı. J_c özelliklerinin artma nedeni katmanların artırılması ile Ag bölgesi yakınında tanecik büyümesi ile ilişkilendirilmiştir. Sıkı yönelimli yapı formu oksit ve Ag katmanı arayüzeyine yakındır. Bu, Ag nin J_c yi artırmadaki önemli rolünü ortaya koyar. J_c nin artırılması, Ag ile Bi-oksit arayüzeyinin artması ile elde edilmiştir.

Anahtar Kelimeler: Bi-2223, Bi-2212, Ag-difüzyonu, Difüzyon katsayısı, Tavlama sıcaklığı, Geçiş sıcaklığı, Kritik akım yoğunluğu, Tanecik sınırı, Arayüzey, Yüksek sıcaklık süperiletkeni.

This Ph.D. thesis is dedicated to my family...

ACKNOWLEDGEMENTS

I would like to thank my Advisor Assoc. Prof. Dr. Cabir Terzioğlu and, Co-Advisor Prof. Dr. İbrahim Belenli and my instructor Prof. Dr. Ahmet Varilci for their support, guidance, patience and encouragement during years of my work as a graduate student at Abant İzzet Baysal University. I am obliged for their continuous guidance and support and thank to them for their help in the revision of scientific content and style of this dissertation. And I want to thank them not only for guidance for scientific content but also their guidance for all contents of life. Their supervision has given me an unforgettable experience for my future career.

This work was supported partly by DPT under grant no. 2004K120200, Tübitak under grant no. TBAG (104T323) and AIBU Research Fund grant no. 2003.03.02.194.

TABLE OF CONTENTS

LIST OF TABLES

LIST OF FIGURES

CHAPTER 1 - INTRODUCTION

Materials are classified as metal, semimetal, semiconductor and insulator via their resistances. It is observed that when some metals and some compounds are cooled enough, nearly to the liquid helium temperature, their resistance falls down to zero and they have no resistance value against current. This process, which is called superconductivity, is a phenomenon occurring in certain materials generally at very low temperatures, characterized by exactly zero electrical resistance and the exclusion of the interior magnetic field (the Meissner effect), discovered by Kamerlingh Onnes for mercury [1]. Like ferromagnetism and atomic spectral lines, superconductivity is a quantum mechanical phenomenon.

Before 1986, superconductivity was a phenomenon restricted to metals, occurring only at very low temperatures and requiring liquid helium as a refrigerant. The highest known critical temperature, T_c, the temperature below which all electrical resistance is lost and the material becomes superconductor, was 23 K for the intermetallic compound Nb_3Ge. In the early part of 1986, Bednorz and Muller [2] realized that a mixed oxide of lanthanum, barium and copper with the nominal composition $La_{5-x}Ba_xCu_5O_{5(3-z)}$, from which later on $La_{2-x}Ba_xCuO_{4-z}$ was identified as the superconducting phase [3], became superconducting at a critical temperature above 30 K.

Within a few months of the announcement of the original discovery another mixed oxide, $YBa_2Cu_3O_7$, (YBCO), was found to have a superconducting critical temperature of 90 K [4]. Superconductivity at liquid nitrogen temperature (77 K) was at last a reality. The intense research effort thus unleashed has led to the discovery of further compounds which are called bismuth, strontium, calcium, copper oxides (BSCCO) with values of T_c up to 100 K [5]. Bismuth based high temperature superconductors were found in 1987 [6]. It is well known that the Bi-Sr-Ca-Cu-O system consists of three different superconducting phases such as $Bi_2Sr_2CuO_{6+x}$ (2201 phases), $Bi_2Sr_2CaCu_2O_{8+x}$ (2212 phase) and $Bi_2Sr_2Ca_2Cu_3O_{10+x}$ (2223 phase), with critical temperatures of about 20, 80 and 110 K, respectively [7, 8]. A large amount of work has been done on this system in order to improve the superconducting properties and to make technical applications possible. A common characteristic of most of these materials is the presence of copper oxygen planes. Superconductivity is confined to these copper-oxygen planes [9] and T_c depends on the free carrier concentration in them. In most of the superconducting compounds which have been discovered so far, holes seem to be the dominant charge carriers [10].

Since the discovery of the high-temperature superconductor system Bi-Sr-Ca-Cu-O [5], many investigators have focused on this system to understand its properties and to improve them. There has been specific interest in its critical current density, J_c. The critical current density is the most important property of a superconductor in transport applications. The critical current capacity of a superconductor is either measured by a four probe test as a transport current, or is calculated from the magnetization measurements. The current density of the high-temperature superconductor (HTSC) is limited by several factors such as second

phases and grain boundaries which act as weak links for the supercurrent. Also critical current densities in high-T_c superconductors can depend on both intragranular flux creep and intergranular weak links [11]. The microstructure of the superconductor, especially the size and shape of the grains and the grain alignment, are also important in determining the critical current density of polycrystalline superconductors [12, 13]. Grain boundaries are usually classified according to the displacement and the rotation of the abutting crystals [14]. For rotational grain boundaries a distinction is made between the tilt and twist components of the misorientation. Here, *tilt* refers to a rotation around an axis in the plane of the grain boundary, and *twist* to a rotation of the crystal grains around the axis perpendicular to the grain boundary plane. Grain boundaries with identical misorientations of the grains with respect to the grain-boundary interface are called *symmetric*; otherwise they are *asymmetric*. In standard polycrystalline high-Tc compounds, the critical currents are limited by the grain boundaries [15]. To increase the critical currents, two strategies have been found. These strategies are based on enhancing the critical current density of the boundaries. The first consists in aligning the grains along all major axes to within few degrees [16]. Second, for a given misorientation angle, the grain boundary critical current density is increased by appropriate doping [17]. Weak link behavior of high temperature superconductors at the grain boundary had been one of the most important research fields. Relationship of the sample features like grain boundary structure and supercurrent conductivity is an important feature which has not been fully understood. SEM measurements provide more important additional information when observing the relationship between material structure and material futures [18]. Formation kinetics of the superconductor Bi-based phases has not been fully understood. Intermediary phases are formed in the course of heat

treatment. Variation in the phase ratio of 2212 and 2223 in a sample complicates the determination of the superconducting properties. Remaining intermediate phases in the sample provide immobilization of the magnetic flux function acting as pinning centers. On the other hand, these stable intermediate phases reduce the volume fraction of superconductor and they cause weak links at the grain boundaries. So it is very important to have a pure phase material in order to investigate the physical properties of the phases separately. Appropriate doping of the grains provides a means to optimize the transport properties of grain boundaries in high-T_c superconductors. So, the critical current is enhanced and normal state conductivity reduced [19].

Size of grains, angles between grain boundaries, chemical composition of the grain boundary and volume concentration of the micro holes in the sample are based on production parameters [7, 8]. Bismuth based superconductor properties heavily sensitive to the initial chemical rates and compositions. With rates of (Bi,Pb) in these initial chemicals are chosen rich so as to compensate the loses at the heat treatment, different heat treatment and chemical mixturing stages changes the appropriate chemical compositional. Thermal process with low oxygen content can provide phase formation with less Pb addition by decreasing initial melting point. Cracks produced in mechanical processes in the ceramic superconductor with Pb rich samples can disappear easily and its performance improves, c-macrocracks can be observed in the materials in effect of oxygen atmosphere [20]. Sample types such as film, bulk, wire and strip need different production parameters. Study on the optimization of production parameters is intensely continuing all over the world.

It has been widely recognized that the Bi-based high-T_c superconductors are suitable for processing into long composite conductors. Wires, but especially tapes,

having a highly densified, oriented and textured ceramic core inside a silver sheath, have been successfully fabricated by means of the powder-in-tube method [21, 22]. Owing to the enormous efforts made in this field, the critical current density (J_c) in short and long specimens are continuously increasing, currently approaching the technical values required for practical applications [23]. In order to get good transport properties in Ag-BSCCO multilayered samples, the superconductor a-b planes should lie almost parallel to the current direction. This preferred orientation is promoted by the proximity of silver, although the mechanism for this particular grain growth is not well understood yet [24]. Penetration of silver to the bismuth based superconductor ceramics causes the changes of the superconductor properties. Silver grains inside the ceramic exist as isolated particles. Near the Ag-sheath, more Ag particles exist. It has been established that Ag penetrates into the ceramics by means of two different mechanisms: (a) ordinary diffusion at elevated temperatures, and (b) indentation of ductile Ag into brittle and porous ceramics in process of plastic deformation of a composite. The effect of this second mechanism is appreciably suppressed when the Ag-sheath alloyed with complex additions of (Ni + Y) and (Zr + Al). Different thermal expansion coefficients of Ag and the ceramics can result in weak connectivity between grains. Strengthened Ag-sheath by alloying is reported to decrease the amount of silver in the ceramics [25].

This thesis is organized as follows. Chapter 2 contains brief background information on aspects of high-T_c superconductivity relevant to the understanding of the results presented in this work. More detailed information can be found in the cited references.

Chapter 3 describes the sample preparation and measurement techniques employed. The experimental results are presented in chapter 4.

The conclusions are presented in chapter 5.

Lastly, the Labview programs that was programmed and used in the research laboratory are presented in the appendix.

CHAPTER 2 – GRAIN BOUNDARIES

2.1 Introduction

Solid materials are made of grains unless they are single crystals. You need a microscope to see the grains and crystal structures. Grain is the region of space occupied by a continuous crystal lattice. Grain structure is the arrangement of grains in a metal, with a grain having a particular crystal structure.

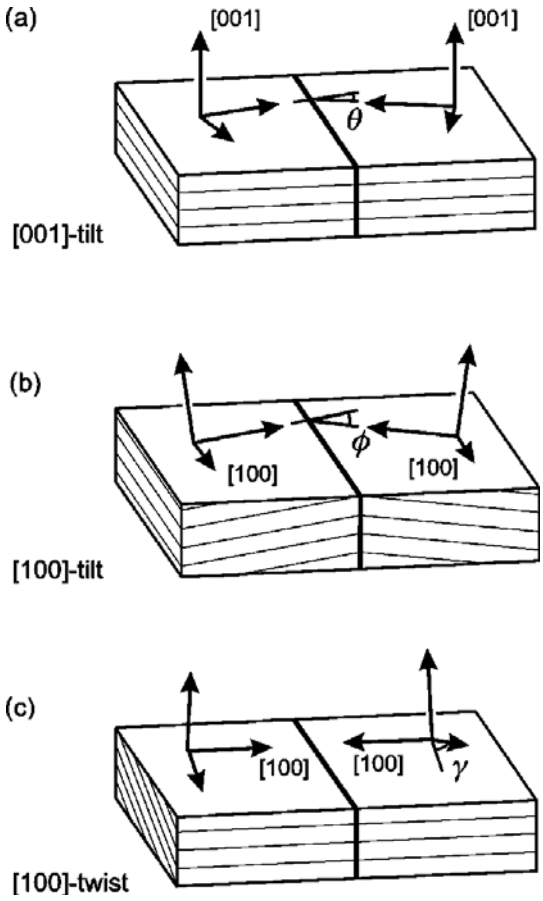

Figure 2-1: Schematic diagram showing the crystallography of a) a [001]-tilt boundary, b) a [100]-tilt boundary, and c) a [100]-twist boundary in a cubic material.

A grain boundary is a single-phase interface, with crystals on each side of the boundary being identical except in orientation. The term "crystallite boundary" is sometimes, though rarely, used. Grain boundary areas contain those atoms that have been perturbed from their original lattice sites, dislocations, and impurities that have migrated to the lower energy grain boundary. Grain boundaries are usually classified according to the displacements and the rotation of the abutting crystals, as shown schematically in Figure 2-1. For rotational grain boundaries a distinction is made between the tilt and twist components of the misorientation. Here, *tilt* refers to a rotation around an axis in the plane of the grain boundary, and *twist* to a rotation of the crystal grains around the axis perpendicular to the grain boundary plane. A 30° [001]-tilt boundary, for example, connects two crystals rotated with respect to each other by 24° around the [001] direction, which is common to both crystals and lies in the grain-boundary plane. Furthermore, combinations of tilt and twist components may occur, leading to so called mixed boundaries. Grain boundaries with identical misorientations of the grains with respect to the grain-boundary interface are called *symmetric*; otherwise they are *asymmetric*. For the high-T_c superconductors with their layered structure, 90° boundaries are particularly noteworthy. Three of these boundaries, which are commonly present in a-axis-oriented high-Tc films, namely, a 90° [010]-twist boundary, a 90° [010]-basal-plane-faced tilt boundary, and a symmetrical 90° [010] tilt boundary, are shown in Figure 2-2. The latter two boundaries are also frequently found in step-edge junctions [14].

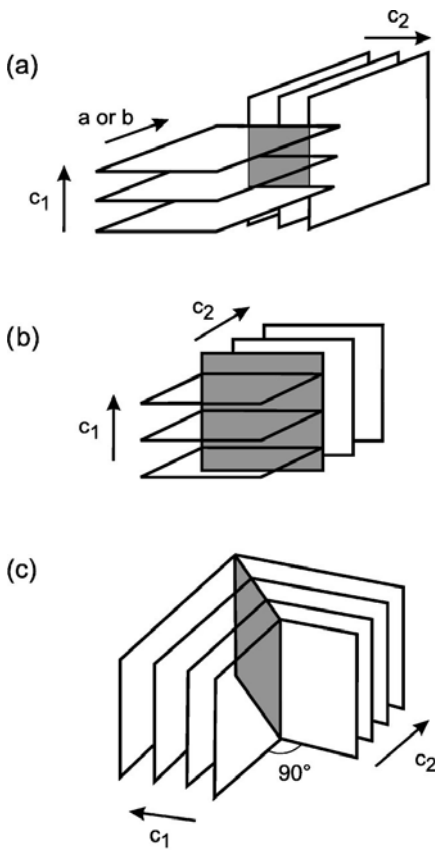

Figure 2-2: Schematic diagram of three types of 90° grain boundaries (drawn in gray); a) a 90° [010] twist boundary; b) a 90° [010] basal-plane-faced tilt boundary; c) a 90° [010] symmetrical tilt boundary. Note that a 90° [010] symmetrical tilt boundary is a [110] twin boundary [26].

In addition to those boundaries associated with a rotation of the crystals, boundaries may also be formed as a result of a translation between two grains.

Grain boundaries disrupt the motion of dislocations through a material. Dislocation propagation is impeded because of the stress field of the grain boundary defect region and the lack of slip planes and slip directions and overall alignment across the boundaries. Reducing grain size is therefore a common way to improve strength, often without any sacrifice in toughness because the smaller grains create more obstacles per unit area of slip plane. The high interfacial energy and relatively weak bonding in grain boundaries makes them preferred sites for the onset of corrosion and for the precipitation of new phases from the solid.

Grain boundary migration plays an important role in many of the mechanisms of creep. Grain boundary migration occurs when a shear stress acts on the grain

boundary plane and causes the grains to slide. This means that fine-grained materials actually have a poor resistance to creep relative to coarser grains, especially at high temperatures, because smaller grains contain more atoms in grain boundary sites. Grain boundaries also cause deformation in that they are sources and sinks of point defects. Voids in a material tend to gather in a grain boundary, and if this happens to a critical extent, the material could fracture.

During grain boundary migration, the rate determining step depends on the angle between two adjacent grains. In a small angle dislocation boundary, the migration rate depends on vacancy diffusion between dislocations. In a high angle dislocation boundary, this depends on the atom transport by single atom jumps from the shrinking to the growing grains [27].

Grain boundaries are generally only a few nanometers wide. In common materials, crystallites are large enough that grain boundaries account for a small fraction of the material. However, very small grain sizes are achievable. In nanocrystalline solids, grain boundaries become a significant volume fraction of the material, with profound effects on such properties as diffusion and plasticity. In the limit of small crystallites, as the volume fraction of grain boundaries approaches 100%, the material ceases to have any crystalline character, and thus becomes an amorphous solid.

Grain boundaries are also present in magnetic domains in magnetic materials. A computer hard disk, for example, is made of a hard ferromagnetic material that contains regions of atoms whose magnetic moments can be realigned by an inductive head. The magnetization varies from region to region, and the misalignment between these regions forms boundaries that are the key to data storage. The inductive head measures the orientation of the magnetic moments of these domain regions and reads

out either a “1” or “0”. These bits are the data being read. Grain size is important in this technology because it limits the number of bits that can fit on one hard disk. The smaller the grain sizes, the more data that can be stored.

Because of the dangers of grain boundaries in certain materials such as superalloy turbine blades, great technological leaps were made to minimize as much as possible the effect of grain boundaries in the blades. The result was directional solidification processing in which grain boundaries were eliminated by producing columnar grain structures aligned parallel to the axis of the blade, since this is usually the direction of maximum tensile stress felt by a blade during its rotation in an airplane. The resulting turbine blades consisted of a single grain, improving reliability.

Generally, polycrystals cannot be superheated; they will melt promptly once they are brought to a high enough temperature. This is because grain boundaries are amorphous, and serve as nucleation points for the liquid phase. By contrast, if no solid nucleus is present as a liquid cools, it tends to become supercooled. Since this is undesirable for mechanical materials, alloy designers often take steps against it.

One of the main characteristics of most high temperature superconductors, and in particular $(Bi,Pb)_2Sr_2Ca_2Cu_3O_x$ (Bi-2223) is the polycrystalline morphology of the material. It is also one of the limiting factors for applications involving long length conductors, such as powder-in-tube (PIT) tapes. Critical current densities (J_c) across grain boundaries are believed to be much lower than intragrain J_c [28]. There has been much effort to analyze and reduce these “weak-link” effects at grain boundaries [28-30]. The focus has been on minimizing secondary phases at grain boundaries [31, 32] and improving grain alignment [33, 34] through the optimization

of both mechanical deformation and heat treatments. There are also other aspects about the size of the Bi-2223 grains [35].

In addition to an increase of the proportion of Bi-2223 phase during processing, a highly aligned Bi-2223 microstructure is essential for a high J_c value because a low J_c value usually results in a grain boundary weak-coupling problem as well as a random growth habit of the superconducting grains. The microstructure of Bi-based oxide superconductors consists of plate-like grains with the *a-b* plane along the flat surface of the platelets. If the grains are aligned by stacking the platelets like a structure of bricks [36], a high J_c can be achieved in the *a-b* plane. To date, there are many reports on deformation-induced texture of Bi-2223 superconductors [37-40] and also there is a report on textured Bi-2223 superconductor formed by partial melting and sintering [41].

CHAPTER 3 - EXPERIMENTAL DETAILS

The aim of the experimental part of this thesis was to determine the properties of grain boundaries and Ag-ceramic interface in bismuth based superconductors. Bi-based superconductor was chosen because of its high temperature transport mechanism. The experimental techniques employed are detailed in this chapter.

3.1 Powder-In-Tube Method and Ag-Ceramic Interface Preparation Steps

In this study, precursor powder from the Alfa Aesar was used for all the sample preparation steps. I researched on five sintering temperature points (830, 835, 840, 845, and 850 °C on the bulk samples), while preparing bulk samples in order to determine the best sintering temperature for high T_c (Bi-2223) phase formation. Therefore, silver-sheathed tapes of (Bi,Pb)-2223 phase sample called as multilayered Ag/BPSCCO tapes were produced on the best temperature (840 °C) by using powder-in-tube (PIT) technique is one of the most promising methods towards practical high-T_c superconducting tapes [42]. For this study, Ag tube 26 cm in length (about 0.3 mm in thickness and 13.134 grams) (Figure 3-1) was used for multilayered sample prepared by PIT technique.

Figure 3-1: Empty Silver Tube

Figure 3-2: One of The Open Edges Sealed Empty Silver Tube

To remove the work hardening on the Ag tube, it was sintered in air at 900 °C for 0.5 hour (using furnace self speed). One of the open edges of the Ag tube was sealed with groove rolling machine (Figure 3-2 and Figure 3-3). After the obtained precursor powder (powder stoichiometry is $Bi_{1.8}Pb_{0.4}Ca_{2.2}Sr_2Cu_3O_x$) (about 10.462 grams) was filled into the Ag tube with 6.3 mm diameter, the total weight was 23.596 grams. Moreover, the diameter of Ag tube decreased from 6.30 mm to 3.54 mm whereas the tube length increased from 26.00 to 43.20 cm by using drawing machine (Figure 3-4). Drawing processes can be seen from the Table 3-1 step by step.

Table 3-1: Step by Step Drawing Processes. This table shows us that the diameter and the length of the tube before and after the process.

Die Diameter	Tube Diameter	Tube Length
6.40	6.30	26
6.20	6.17	26.5
6.00	5.98	26.8
5.80	5.74	27.1
5.65	5.64	27.4
5.50	5.47	28.2
5.30	5.28	28.6
5.15	5.12	29.0
5.00	4.94	30.0
4.85	4.84	31.1
4.70	4.67	32.0
4.55	4.52	33.0
4.40	4.34	35.0
4.25	4.24	35.4
4.15	4.14	35.8
4.00	3.95	37.7
3.90	3.86	38.5
3.80	3.77	40.2
3.70	3.70	40.9
3.55	3.54	43.2

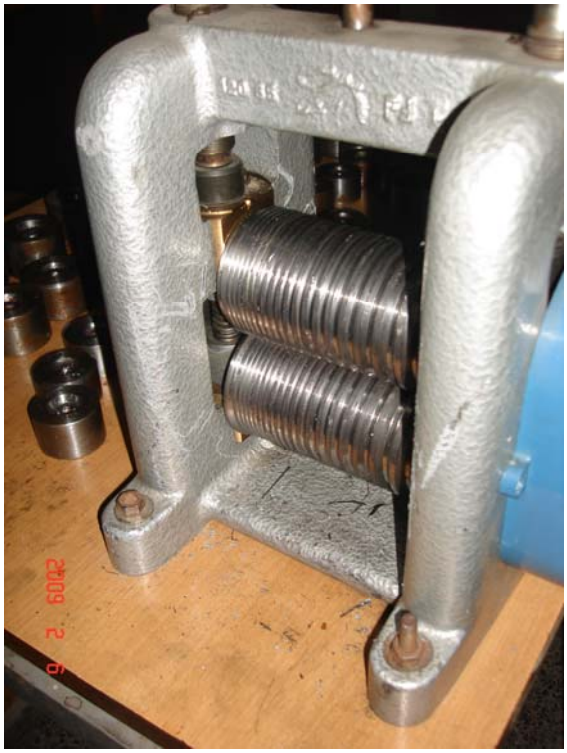

Figure 3-3: Groove Rolling Machine

Figure 3-4: Drawing Machine

Furthermore, after rolling process (Figure 3-5) was applied on the sample, the tape thickness was changed to 0.99 mm in thickness.

Figure 3-5: Rolling Machine

I have cut tape into 5 pieces about 4 cm in length (Figure 3-6). The tapes were sintered under the atmosphere of open air at 830 °C for 2 hours (with 4 °C/min. heating and 1 °C/min. cooling rates using programmable three-zone furnace from Protherm (Figure 3-7)).

Figure 3-6: Ag/BPSCCO Tape

Figure 3-7: Protherm PZF 12/75/700 Three Zone Tube Furnace

Some of the tapes (5 tapes) were cut into 2 peaces throughout longitudinal (Figure 3-8) to produce the 10-layered Ag-ceramic interfaced sample; similarly, 2- and 4-layered samples were prepared from the others. All samples look like sandwich structure, since they were prepared by Ag-ceramic interface (arranging two sheets on the upper and lower side). Samples placed into the metal dies top by top (Figure 3-9).

Figure 3-8: One of the Ag/BPSCCO tapes which is cut into two pieces.

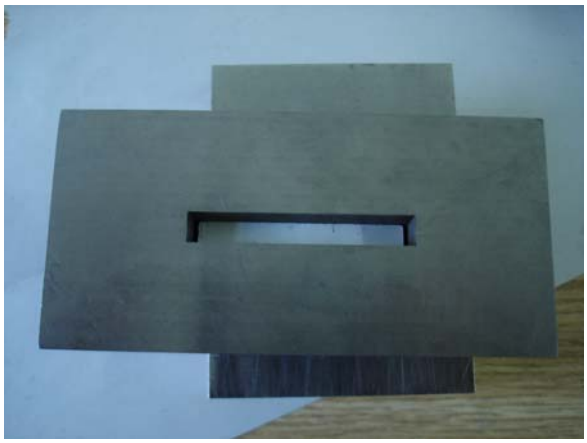

Figure 3-9: Stainless Steel Pressing Apparatus

In addition to avoid touching silver faces of the samples with each other, precursor powder has been planted on each sample again during pressing process. Then, all the samples was pressed under 344 MPa pressure with mechanical press (Figure 3-10). All layered samples were sintered in air at 840 °C for 48 hours (with 4 C/min. heating and 1 C/min. cooling rates). After the heat treatment layered samples pressed

under 418 MPa pressure with mechanical press and sintered in air at 840 °C for 48 hours again (with 4 °C/min. heating and 1 °C/min. cooling rates). Thus, layered sample with Ag-ceramic interface was achieved (Figure 3-11).

Figure 3-10: Mechanical Press

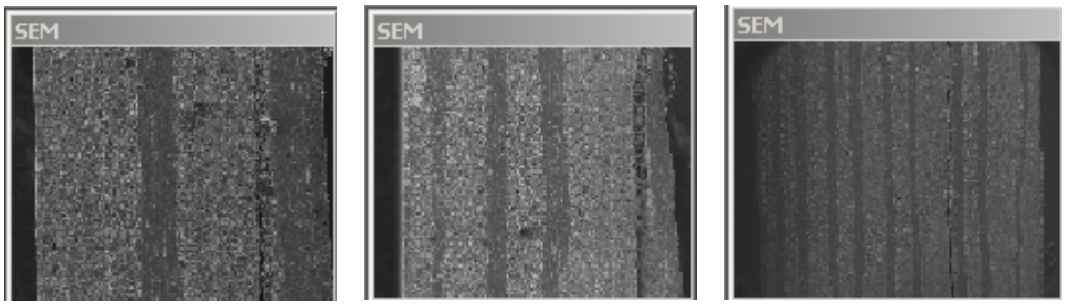

a) **b)** **c)**

Figure 3-11: SEM images for a) 2 layered, b) 4 layered, c) 10 layered samples

3.2 X-Ray Diffraction Analysis

X-ray diffraction (XRD) data were taken using a Rigaku MultiFlex 2kW diffractometer (Figure 3-12) with CuK_{α} radiation in the range of $2\theta = 3° - 60°$ with a scan speed of 3 °/min and a step increment of 0.02° at room temperature. The XRD measurements provide data about lattice parameters for only a thin surface layer of layered sample, since the effective penetration depth of the x-rays is about 15 μm into the sample. Phase purity and the lattice parameters were determined from these XRD patterns. The mean value of the lattice parameter c of layered samples is determined from the high-angle (00l) peaks of the XRD measurements.

Figure 3-12: Rigaku MultiFlex 2kW X-Ray Diffractometer

3.3 SEM Analysis

The surface morphologies of the multilayered and pure samples were studied by using a JEOL JSM-6390LV scanning electron microscope (Figure 3-13). SEM micrographs were taken from fracture surfaces of the bulk samples. Micrographs of the samples were magnified approximately 5000 times. We investigated microstructure of the sample, connectivity and size of the grains.

Figure 3-13: JEOL JSM-6390LV Scanning Electron Microscope

3.4 EDS Analysis

Electron dispersive X-ray analysis, also known as EDS, EDX or EDAX, is a technique used to identify the elemental composition of a sample or small area of interest on the sample. During EDS, a sample is exposed to an electron beam inside a scanning electron microscope (SEM) which can be seen from the Figure 3-14. These electrons collide with the electrons within the sample, causing some of them to be knocked out of their orbits. The vacated positions are filled by higher energy electrons which emit x-rays in the process. By analyzing the emitted x-rays, the elemental composition of the sample can be determined. EDS is a powerful tool for microanalysis of elemental constituents. EDS analysis is best suited for:

- Metals and metal alloys
- Ceramics
- Minerals

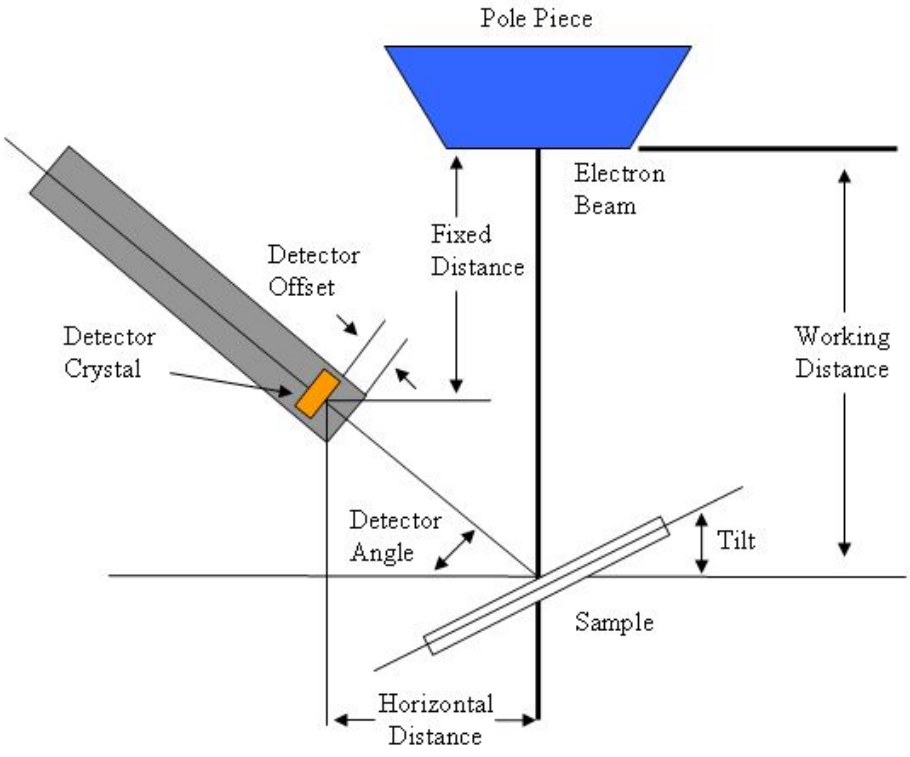

Figure 3-14: EDS detector is embedded to the SEM system.

Our EDS system which is embedded to the SEM includes IXRF SYSTEMS Model 550i Analyzer for analyzing emitted x-rays from the sample with detector crystal (Figure 3-15). Detector crystal can detect the x-rays of atoms range from Bor to Uranium in the periodic table.

Figure 3-15: IXRF Systems Model 550i Analyzer.

3.5 Resistivity Measurements

The low temperature DC electrical resistivity measurements were carried out by using Oxford Edwards Model CS2/9 (Figure 3-16).

Figure 3-16: OXFORD, Edwards Model CS2/9 cryogenic system.

The measurements of DC resistivity were performed with the four-probe method on all samples (Figure 3-17). Both voltage and current contacts were made with silver paint, the contact resistance being in the order of 0.1 Ω or lower. Resistive contacts caused heating and the test was completed in possible shortest time to avoid extensiveness of this effect. We measured temperature (70 K – 130 K) dependence of resistivity of the samples running 20 mA, 50 mA DC current through the samples in the cryostat for bulk and multilayered samples respectively. Throughout the measurements copper plates were used to increase cooling and warming efficiency in the multilayered samples as shown at the Figure 3-18.

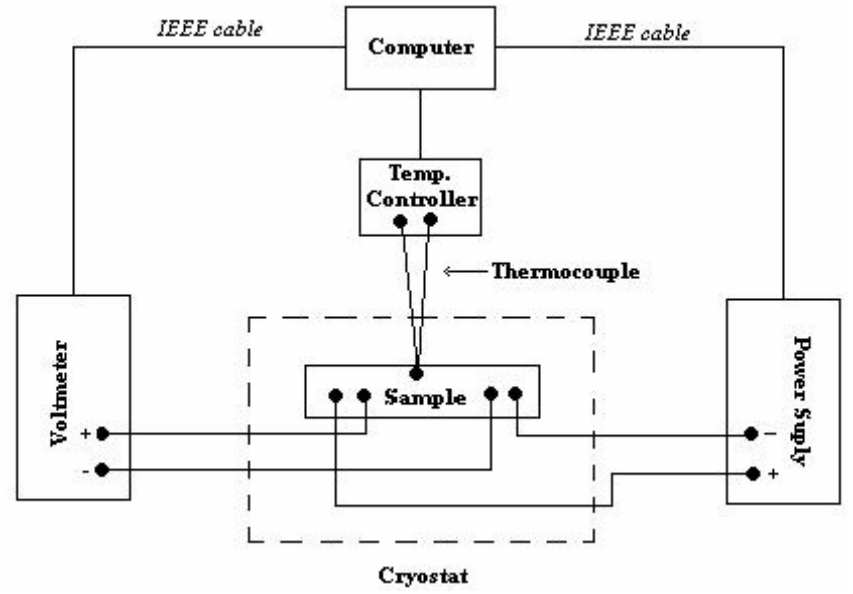

Figure 3-17: Schematic diagram of the four-probe method.

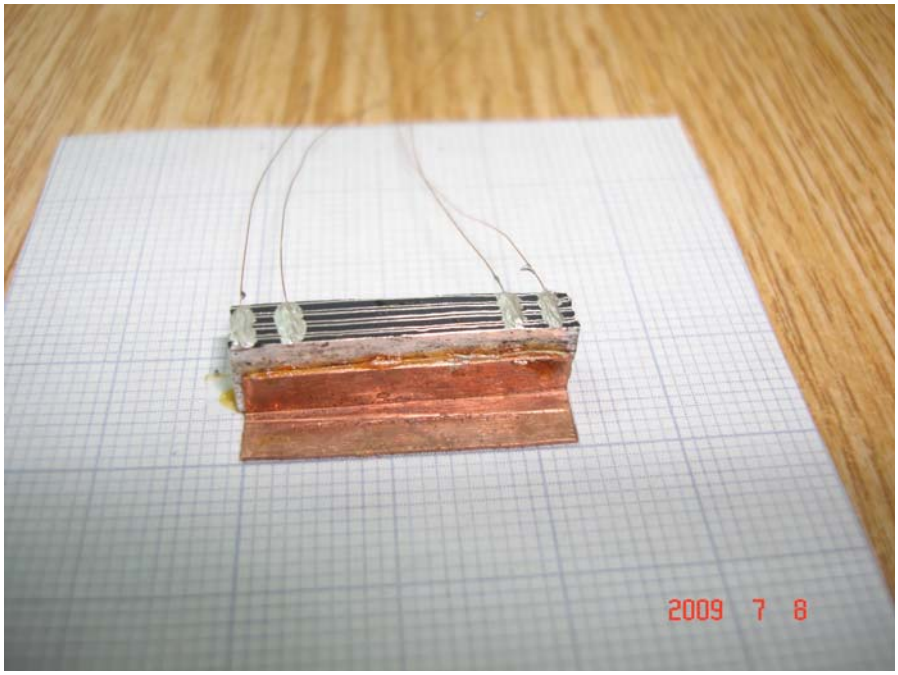

Figure 3-18: The multilayered sample between two copper plates for increasing the cooling and warming efficiency.

A Keithley 220 programmable current source, a Keithley 2700 nanovoltmeter and Oxford ITC503 temperature controller were used for the resistivity measurements. The transition temperature was defined as temperature at which the material conducts electricity without any detectable resistance. To convert voltage to resistivity the calculation is made as fallowing:

$$\rho = \frac{RA}{L}$$

where L is the distance between the inner electrical contacts, A is the cross-section of the sample.

3.6 Critical Current Density Measurements

Critical current density, J_c, measurements were performed with the four-probe method on all samples. The current was applied to the two outer electrical contacts and the voltage drops across the two inner electrical contacts were measured against current. Both voltage and current contacts were made with silver paint, the contact resistance being in the order of 0.1 Ω or lower. We determined J_c from the I-V curves at 77 K, the criterion for critical current was 1 μV/cm. Resistive contacts caused heating and the test was completed in possible shortest time to avoid extensiveness of this effect. A PCE Power Control GEN1500 programmable current source (6V-200A) and a Keithley 2700 Multimeter were used for I-V measurements. The schematic diagram of critical current measurement system is shown in Figure 3-19.

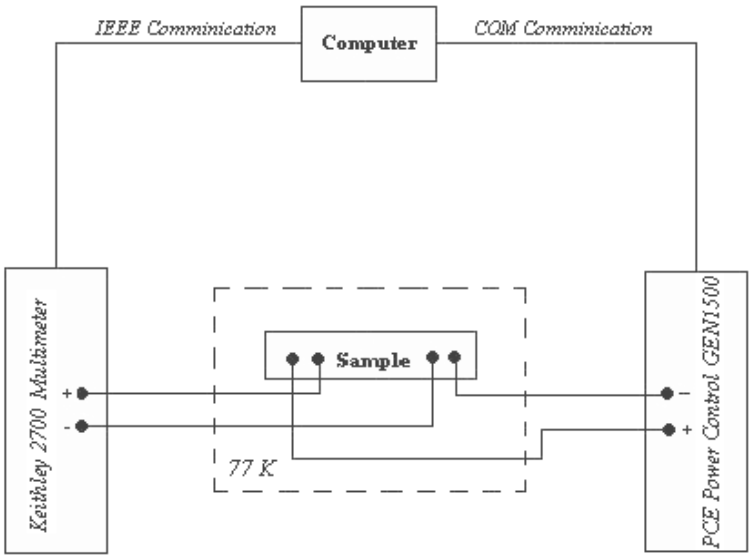

Figure 3-19: The schematic diagram of critical current measurement system.

3.7 Magnetoresistivity Measurements

We measured temperature (60-140 K) and DC magnetic field (0-0.5 T) dependent of resistivity of the samples with 20mA DC current for bulk sample and 50 mA for multilayered samples in a cryostat. The magnetic field was applied parallel and perpendicular to the current direction. The external dc magnetic fields for resistivity measurements were provided by an electromagnet. The transition temperature T_c was determined as the temperature at which the material conducts electricity without any detectable resistance. Magnetoresistivity measurement system is shown in Figure 3-16.

CHAPTER 4 – RESULTS AND DISCUSSIONS

4.1 Introduction

An enormous effort has been made on *Bi(Pb)-Sr-Ca-Cu-O* system to improve the superconducting properties by partial substitution and diffusion since its discovery [43-50]. The noble metals such as silver and gold, in the same column as copper in the periodic table, are of special interest for high-T_c superconductors. As to *Bi*-based HTSC-*Ag* compounds, a variety of structures, such as films on silver substrates [51, 52], wires with silver-cores [53-56], and silver-sheathed tapes [57-59], are used to obtain superconducting materials with high stability and a high value of the critical current density J_c [60]. It has been reported that J_c can be enhanced in $(Bi,Pb)_2Sr_2Ca_2Cu_3O_y/Ag$ multilayered (*Bi/Ag*) systems prepared by stacking *Ag* sheets alternatively between the oxide superconductor layers, and that J_c is proportional to the number of *Ag* sheets *NAg* [61]. The reason for the improvement is generally attributed to a high *c*-axis alignment and dense structure of the *Bi-2223* phase formed on both surface sides of the inserted *Ag* layer [62].

The effect of *Ag* diffusion on the properties of *BiPbSrCaCuO* thin films [63], and bulks [44, 46, 64] was investigated by several groups. Dzhafarov et al. [63] studied the effect of *Ag* diffusion on the properties of *BiPbSrCaCuO* thin films. In that work, superconducting *BiPbSrCaCuO* films have been evaporated on *Ag/MgO*

and *MgO* substrates by the electron-beam technique. It was found that the annealing of both types of films at 835 or 845°C resulted in formation of the mixed *Bi-2223* and *Bi-2212* phases with a high degree of preferential orientation with the c-axis perpendicular to the substrates. They also calculated the diffusion coefficient of silver and the activation energy in the temperature range of 650-800°C and the coefficient was described by the relation $D=2.2x10^{-5}\ exp(-1.2eV/k_BT)$. In addition, effects of *Ag*, *Cu*, *Sr* electro-migration on crystal structure, composition, surface morphology and superconducting properties of the near-anode and the near-cathode region of *BiPbSrCaCuO* samples have been investigated by XRD, SEM and resistivity measurements by Dzhafarov et al. [44]. They found that electro-migration of silver and components of *BiPbSrCaCuO* are accompanied by the formation of predominantly the *Bi-2223* phase and by an increase of the T_c on the cathode side in comparison with that on the anode side of the sample. Cömert et al. [64] investigated the effect of *Ag* diffusion on the crystal structure and electrical properties of *Bi(Pb)SrCaCuO* bulk superconductors. They observed that diffusion of silver in *Bi*-based superconductors stimulates a high degree of grain orientation along the *c*-axis, decreases the lattice parameters *a* and *c*, increases the critical transition temperature and the critical current density in comparison with the undoped samples. Dzhafarov et al [46] calculated the silver diffusion coefficient in *BiPbSrCaCuO* over the temperature range of 350-800 °C using the technique of successive removal of thin layers and measurement of the sample resistivity at room temperature and found that the coefficient could be described by the relation $D=5.2x10^{-3}\ exp(-0.70eV/k_BT)$. To our knowledge, no detailed work has been published on the diffusion coefficient of silver in *Bi(Pb)SrCaCuO* bulk superconductors. The only publication on this topic is a previous work on the calculation of the diffusion coefficient via the sample

resistivity measurements by removing the thin layer of silver diffused samples [46].

In this thesis, in order to obtain the optimum annealing temperature we studied the microstructure and superconducting properties of $Bi_{1.8}Pb_{0.4}Ca_{2.2}Sr_2Cu_3O_x$ samples that were annealed at various temperatures by performing XRD, SEM, temperature dependent dc resistivity and critical current density measurements. In addition, the *Ag* diffusion and its effects on the structural and superconducting properties of the $Bi_{1.8}Pb_{0.4}Ca_{2.2}Sr_2Cu_3O_x$ were studied. Besides, the silver diffusion in $Bi_{1.8}Pb_{0.4}Ca_{2.2}Sr_2Cu_3O_x$ has been studied over the temperature range 500-800°C using the technique of successive removal of thin layers and calculation of the lattice parameter *c* from XRD patterns, at room temperature, for each diffusion-annealing temperature (500, 600, 700, 750 and 800°C for 48 h).

4.2 Optimization of the annealing temperature

Since the discovery of superconductivity in the *Bi(Pb)-Sr-Ca-Cu-O* system, considerable progress has been made in preparing samples with high critical transition temperature, high critical currents and strong pinning force.

In this study, in order to find the optimum annealing temperature precursor powder (Alfa Aesar) was used as starting material for the preparation of $Bi_{1.8}Pb_{0.4}Ca_{2.2}Sr_2Cu_3O_x$ samples that were annealed at 830, 835, 840, 845, and 850 °C for 48 h in air. The heating and cooling rates of temperature were chosen to be 10 and 3 °C min^{-1}, respectively. The dimension of the pellet is 1.37x3.65x5.16 mm^3. The samples annealed for 48 h at 830, 835, 840, 845, and 850 °C will be hereafter denoted as *B830*, *B835*, *B840*, *B845*, and *B850*, respectively. XRD, SEM, EDS, dc electrical resistivity and critical current density measurements on annealed at different temperature samples were made to find optimum annealing temperature.

Fig. 4-1 shows the X-ray spectra of precursor powder bulk (which is named "Bulk with PP"), *B830*, *B835*, *B840*, *B845* and *B850* samples which are used to determine the optimum annealing temperature. Miller indices are indicated in the figure. One star (*), two stars (**), and three stars (***) in this figure indicate the high-T_c (*Bi-2223*), low-T_c (*Bi-2212*) and Ca_2PbO_4 phase, respectively. As annealing temperature increased from 830 to 840 °C, the intensities of the peaks corresponding to the *Bi-2223* phase increased while the intensities of the peaks corresponding to the *Bi-2212* phase decreased. When the annealing temperature was above 840 °C, the Ca_2PbO_4 phase was completely absent. The lattice parameter *c* determined from the (*00l*) peaks of the XRD data and tabulated in Table 4-1. The *c* lattice parameter is found to expand linearly with annealing temperature; it increases from 36.950 $\mathring{A}$ for B830 to 37.060 $\mathring{A}$ for B850 sample.

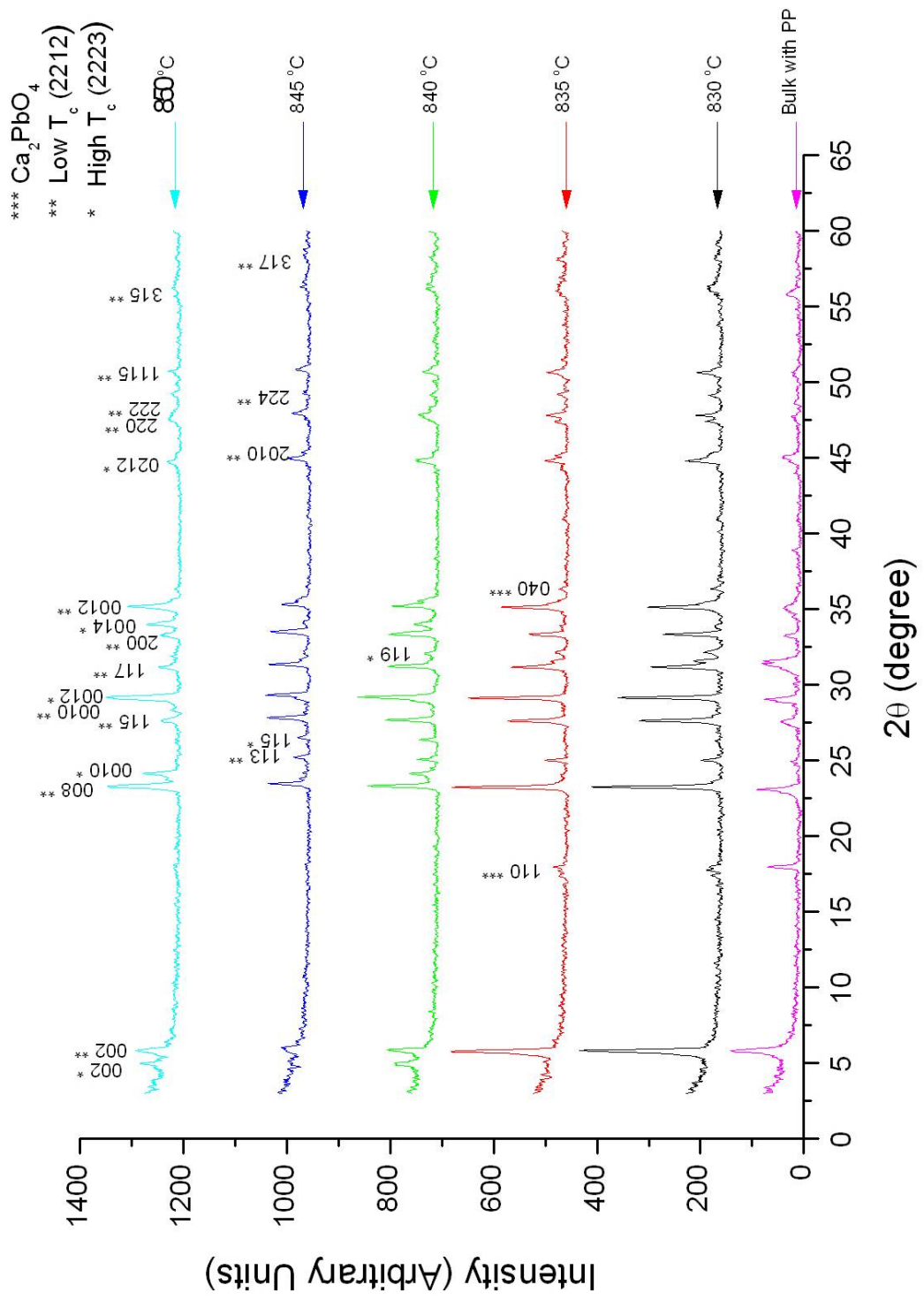

Figure 4-1: XRD analysis for the bulk samples.

Table 4-1: T_{c0}, lattice parameter *c* and critical current density values of the samples.

Samples	T_{c0} (K)	Lattice parameter *c* Å	Critical Current Density (A/cm^2)
B830	99	36.950	3.5
B835	104	36.968	54
B840	106	37.050	124
B845	105	37.058	121
B850	104	37.060	103

The surface morphology of the *B830*, *B835*, *B840*, *B845* and *B850* samples are studied by SEM and the surface micrographs are displayed in Fig. 4-2. The microstructure of *B830* and *B835* samples are remarkably different from that of *B840*, *B845* and *B850* samples. The grains are found to be much larger for the samples *B840*, *B845* and *B850* compared to those of *B830* and *B835*. This result is consistent with the XRD results. There are voids in the samples annealed at 845 and 850 °C while the surface of the *B840* sample is smoother and denser from that of other sample. These results indicate that the surface morphology of the sample is worsened with increasing the annealing temperature from 840 to 845 °C.

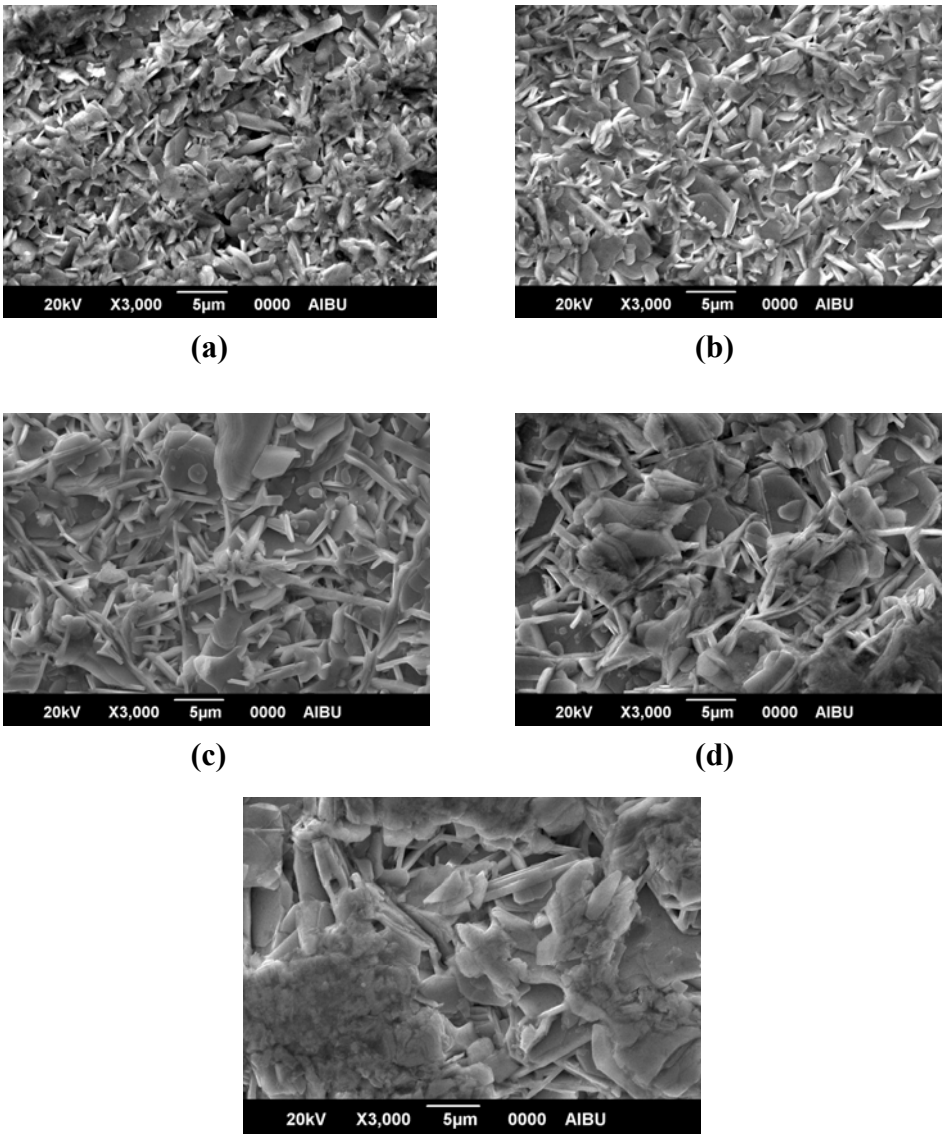

Figure 4-2: SEM analysis for the bulk samples. a) 830 °C, b) 835 °C, c) 840 °C, d) 845 °C, and e) 850 °C.

To investigate the effect of annealing temperature on the superconducting properties of the samples, we carried out dc electrical resistivity measurements as a function of both temperature and the dc magnetic field. The electrical resistivity was measured by using the standard four-probe dc technique in the temperature range of 90-140 K and the results are displayed in Fig. 4-3. The transition temperatures obtained from the dc resistivity as a function of temperature are given in Table 4-1.

Zero resistivity transition temperatures of the *B830*, *B835*, *B840*, *B845* and *B850* samples are determined as 99, 104, 106, 105, and 104 K, respectively. The highest T_c value was observed for the *B840* sample. As can be seen from the figure, the *B830*, *B835*, and *B850* samples showed a broad transition, which indicates the presence of impurities and weak links between the superconducting grains, which is in agreement with the SEM measurements. Metallic behavior was observed for all the samples above the onset temperature. The resistivity of the *B840* sample is smaller than that of the others above the onset temperature.

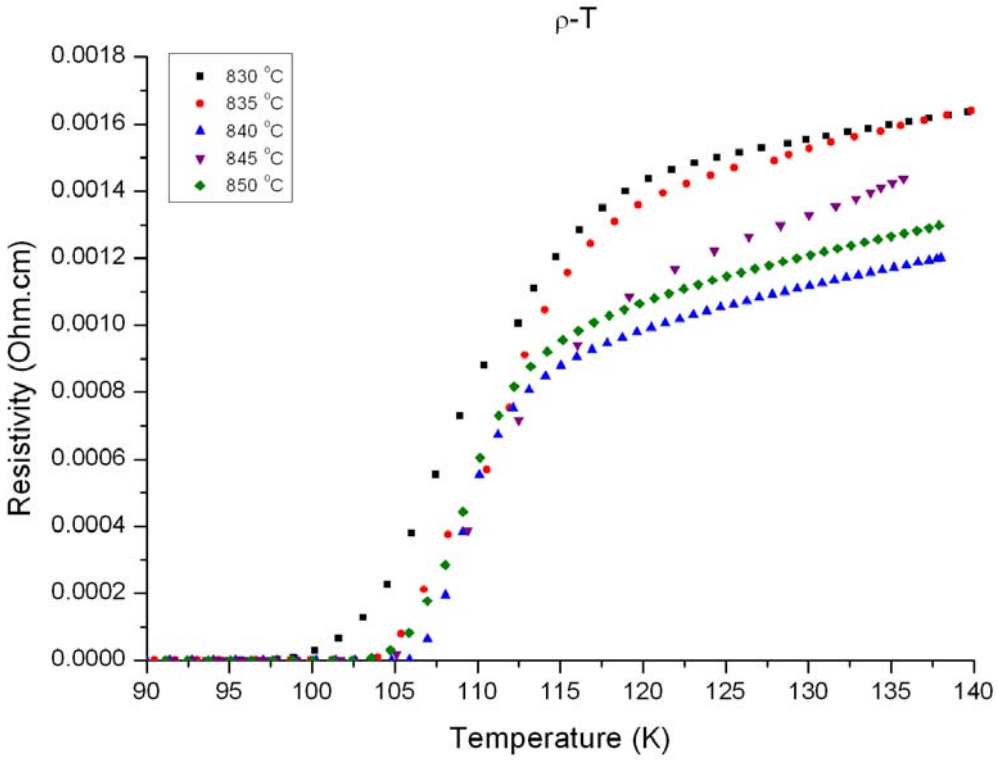

Figure 4-3: Resistivity versus Temperature Graph for The Bulk Samples.

We also carried out magnetoresistivity measurements as a function of temperature under dc magnetic fields of 0, 100, 200, 300, 400 and 500 mT for the *B840* samples. The measurements are taken in two different configurations; the first one has the current perpendicular to the dc field direction while for the second one

the current is parallel to the dc field, the schematic of the configurations are shown in the inset of Figs. 4-4a and 4b, which also display the measured temperature and dc field dependence of the resistivity. We observed that the zero resistivity transition temperature of the *B840* sample was 106 K for both configurations. The transition temperature of the sample for both configurations was found to decrease from 106 K to 88 K when the dc magnetic field is increased up to 0.5 T. No appreciable difference in temperature dependence of resistivity was found between the two different configurations, as an example we display the magnetoresistivity measurements at 300 mT for both configurations in Fig. 4-5. This behavior is the same for other field values.

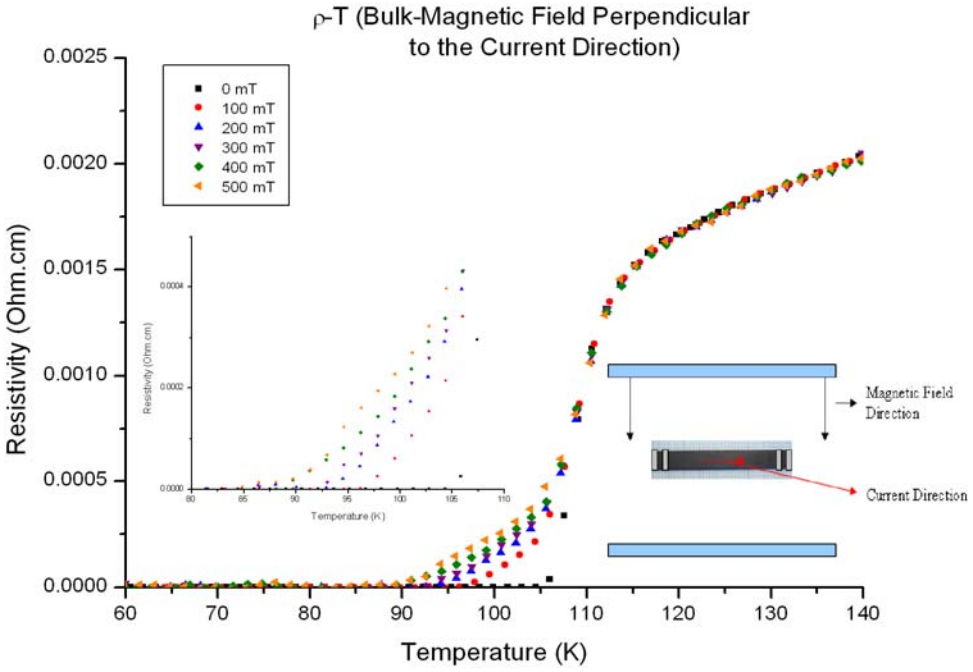

(a)

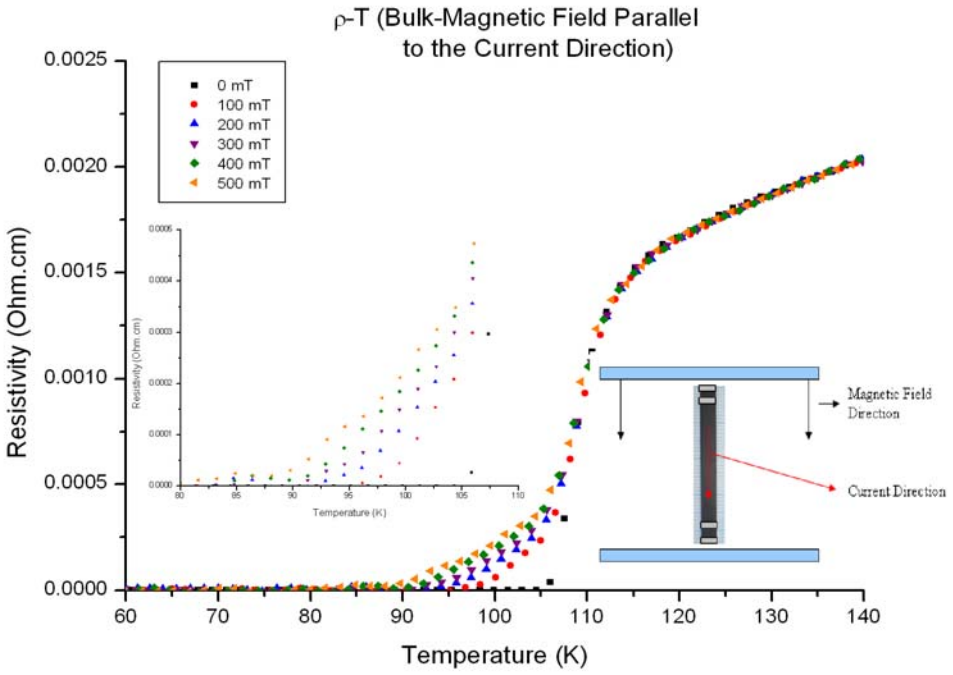

(b)

Figure 4-4: Magnetoresistivity as a function of temperature for the B840 sample with a) Perpendicular and b) Parallel magnetic fields.

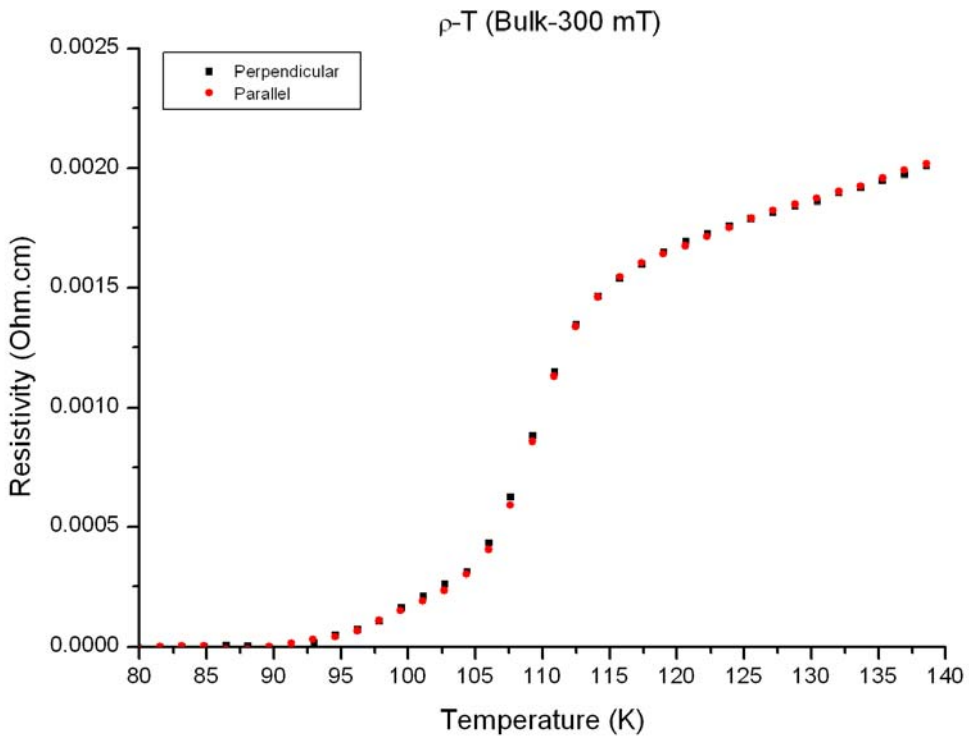

Figure 4-5: Magnetoresistivity measurement at 300 mT for both configurations for the B840sample.

We also measured the transport critical current density of the samples in the liquid nitrogen at zero magnetic fields. Fig. 4-6 shows the electric field as a function of critical current density for the samples. From I-V measurements, the critical current density value of the sample was calculated and is tabulated in Table 4-1. The critical current density is found to increase in the 830 to 840 °C annealing temperature range while it decreases above 840 °C.

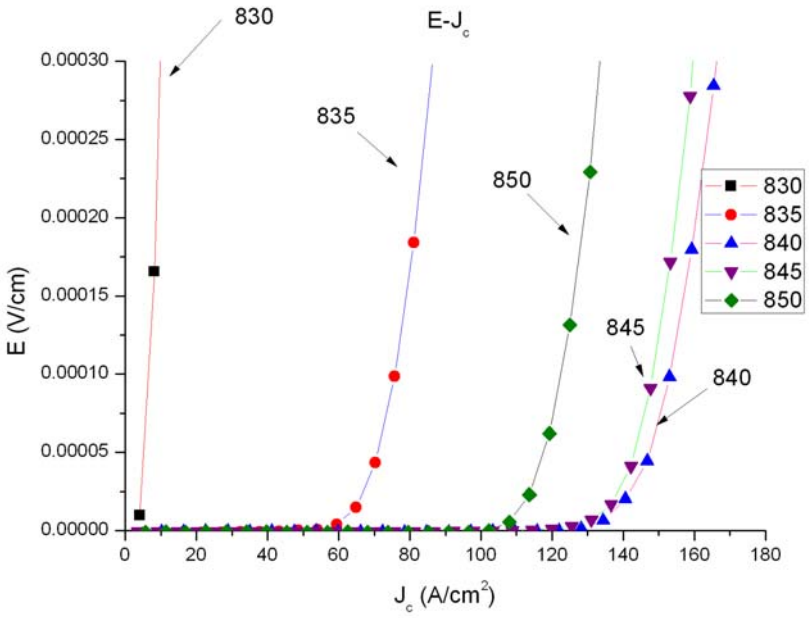

Figure 4-6: Electric Field versus Critical Current Density Graph for The Bulk Samples.

Based on XRD, SEM, dc resistivity and critical current density measurements and their analysis detailed above, we can conclude that the ideal annealing temperature for the $Bi_{1.8}Pb_{0.4}Ca_{2.2}Sr_2Cu_3O_x$ samples is 840 °C.

4.3 The effect of Ag Diffusion on superconducting and microstructure properties of $Bi_{1.8}Pb_{0.4}Ca_{2.2}Sr_2Cu_3O_x$

To investigate the effect of *Ag* diffusion on properties of $Bi_{1.8}Pb_{0.4}Ca_{2.2}Sr_2Cu_3O_x$, the sample annealed at 840 °C for 48 h was doped with silver by evaporating *Ag* film on the pellet. Doping of *Ag* in $Bi_{1.8}Pb_{0.4}Ca_{2.2}Sr_2Cu_3O_x$ was carried out by means of diffusion from an evaporated *Ag* film on pellets. The *Ag* coated superconducting samples were annealed at 840°C for 48 h. At the end of this procedure, *Ag* diffusion was realized through the samples. The *Ag*-diffused samples annealed for 48 h at 840°C will be hereafter denoted as *S840*. For comparison, an undoped sample (*B840*) was also annealed under the same conditions. In order to

calculate the *Ag* diffusion coefficient, virgin bulk samples were coated with an *Ag* layer and diffusion annealing was carried out at 500, 600, 700, 750 and 800 °C for 48 h. XRD patterns taken after the annealing indicates that *Ag* is incorporated into the samples. After diffusion runs, the layers of *Ag* diffused sample were removed from surfaces of the samples by etching in $HCl+H_2O$ solution for different times and by taking the XRD patterns to calculate the diffusion coefficient.

4.3.1 The effect of silver diffusion doped in $Bi_{1.8}Pb_{0.4}Ca_{2.2}Sr_2Cu_3O_x$ on microstructural and superconducting properties

We have studied the effect of *Ag* diffusion on the microstructure and superconducting properties of *Ag*-doped sample by performing XRD, SEM, dc resistivity and the critical current density measurements. The XRD patterns from the surface of the *B840* and *S840* samples are shown in Fig. 4-7. Some of the Miller indices are indicated in the figure. The lattice parameter *c* determined from the (*00l*) peaks of the XRD data are 37.050 $\mathring{A}$ for the B840 sample and 37.190 $\mathring{A}$ for the *S840* sample. The diffusion of silver is found to increase the lattice parameter *c* and the intensity of the peaks for the *Ag*-diffused sample (*S840*) in comparison with that for the undoped sample (*B840*). *Ag* diffusion also causes the peaks to shift to left uniformly, as can be seen from Fig. 4-7. Our measurements showed an increase of *c*-parameter by about 0.15%. The observed increase in *c* indicates that silver atoms diffused into the lattice of $Bi_{1.8}Pb_{0.4}Ca_{2.2}Sr_2Cu_3O_x$. This finding is in contrast with the results of Ref. [64] in some respects; while the intensity increase is also found in Ref. [64], they report a decrease in both *a* and *c* lattice parameters with silver doping of $Bi_{1.6}Pb_{0.4}Ca_2Sr_2Cu_3O_x$. We should note that the stoichiometry of the samples studied in Ref. [64] and the one used in the present study are not the same. We have compared the *c* parameters measured from the bulk and powder forms of *Ag*-diffused

samples to understand the behavior of silver-diffusion at the microscopic level. The larger *c* found for the bulk indicates that silver is incorporated into the crystal structure by diffusion which suggests that it substitutes one of the cations of the system (Bi^{3+}, Sr^{2+}, Ca^{2+}). The increase in the intensities of the peaks for the *Ag*-doped sample may testify the enhancement of grain growth and better orientation of grains with *Ag* diffusion, which is in agreement with the present SEM investigations which are detailed in the next paragraph. These findings are expected to increase the critical current density which is confirmed by critical current density measurements in the present work.

The relative volume fraction of the *Bi-2223* and *Bi-2212* phases in all the samples were estimated from the peak heights of the reflections belonging the same particular crystallographic plane, using the following well-known expressions [65, 66]:

$$f(2223) = \frac{\sum I_{H(hkl)}}{\sum I_{H(hkl)} + \sum I_{L(hkl)}} \qquad (2)$$

$$f(2223) = \frac{\sum I_{L(hkl)}}{\sum I_{H(hkl)} + \sum I_{L(hkl)}} \qquad (3)$$

Here $I_{H(hkl)}$ and $I_{L(hkl)}$ are the intensities of the (*hkl*) diffraction lines for *Bi-2223* and *Bi-2212* phases, respectively. Sample *S840* has higher volume fraction of *Bi-2223* phase than sample *B840* indicating that the formation of *Bi-2223* phase is enhanced by silver doping.

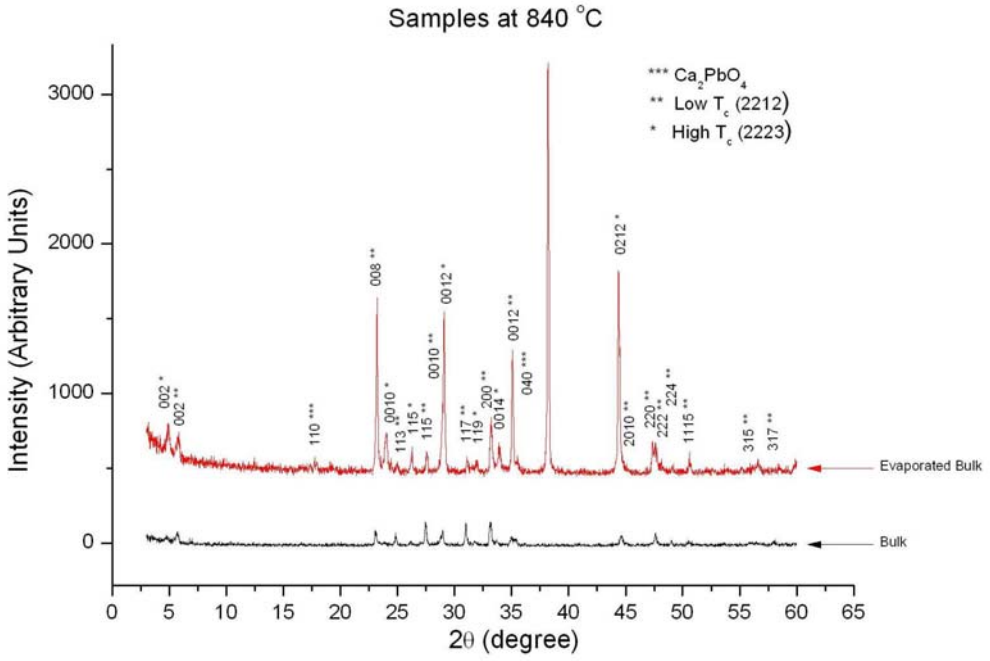

Figure 4-7: The XRD patterns for the B840 and S840 samples.

Surface morphology of the *B840* and *S840* samples was investigated by SEM in order to determine the grain sizes and the possible precipitation at the grain boundaries. Fig. 4-8 displays the surface micrographs for the *S840* and *B840* samples. It was observed that the grain size of the *S840* sample is quite larger than that of the *B840* sample. SEM pictures show better connectivity in *Ag*-diffused sample (*S840*). It was also found that the grains in the *B840* sample are oriented randomly and poorly connected. The surface of the *S840* sample is also smoother and denser. These results are in agreement with our XRD investigations discussed in the previous paragraphs and indicate that the surface morphology of the sample is appreciably improved by *Ag*-doping. The silver on the surface is thought to form a metallic connection between the grains. This connection acts like a resistive short-circuit and lowers the room temperature resistivity as will be confirmed by dc resistivity measurements in the next paragraph. From the SEM results, it is inferred that *Ag*-doping has a positive effect of decomposing the structure of the *Bi-2212*

phase, enhancing the *Bi-2223* phase formation, and improving the connections between the grains.

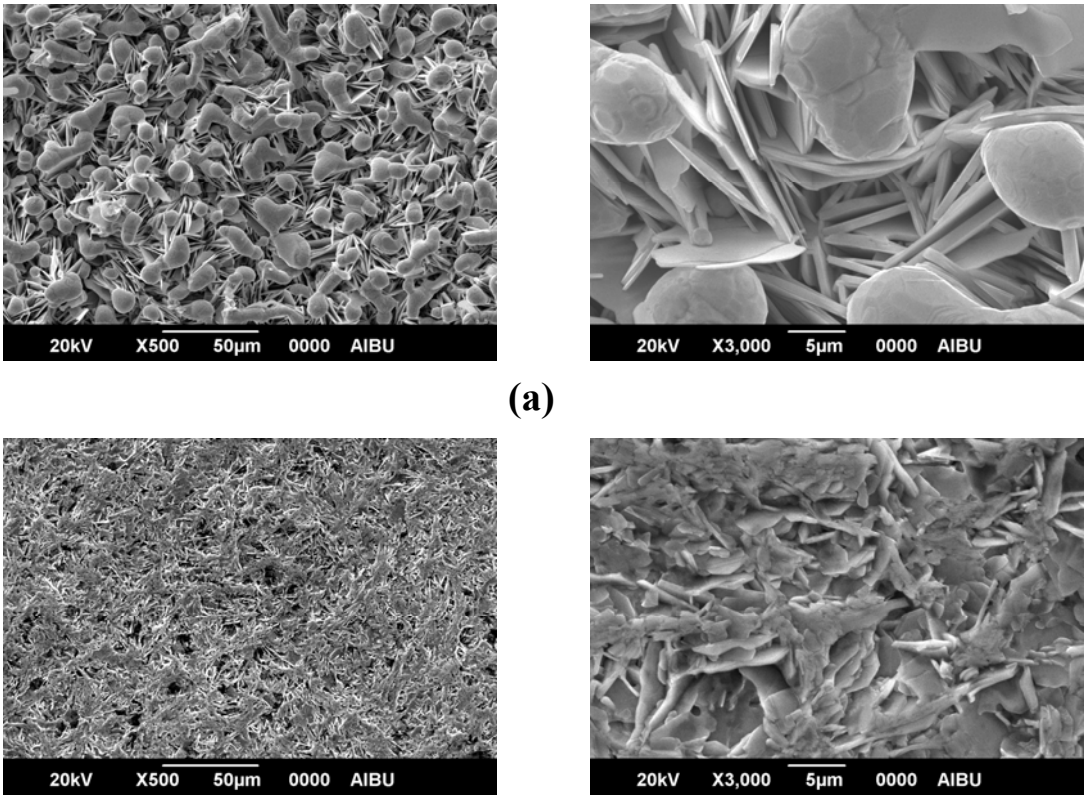

Figure 4-8: SEM micrographs of the a) S840 and b) B840 sample.

We have also performed EDS measurements for elemental analysis as presented in Fig. 4-9 which shows *Bi, Pb, Sr, Ca, Cu, O* and *Ag* element composition mappings taken on the cross-section of the S840 and B840 samples, respectively. On the Bi composition, distribution for the B840 sample in the figures is distributed homogeneously in the oxide layer, which implies that 48 h of annealing duration at 840°C was enough to cause transformation from low-T_c phase to high-T_c phase. As can be seen from the figure, it was observed that the silver is distributed in the *S840* sample.

Component	Type	Conc.	Units	
Bi	Calc	22.700	wt.%	
Pb	Calc	3.320	wt.%	
Sr	Calc	7.695	wt.%	
Ca	Calc	2.112	wt.%	
Cu	Calc	7.938	wt.%	
O	Calc	3.401	wt.%	
Ag	Calc	52.833	wt.%	
		100.000	wt.%	Total

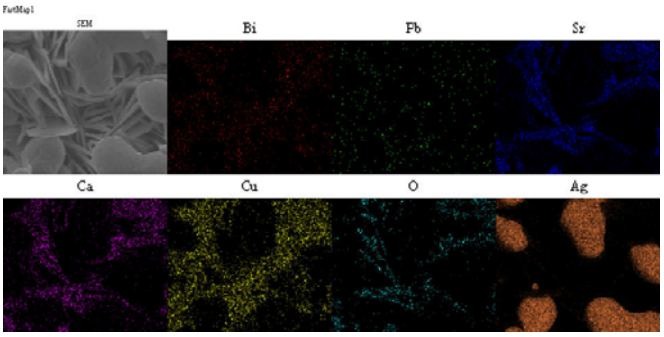

(a)

Component	Type	Conc.	Units	
Bi	Calc	31.740	wt.%	
Pb	Calc	3.931	wt.%	
Sr	Calc	23.289	wt.%	
Ca	Calc	7.534	wt.%	
Cu	Calc	14.750	wt.%	
O	Calc	18.757	wt.%	
		100.000	wt.%	Total

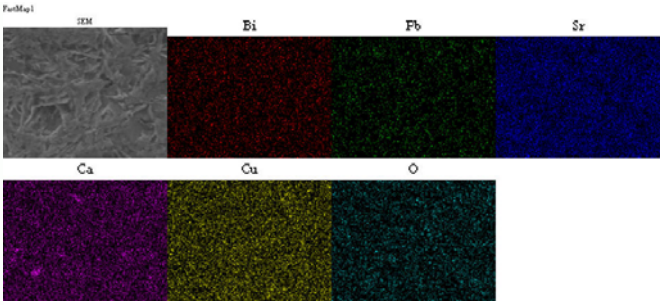

(b)

Figure 4-9: The results of EDS measurements of (a) *S840* and (b) *B840* samples.

The electrical resistivity was measured by using the standard four-probe dc technique. The resistivity as a function of temperature for *Ag*-doped and undoped samples is shown in Fig. 4-10. Both samples were annealed isothermally at 840°C for 48 hours. These samples show the resistive behavior above the onset critical transition temperature with the zero resistivity transition temperatures of 106 and 109 K for B840 and S840, respectively. The same increment in T_c was observed by Cömert et al. [64]. Data of increasing T_c by about 3 K in the *S840* sample over that for undoped samples are reproducible using different batches of the sample. The observed increase of T_c by silver diffusion makes the substitution at the *Cu* site less likely [67]. Room temperature resistivities calculated from the room temperature *I-V* curves are 0.0048 ohm-cm for the *B840* sample and 0.0013 ohm-cm for the *S840*

sample. It was observed that *Ag*-doping decreased the room temperature resistivity which can be explained by noting the role of Ag in connecting the grains as mentioned above.

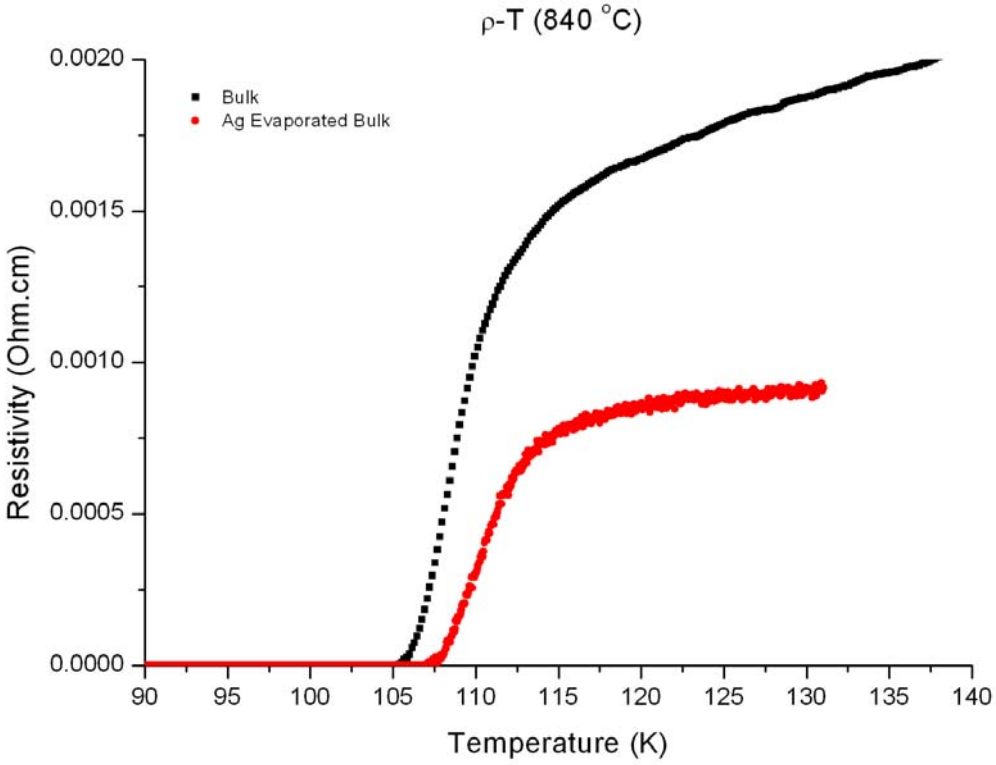

Figure 4-10: Temperature dependence of resistivity for the B840 and the S840 samples annealed at 840 °C for 48 hours.

We have carried out the critical current density measurements on *B840* and *S840* samples to study the effect of *Ag*-doping on the critical current density. The measured transport J_c values are found to be 123 and 696 A/cm^2 for *B840* and *S840*, respectively. The approximately 500% increase in J_c is in contrast with the results given in Ref. [64] which reported that *Ag*-doping did not change J_c at all. The increase of J_c in $Bi_{1.8}Pb_{0.4}Ca_{2.2}Sr_2Cu_3O_x$ by addition of silver might be due to: i) increase of the flux pinning centers due to the presence of silver in the intergrain regions [68], ii) improved coupling between the silver-coated superconducting grains [69] or iii) silver-stimulated grain growth through partial melting of *Bi(Pb)SrCaCuO*

and creation of uniform grain size distribution [70, 71]. The increase in the intensities of the peaks for the *Ag*-doped sample in XRD figure (Fig. 4-7) may indicate an enhancement of the grain growth and better orientation of grains with *Ag* diffusion, which supports the findings from the SEM micrographs. Larger grains and better grain orientation lead to an increased critical current density. A similar effect of *Ag*-diffusion in J_c is also found for the T_c in the present study. In short, one can say that in silver doped $Bi_{1.8}Pb_{0.4}Ca_{2.2}Sr_2Cu_3O_x$, silver is deposited in the intergrain boundaries as well as diffused into the lattice which leads to two main modifications; (i) the lattice parameter *c* is increased by 0.15%, (ii) the morphology of the surface is improved as indicated by larger and better oriented grains. These modifications have positive effect on both T_c and J_c of the samples: T_c increases from 106 to 109 K while J_c increases from 123 to 696 A/cm^2. *Ag*-doping also changes the room temperature resistivity from 0.0048 to 0.0013 ohm-cm. In addition, *Ag* diffusion improved the surface morphology and increased the *Bi-2223* phase formation [72-79].

4.3.2 Calculation of diffusion coefficient and activation energy of silver in $Bi_{1.8}Pb_{0.4}Ca_{2.2}Sr_2Cu_3O_x$

In the present work, in order to calculate the diffusion coefficient and activation energy of silver in $Bi_{1.8}Pb_{0.4}Ca_{2.2}Sr_2Cu_3O_x$, virgin bulk samples were coated with an *Ag* layer and diffusion annealing was carried out at 500, 600, 700, 750 and 800 °C for 48 h. As mentioned in the experimental details section, layers containing *Ag* from the top of the sample were removed by etching in $HCl+H_2O$ solution for different times. One would expect that the change of *c*-parameter with thickness of the samples resembles the concentration distribution of diffused silver impurity. From these considerations, the change of lattice parameter *c* is studied by successive removal of thin layers from the sample and by XRD measurements.

In this study, it is supposed that the conditions of impurity diffusion from a constant source into a semi-infinite solid can be descried by the following equation [72]:

$$N(x,t) = N_0[1 - erf(x/2\sqrt{Dt})] \quad (1)$$

where $[erf(x/2\sqrt{Dt})]$ is the error function with argument $y = (x/2\sqrt{Dt})$;

$$erf(y) = \frac{2}{\sqrt{\pi}} \int_0^y \exp(-y^2).$$

Here N_0=*N(0,t)* is the constant concentration on the surface of the sample, *N(x,t)* is the impurity concentration at the distance *x*, *D* is the diffusion coefficient, and *t* is the diffusion-annealing time.

Fig. 4-11 displays the variation of the lattice parameter $\Delta c/c_0$ (c_0 is the lattice parameter of the undoped region of the sample) as a function of thickness of the sample, exposed to silver diffusion at 750 °C for 48 h. The data in Fig. 4-11 are fitted to Eq. (1) by using a non-linear least-square fit procedure; the resulting concentration profile is plotted with the solid curve in Fig. 4-11.

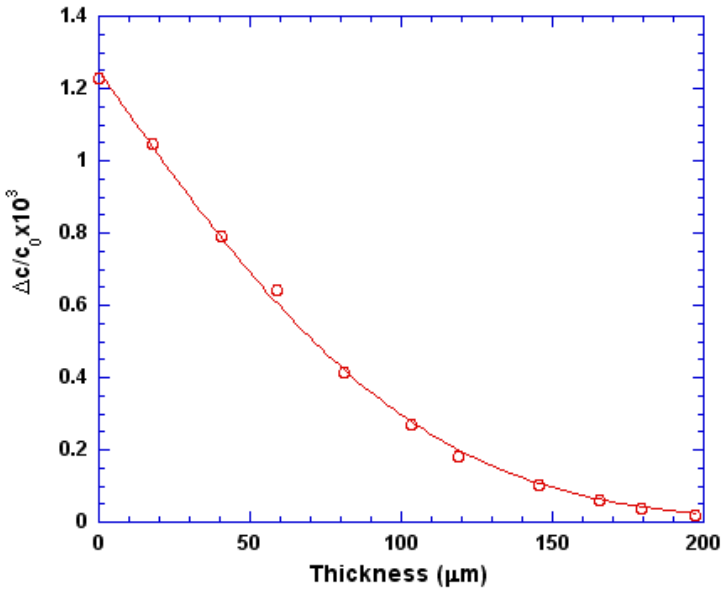

Figure 4-11: Deformation $\Delta c / c_0$ versus the thickness of $Bi_{1.8}Pb_{0.4}Ca_{2.2}Sr_2Cu_3O_x$ diffusion-doped by silver at 750 °C for 48 h (the solid line is calculated according to equation (1)).

The regression R= 0.9995 indicates a good fit, and we found $D = (5.8 \times 10^{-9} \pm 1.2 \times 10^{-11})$ cm^2s^{-1} for the sample annealed at $750^\circ C$ for 48 h. The same fitting was performed for the samples that were diffusion annealed at 500, 600, 700, and 800 °C for 48 h, and the values of diffusion coefficient were found to be 1.15×10^{-8} for 800 °C, 3.40×10^{-9} for 700 °C, 9.2×10^{-10} for 600 °C, and 2×10^{-10} for 500 °C. As can be clearly seen, diffusion at lower temperatures is much less significant. The mean value of the diffusion coefficient of silver in $Bi_{1.8}Pb_{0.4}Ca_{2.2}Sr_2Cu_3O_x$ as a function of temperature is given in Fig. 4-12. The results of this study showed that the silver diffusion coefficient in the temperature range 500-800°C increases in accordance with the Arrhenius relation

$$D = 2.9 \times 10^{-4} \exp(-1.05 \text{ eV}/k_B T)$$

The activation energy obtained from the present work is 1.05 eV which can be compared to the value reported by Dzhafarov et al. [46] who determined it via resistivity versus thickness measurements and found it to be 0.70 eV. Moreover, the

values of the diffusion coefficient of silver in this study are almost ten times smaller than that in Ref. [46]. These discrepancies may be related to the differences in chemistry (stoichiometry) and structure (high porosity) of the BiPbSrCaCuO samples used in Ref. [4] and the present study. Diffusion rate depends on the number of vacancies, temperature and activation energy (energy barrier for diffusion). The porosity would mean a lower activation energy which is also an indication of higher diffusivity.

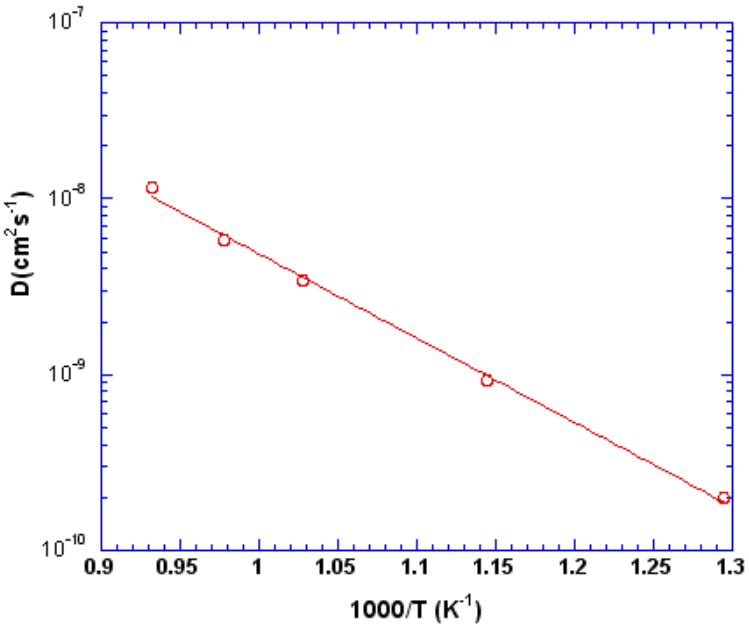

Figure 4-12: Temperature dependence of the silver diffusion coefficient and activation energy in the $Bi_{1.8}Pb_{0.4}Ca_{2.2}Sr_2Cu_3O_x$.

4.4 The effect of multilayered $Bi_{1.8}Pb_{0.4}Ca_{2.2}Sr_2Cu_3O_x$/Ag on superconducting and microstructure properties of $Bi_{1.8}Pb_{0.4}Ca_{2.2}Sr_2Cu_3O_x$

The powder-in-tube method (PIT), among various methods to fabricate metal/superconductor composites, has proved to be an attractive route for producing superconducting wires, tapes and filaments. The PIT process, the quality and reactivity of the precursors are of vital importance to the properties of superconducting grown tapes. A precursor powder with a nominal chemical

composition of $Bi_{1.8}Pb_{0.4}Ca_{2.2}Sr_2Cu_3O_x$ was used to fabricate the multilayered $Bi_{1.8}Pb_{0.4}Ca_{2.2}Sr_2Cu_3O_x$/Ag samples using the powder-in-tube method. Ag tube 26 cm in length (about 0.3 mm in thickness and 13.134 grams) was used for producing multilayered sample prepared by PIT technique. The multilayered bulk was prepared by filling the precursor powder into the Ag tube. Number of produced layers was 2, 4 and 8. 10. 462 grams of precursor Bi-based powder ($Bi_{1.8}Pb_{0.4}Ca_{2.2}Sr_2Cu_3O_x$) was filled inside the silver tube of 6.3 mm outer diameter with total mass of 23.596 grams, and then both sides of the Ag tube were sealed with groove rolling machine. At the initial stage the powder density was low, as expected. After sealing the Ag tube, it was cold drown to 3.54 mm outer diameter and 43.2 cm in length by using the drawing machine. Drawing process steps can be seen from Table 3-1. The density increased during the drawing process. To remove the work hardening on the Ag tube, it was sintered in air at 900 °C for 0.5 hour (at furnace self speed). By an intermediate rolling, pressing and sintering procedure, the wire was rolled to obtain a tape which is 0.99 mm thick. The rolling procedure was not effective in obtaining further substantial increases of the powder density, but greatly improved the orientation of the ceramic grains inside the silver sheath. Tapes were cut into 5 pieces about 3.97 cm in length, and then they were sintered under the atmosphere of open air at 830 °C for 2 hours. Some of the tapes (5 of them) were longitudinally cut into 2 pieces to produce the 10-layered Ag-ceramic interfaced sample; similarly, 2- and 4-layered samples were prepared in the same manner of ten-layered sample. The preparation of layered structures involves the following steps: 1) The tapes have silver on top and bottom and Bi-oxide in between the Ag layers. 2) We put these tapes on top of each other and fill the interface regions Bi-oxide powder. 3) Press the sandwich to obtain a stacked multilayer structure, such that the bottom has Ag, top

has Bi-oxide and between there are several layers of Bi-oxide and Ag in alternating fashion. The pressure used to press the tapes together was 344 MPa which is obtained with a mechanical press. All layered samples were sintered in air at 840 °C for 48 hours (with 4 °C/min. heating and 1 °C/min. cooling rates). After sintering, the multilayered samples were pressed at 418 MPa pressure for five minutes. They were annealed at 840 °C for 48 hours in the atmosphere of open air. Dimensions of the final two-, four-, and eight-layered annealed samples were approximately 4.96x42.00x1.11 mm^3, 5.98x44.00x1.49 mm^3, 6.98x46.00x3.96 mm^3, respectively. In order to investigate the effect of Ag layers, we performed XRD, SEM, EDS, dc resistivity and critical current density measurements on the prepared samples.

4.4.1 XRD investigations

In order to investigate the effect of Ag on the inhomogeneity of the grain alignment and crystallite structure in Bi-2223 layer, we have taken two XRD measurements in which one is far away from the Ag layer (Figure 4-13) and the other is near the Ag layer (Figure 4.14). For comparison, we have also taken the XRD pattern of the bulk $Bi_{1.8}Pb_{0.4}Ca_{2.2}Sr_2Cu_3O_x$ sample. Some of the Miller indices were indicated in Figures 4-13 and 14. From XRD patterns in the region near the Ag layer, lattice parameter *c* calculated from *(00l)* peaks of the XRD patterns were 37.195 $\mathring{A}$ for the two-layered sample, 37.205 $\mathring{A}$ for the four-layered sample and 37.210 $\mathring{A}$ for the eight-layered sample. As can be clearly seen from Figure 4-14, most of the peaks, especially (0010) peak, shifted to the lower angle when the number of layers increased. The observation indicates that c parameter increases for BSCCO near Ag layer as the number of layer is increased. It was also obtained that the intensities of the peaks increase with increasing the number of layers. The increase in the intensities of the peaks may testify the enhancement of grain growth and better

orientation of grains with increasing the number of layers, which is in agreement with present SEM investigations that will be discussed below. These results cause the critical current density to increase, as will be confirmed in the critical current density measurements in the present work. In the case of far away from the Ag layer, the calculated c parameters are less then that of the region near the Ag layer. As the number of Ag layers increased most of the peaks shifted to the lower angle, which implies that the lattice parameter c increases with increasing the number of layers in the region of BSCCO away from the Ag layer. Comparing the (0010) peak in both cases, the strong intensity and the small value of full width at half maximum (FWHM) in the (0010) peak were observed in the region near the Ag layer while the weak intensity and the large value of FWHM were observed in the region far away from the Ag layer. These results imply that there are two regions, highly *c*-axis aligned region (near to Ag layer) and low aligned region (far away from Ag layer) in the $Bi_{1.8}Pb_{0.4}Ca_{2.2}Sr_2Cu_3O_x$ layer [61].The increase in lattice parameter *c* in the region near to Ag layer implies that Ag diffused into the $Bi_{1.8}Pb_{0.4}Ca_{2.2}Sr_2Cu_3O_{x.}$ We have already presented the results of the interpretation of Ag diffusion into $Bi_{1.8}Pb_{0.4}Ca_{2.2}Sr_2Cu_3O_x$ in Chapter 5 Section 1.3. In that investigation, the increase in the lattice parameter *c* by Ag diffusion-doping was observed. The volume fractions for the samples were determined by comparing the peak intensities of different phases, deduced from the XRD patterns. It was obtained that the high-T_c phase increased with increasing the layer number.

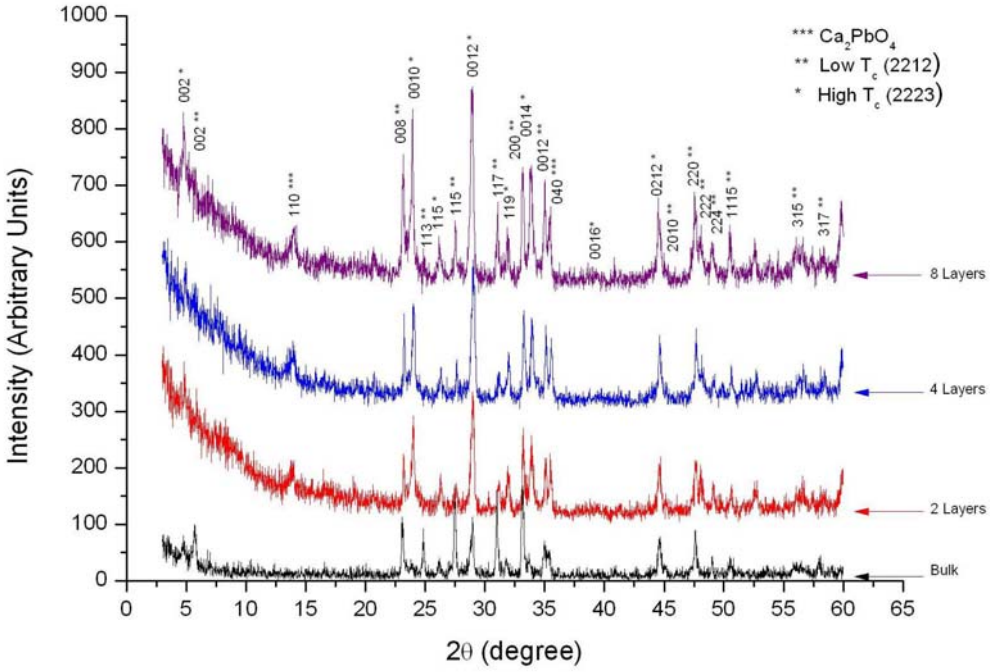

Figure 4-13: XRD pattern taken from a region far away from the Ag layer in the multilayered samples.

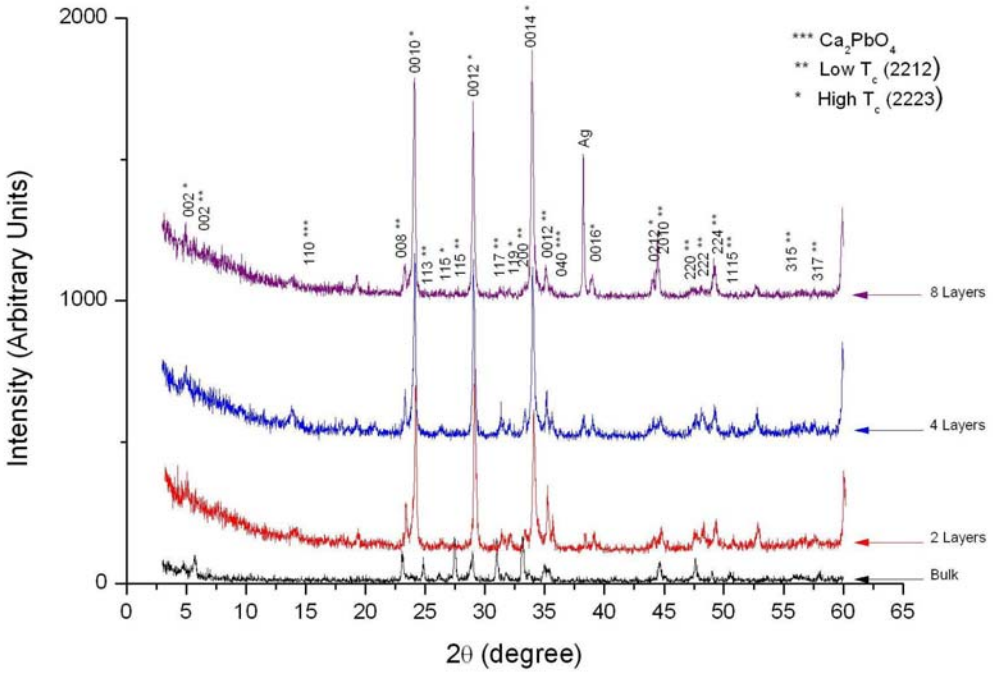

Figure 4-14: XRD pattern obtained from a region near the Ag layer in the multilayered samples.

4.4.2 SEM and EDS analyses

We have investigated the change of distribution of elemental composition with number of Ag layers in the $Bi_{1.8}Pb_{0.4}Ca_{2.2}Sr_2Cu_3O_x$/Ag using EDS technique. Using this technique, we studied distribution of different elements in the interface region between the $Bi_{1.8}Pb_{0.4}Ca_{2.2}Sr_2Cu_3O_x$ and Ag layers. Figures 4-15a, b, and c show Bi, Pb, Sr, Ca, Cu, O and Ag element composition mappings taken on the cross-section of the two-layered, four-layered and ten-layered samples, respectively. In the figure, the longitudinal cross-section of the multilayered samples having 2, 4, and 8 thin Bi(Pb)-2223/Ag layers are visible in detail. Since Bi has highly subliminal, its distribution in EDS is a good indication of superconductive properties of the samples. In Fig. 4-15, it can be seen that Bi is distributed homogenously for all the considered layer structures. This finding indicates that 48 h of annealing duration at 840°C was enough to cause transformation from low-T_c phase to high-T_c phase. It is also seen that the thickness of HTS layers and the Ag interlayers are fairly uniform for all the layered samples.

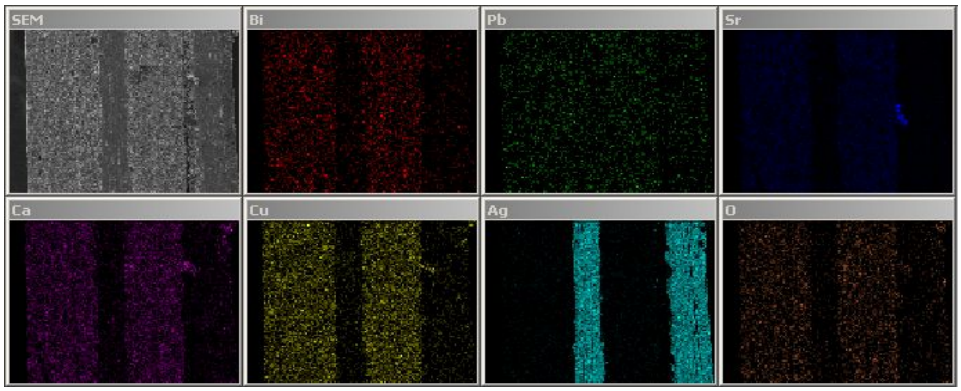

(a)

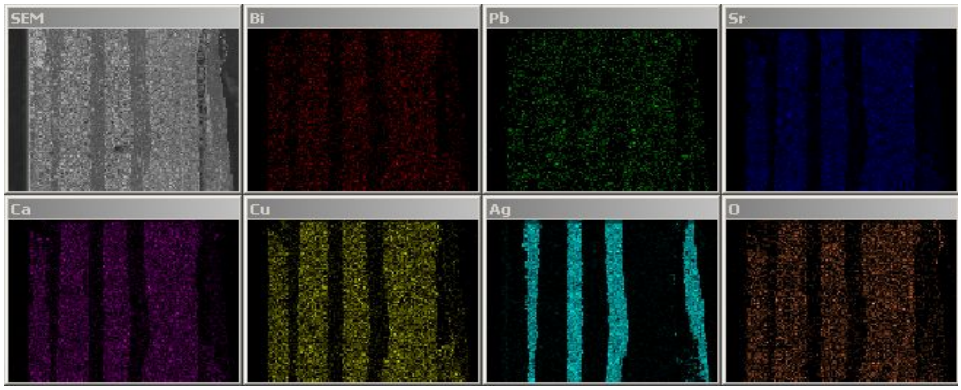

(b)

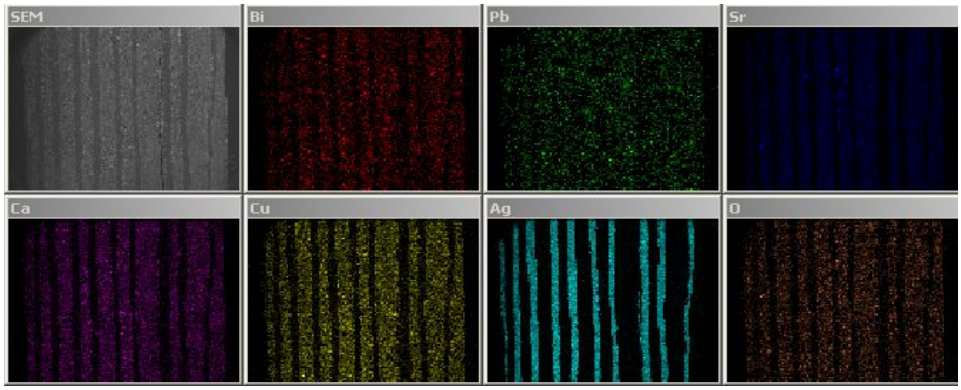

(c)

Figure 4-15: EDS analysis of Ag-BPSCCO site of a) 2-layered, b) 4-layered and c) 10-layered (before 2 layers broken) samples.

In order to investigate the grain size and microstructure properties in the multilayered samples, we took SEM measurements. Figure 4-16a corresponds mainly to the outer oxide layer and Figure 4-16b obtained from the center of the tape. From

the figures, high alignment of large crystallites and dense structure were observed when the number of Ag layers increased. From SEM results, high alignment of large plate-like crystallites and dense structure of Bi(Pb)-2223 were observed near the region of the interface between Bi(Pb)-2223 and Ag layers (Fig. 4.16b). On the other hand, the regions far away for the Ag layer in the oxide have low alignment and porous structures (Fig. 4.16a), which is consistent with the literature [80, 81]. The results of SEM observations agree with the results of XRD measurements.

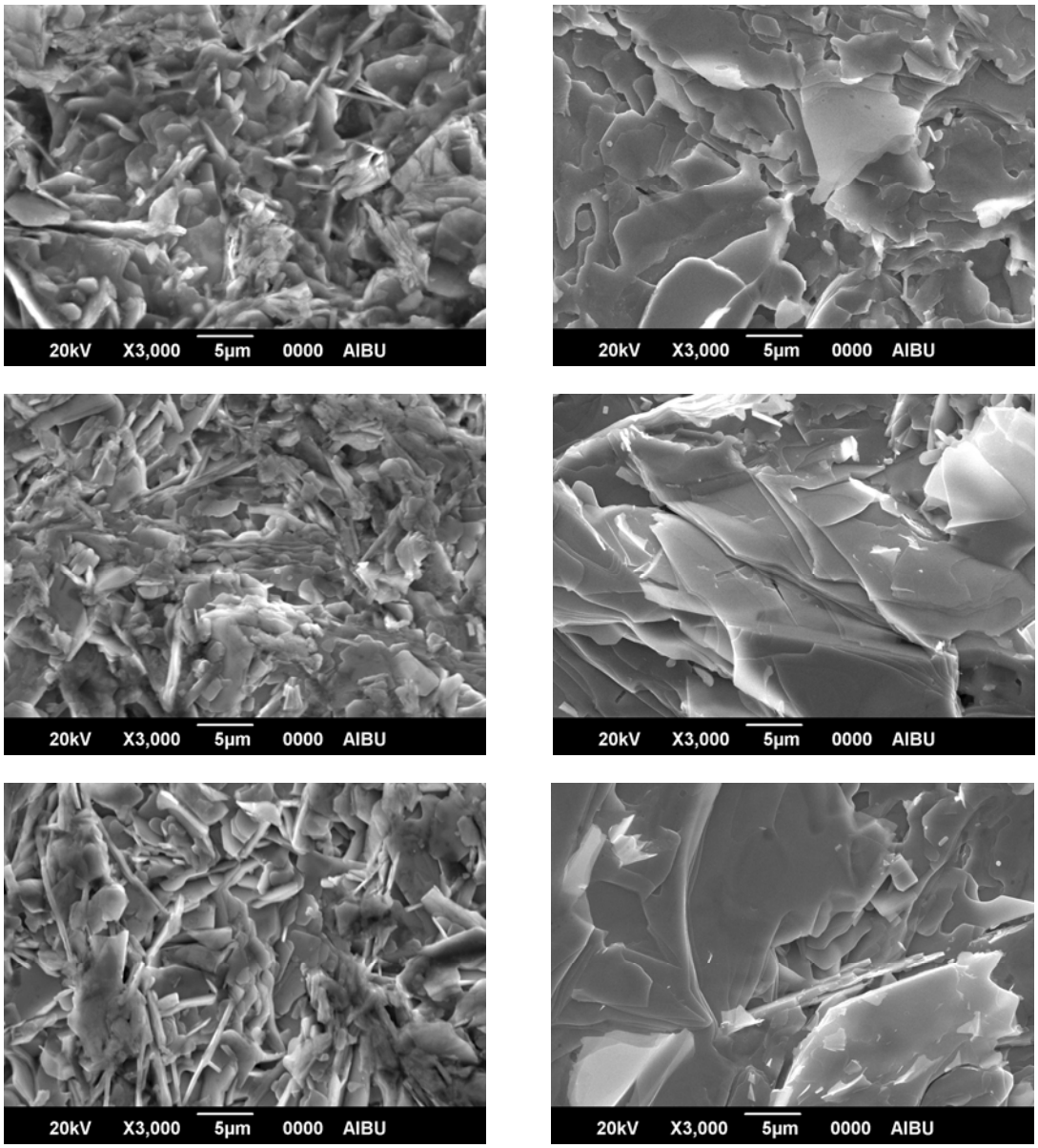

Figure 4-16: SEM micrographs of BPSCCO of the a) region far away from the Ag layers for i) 2-layered, ii) 4-layered and iii) 8-layered samples b) region near the Ag layers for i) 2-layered, ii) 4-layered and iii) 8-layered samples.

4.4.3 Transport measurements (T_c and J_c)

Electrical resistivity was measured by using the four-probe dc technique, in temperature range between 60 and 140 K for the Bi-oxide, two-, four-, and eight-layered samples as shown in Figure 4-17. These samples show the resistive behavior above the onset critical transition temperature with the zero resistivity transition temperature of 106.0 ∓ 0.2 and 107.3 ∓ 0.2, 108.3 ∓ 0.2, and 109.2 ∓ 0.2 K, respectively. The T_c of multilayered tapes is greater than that of the undoped one (B840). From these results, the T_c value gradually increases as the number of Ag layers increased. In addition, there is a little broadening of transition width in the two-layered sample, which indicates impurity phases. However there is no evident transition plane in the Bi-2212 transition range, which shows that the main phase is Bi-2223.

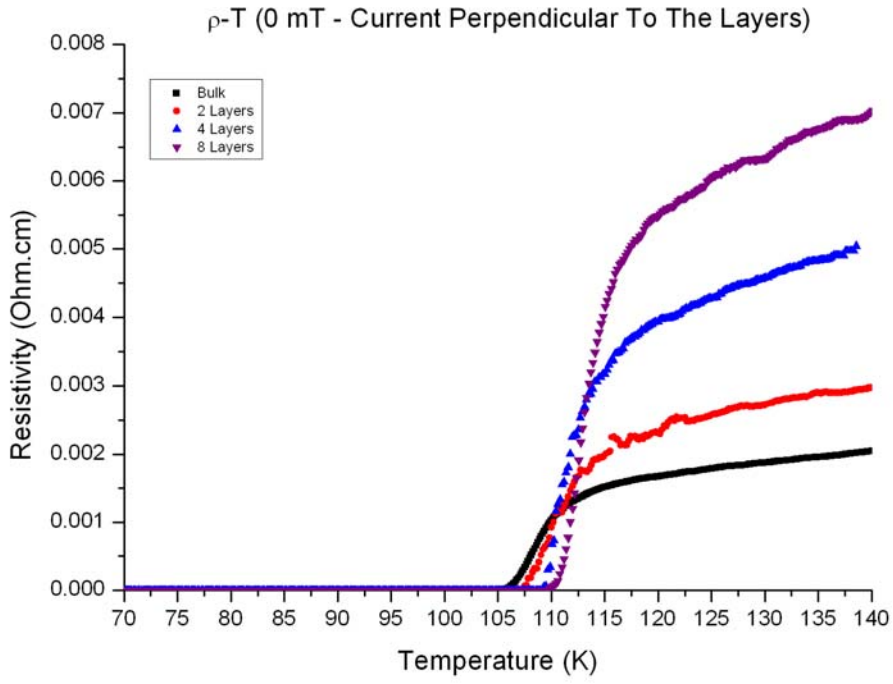

Figure 4-17: Resistivity vs. Temperature at zero magnetic field for bulk (Bi-oxide), two-, four-, and eight-layered samples.

We have carried out magnetoresistivity measurements for the layered samples at 0, 0.1, 0.2, 0.3, 0.4 and 0.5 T. In these measurements, we took four magnetoresistivity measurements for each sample in the configuration depicted in Figures 4-18a, b, c, and d. In Figure 4-18a, configuration is called C1 and it corresponds to magnetic field parallel to growth direction, current is along the surface of the film and perpendicular to the magnetic field. In Figure 4-18b, configuration is called C2 and it corresponds to magnetic field perpendicular to growth direction, current is along the surface of film and parallel to magnetic field. In Figure 4-18c, configuration is called C3 and it corresponds to magnetic field parallel to growth direction, current is across the surface of the film and parallel to the magnetic field. In Figure 4-18d, configuration is called C4 and it corresponds to magnetic field perpendicular to the growth direction, current is across the surface of the film and perpendicular to the magnetic field.

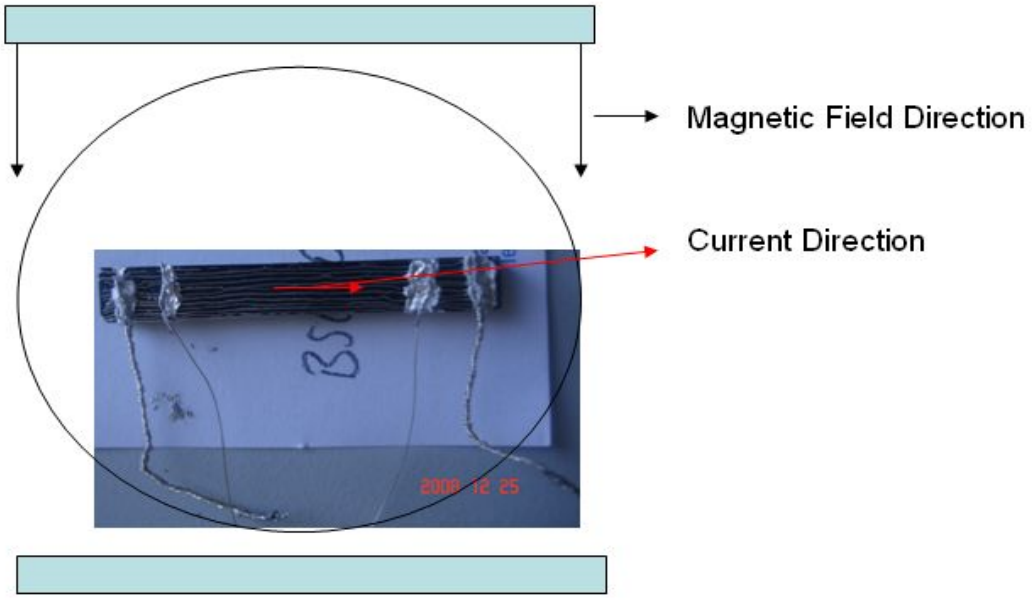
Magnetic Field Direction
Current Direction

(a)

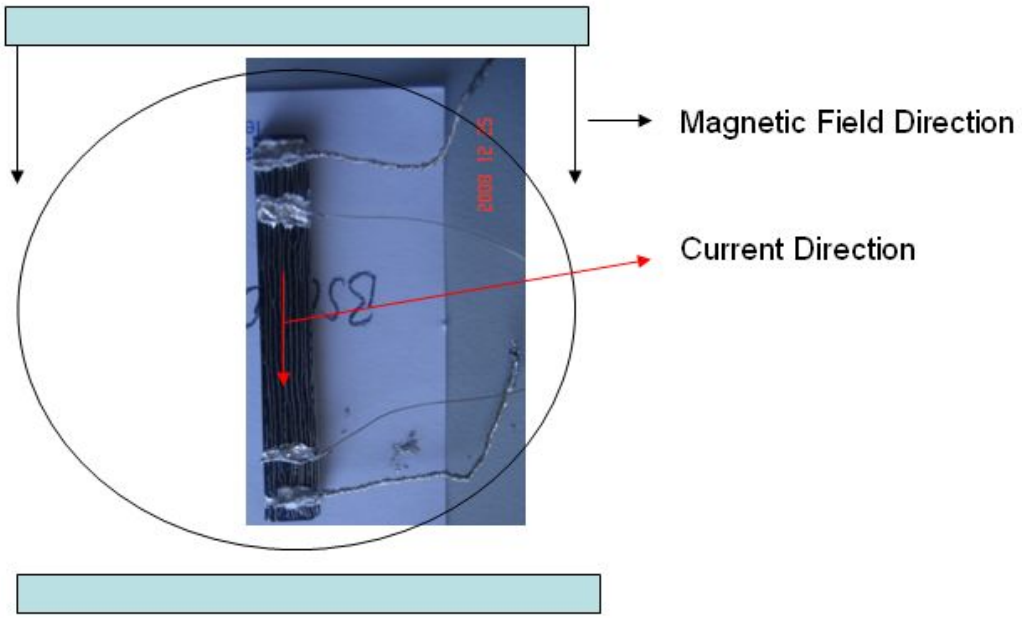
Magnetic Field Direction
Current Direction

(b)

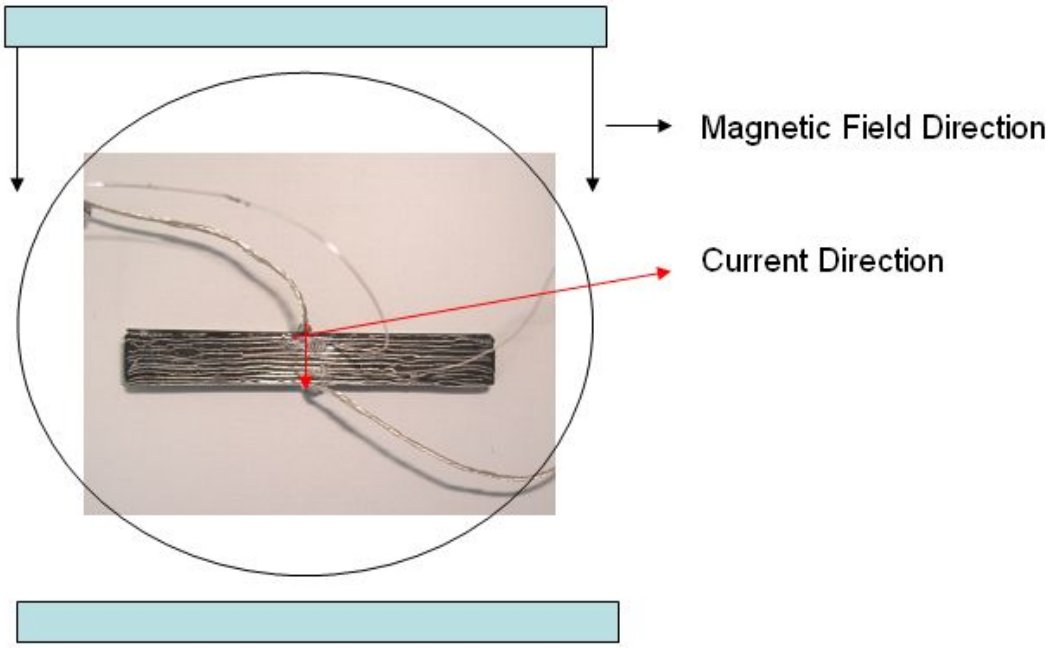

(c)

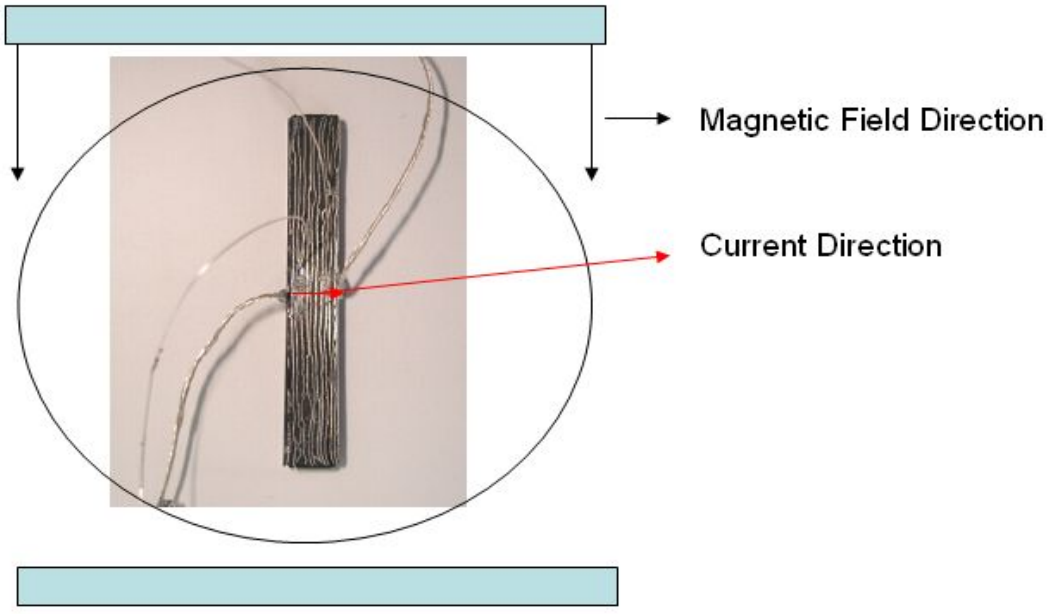

(d)

Figure 4-18: Schematic diagrams of applied magnetic field and current direction for the multilayered samples. They correspond to a) C1, b) C2, c) C3 and d) C4 detailed in the main text, respectively.

Figures 4-19, 20, 21 and 22 display the results of the magnetoresistivity measurements in the configuration C1, C2, C3 and C4 configurations for the two-, four- and eight-layered samples.

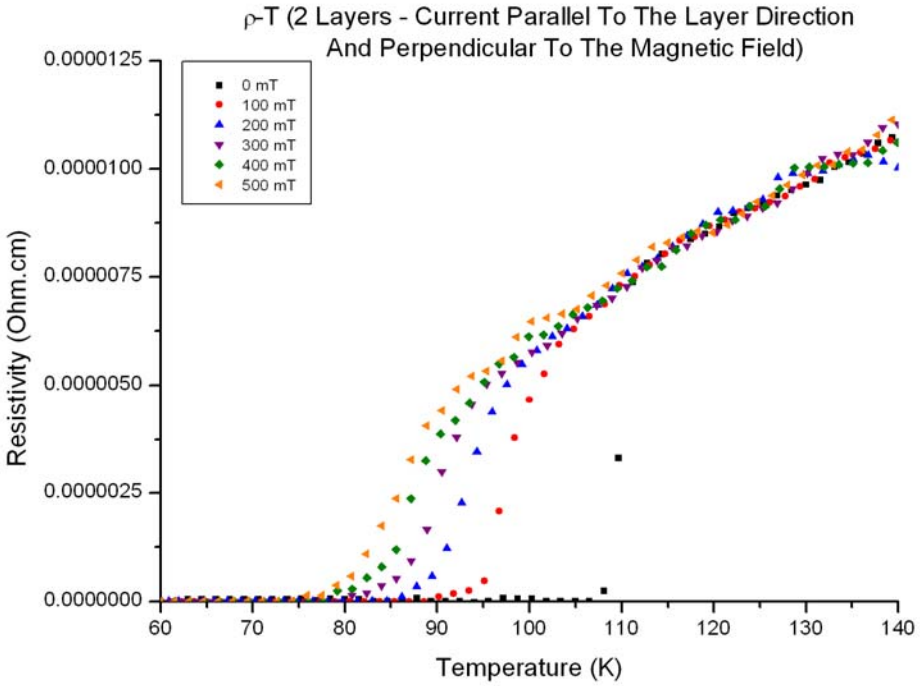

(a)

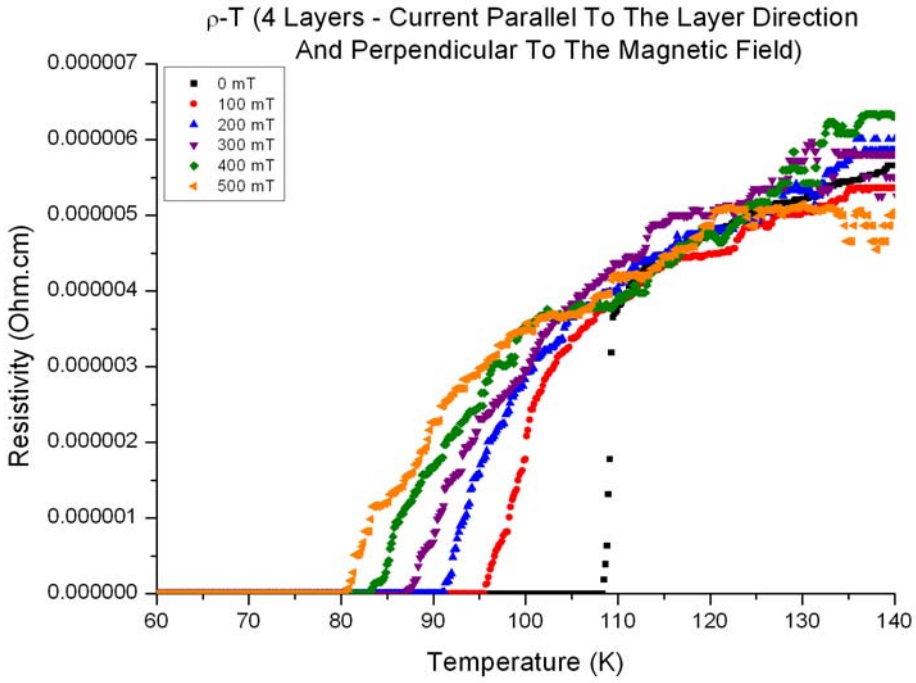

(b)

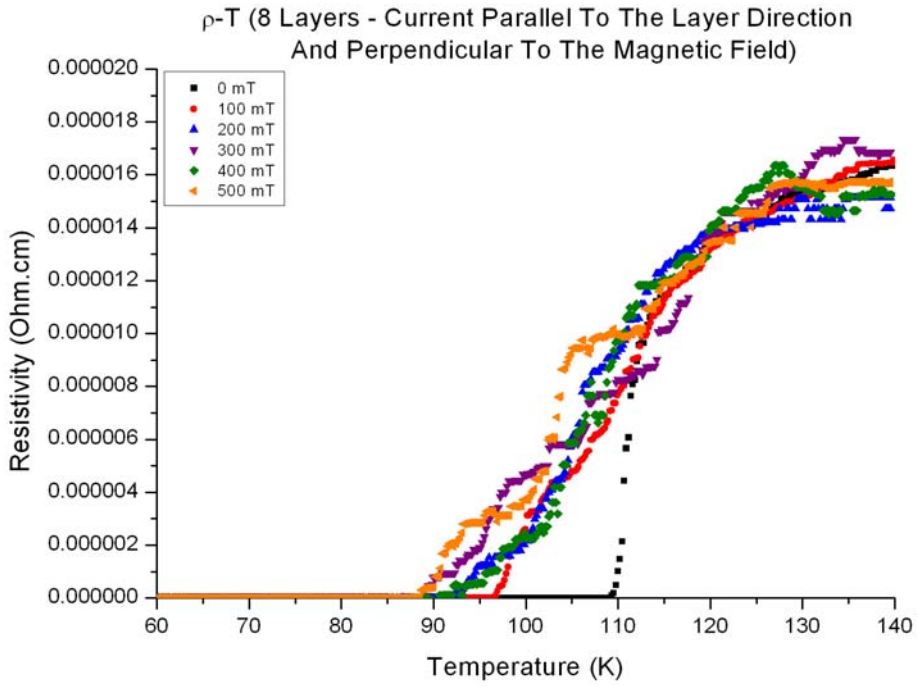

(c)

Figure 4-19: Magnetoresistivity measurements at 0, 100, 200, 300, 400 and 500 mT for a) 2-layered, b) 4-layered and c) 8-layered samples using the configuration C1 (Figure 4-18a).

The figures indicate that the critical transition temperature is lowered when an external magnetic field is applied for all the layered tapes. Specifically, with increasing dc magnetic field up to 0.5 T, zero resistivity transition temperature value decreases from 107.3 to 74.3 K for the two-layered sample, 108.3 to 80.4 K for the four-layered sample and 109.3 to 88.3 K for the eight-layered sample in the case of C1 configuration. In the C2 configuration, critical transition temperature decreases from 107.3 to 86.5 K for the two-layered sample, 108.3 to 90.2 K for the four-layered sample and 109.2 to 92.6 K for the eight-layered sample with increasing dc magnetic field up to 0.5 T (Fig. 4-20). The broadening (33.0 K) in the configuration C1 is larger than that (20.8 K) in the configuration C2 for the two-layered sample. Transition temperature decreased from 107.6 to 84.1 K for the two-layered sample, 109.2 to 86.5 K for the sample four-layered sample and 110.3 to 87.0 K for the eight-layered sample when dc magnetic field increased up to 0.5 T in the case of C3

configuration (Figure 4.21). In the C4 configuration, the transition temperature decreased from 107.6 to 90.0 K for the two-layered sample, 109.2 to 92.4 K for the sample four-layered sample and 110.3 to 96.3 K for the eight-layered sample when dc magnetic field increased up to 0.5 T (Figure 4.22). We observed that the broadening of the resistivity transition width increases with increasing the external dc magnetic field.

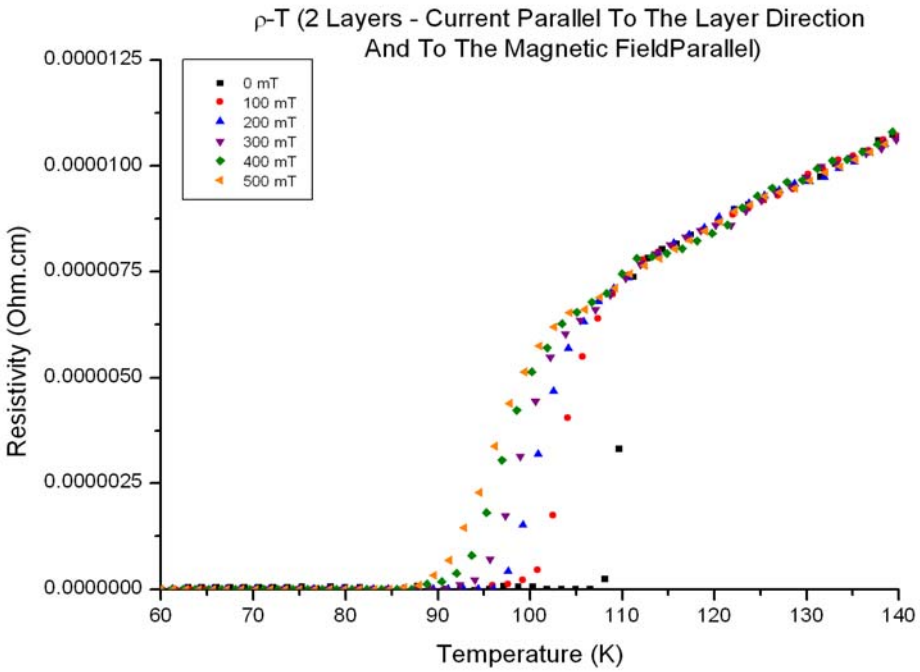
ρ-T (2 Layers - Current Parallel To The Layer Direction
And To The Magnetic FieldParallel)
0 mT
100 mT
200 mT
300 mT
400 mT
500 mT
Resistivity (Ohm.cm)
0.0000125
0.0000100
0.0000075
0.0000050
0.0000025
0.0000000
60
70
80
90
100
110
120
130
140
Temperature (K)

(a)

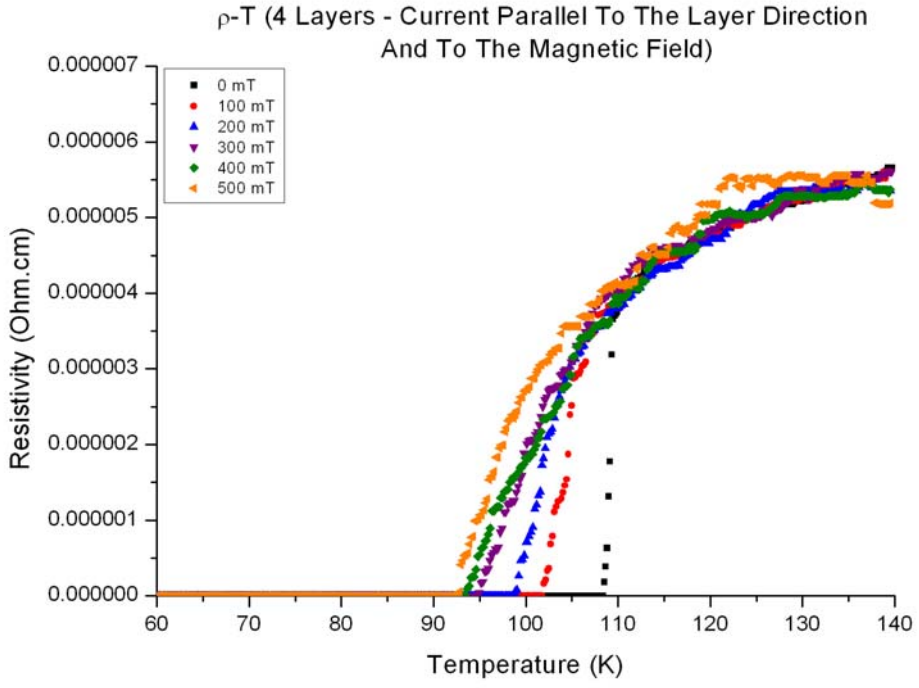
ρ-T (4 Layers - Current Parallel To The Layer Direction
And To The Magnetic Field)
0 mT
100 mT
200 mT
300 mT
400 mT
500 mT
Resistivity (Ohm.cm)
0.000007
0.000006
0.000005
0.000004
0.000003
0.000002
0.000001
0.000000
60
70
80
90
100
110
120
130
140
Temperature (K)

(b)

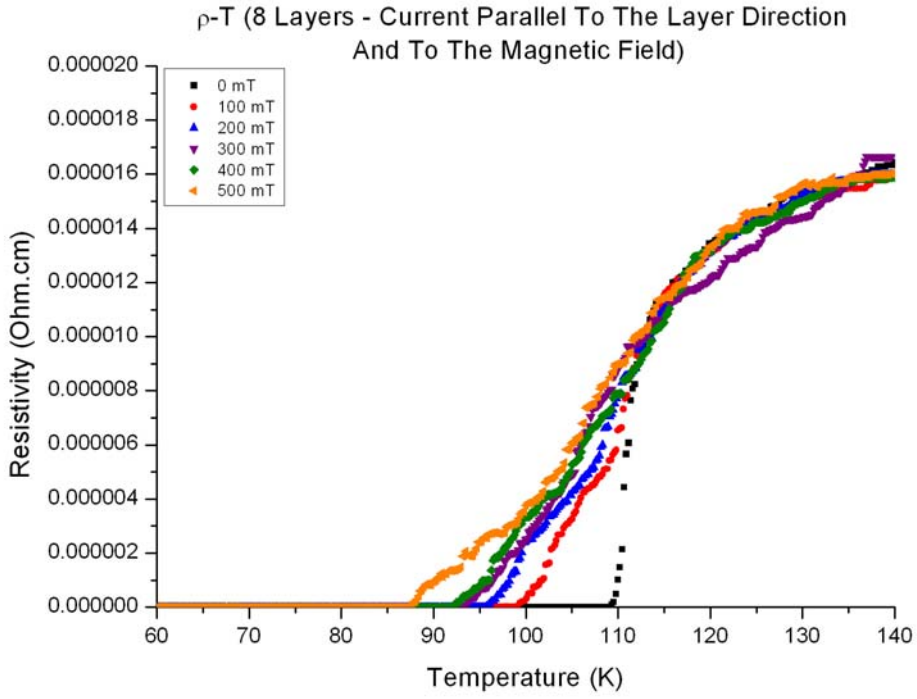

(c)

Figure 4-20: Magnetoresistivity measurements at 0, 100, 200, 300, 400 and 500 mT for a) 2-layered, b) 4-layered and c) 8-layered samples using the configuration C2 (Figure 4-18b).

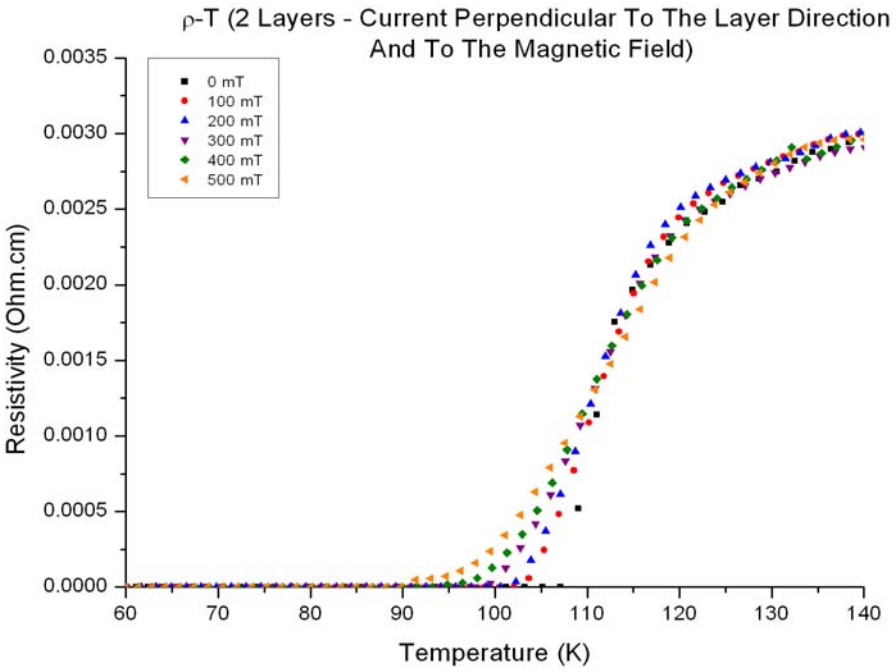
ρ-T (2 Layers - Current Perpendicular To The Layer Direction
And To The Magnetic Field)
0 mT
100 mT
200 mT
300 mT
400 mT
500 mT
Resistivity (Ohm.cm)
0.0035
0.0030
0.0025
0.0020
0.0015
0.0010
0.0005
0.0000
60
70
80
90
100
110
120
130
140
Temperature (K)

(a)

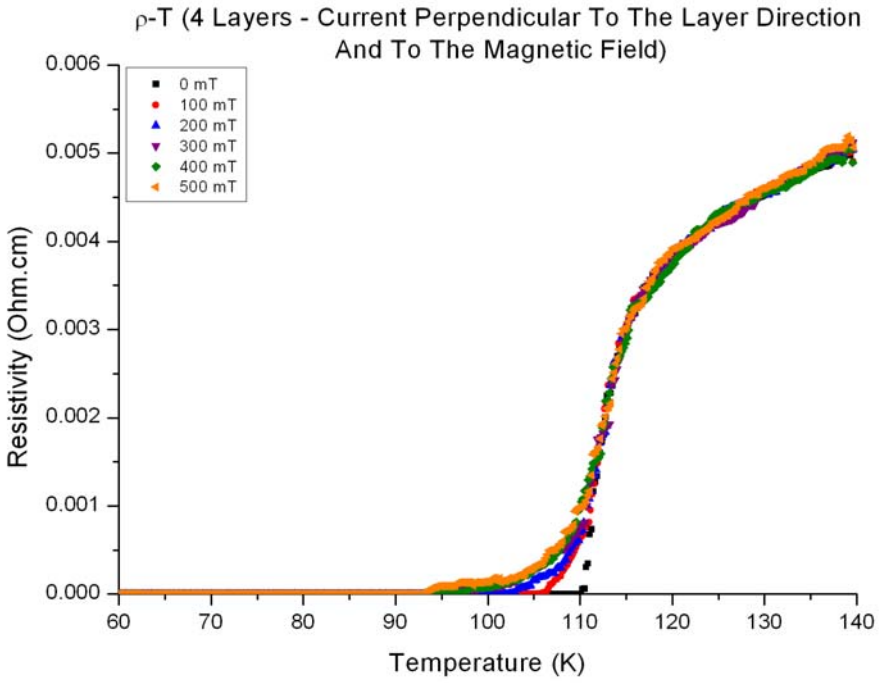
ρ-T (4 Layers - Current Perpendicular To The Layer Direction
And To The Magnetic Field)
0 mT
100 mT
200 mT
300 mT
400 mT
500 mT
Resistivity (Ohm.cm)
0.006
0.005
0.004
0.003
0.002
0.001
0.000
60
70
80
90
100
110
120
130
140
Temperature (K)

(b)

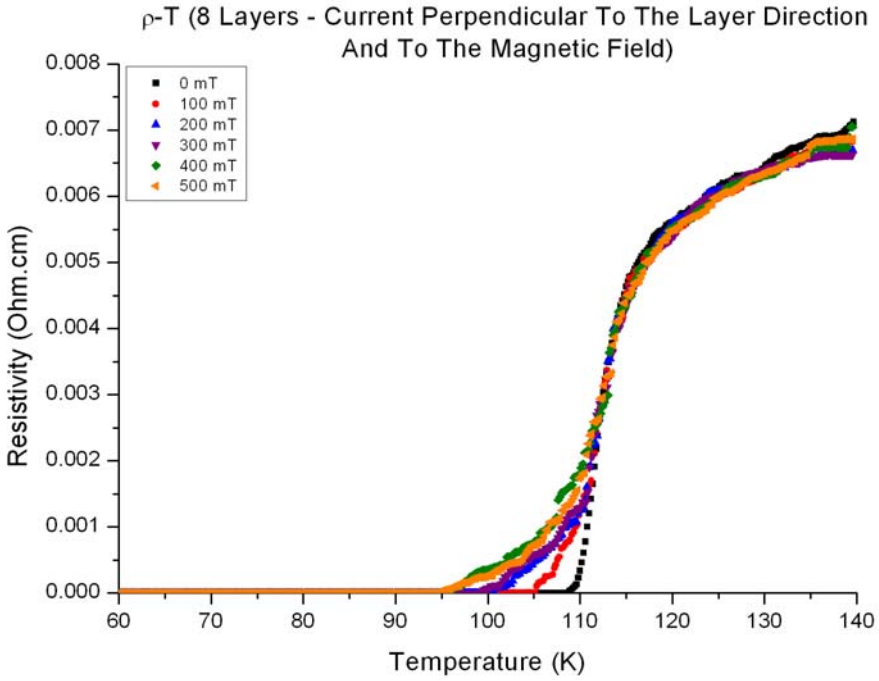

(c)

Figure 4-21: Magnetoresistivity measurements at 0, 100, 200, 300, 400 and 500 mT for a) 2-layered, b) 4-layered and c) 8-layered samples using the configuration C3 (Figure 4-18c).

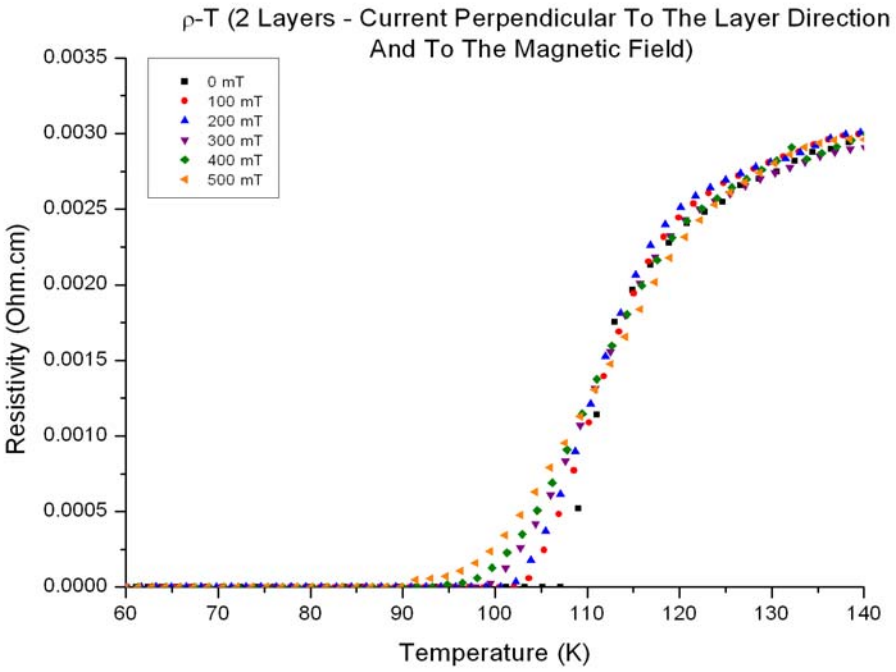
ρ-T (2 Layers - Current Perpendicular To The Layer Direction And To The Magnetic Field)
0 mT
100 mT
200 mT
300 mT
400 mT
500 mT
Resistivity (Ohm.cm)
0.0035
0.0030
0.0025
0.0020
0.0015
0.0010
0.0005
0.0000
60
70
80
90
100
110
120
130
140
Temperature (K)

(a)

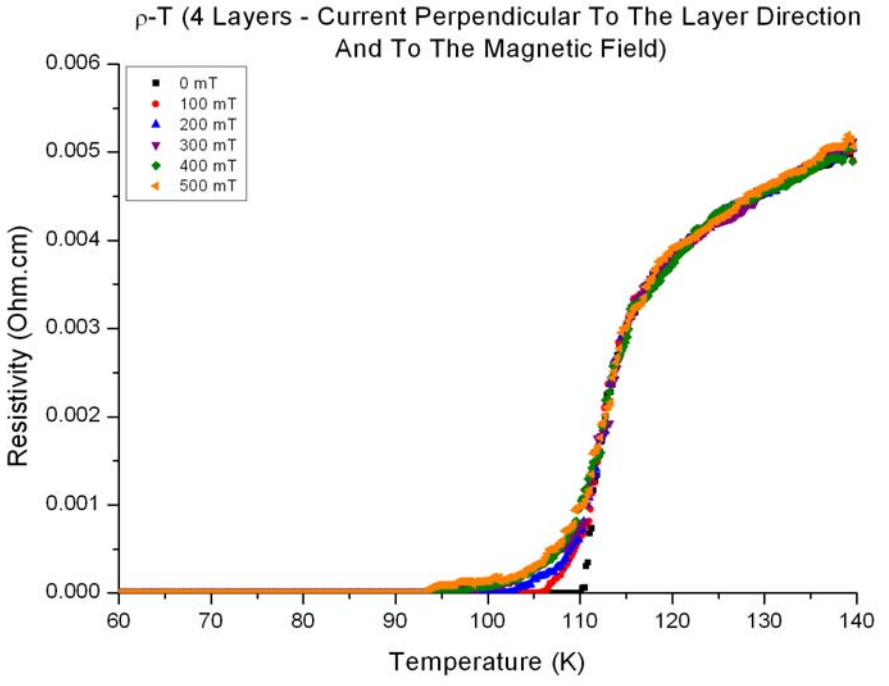
ρ-T (4 Layers - Current Perpendicular To The Layer Direction And To The Magnetic Field)
0 mT
100 mT
200 mT
300 mT
400 mT
500 mT
Resistivity (Ohm.cm)
0.006
0.005
0.004
0.003
0.002
0.001
0.000
60
70
80
90
100
110
120
130
140
Temperature (K)

(b)

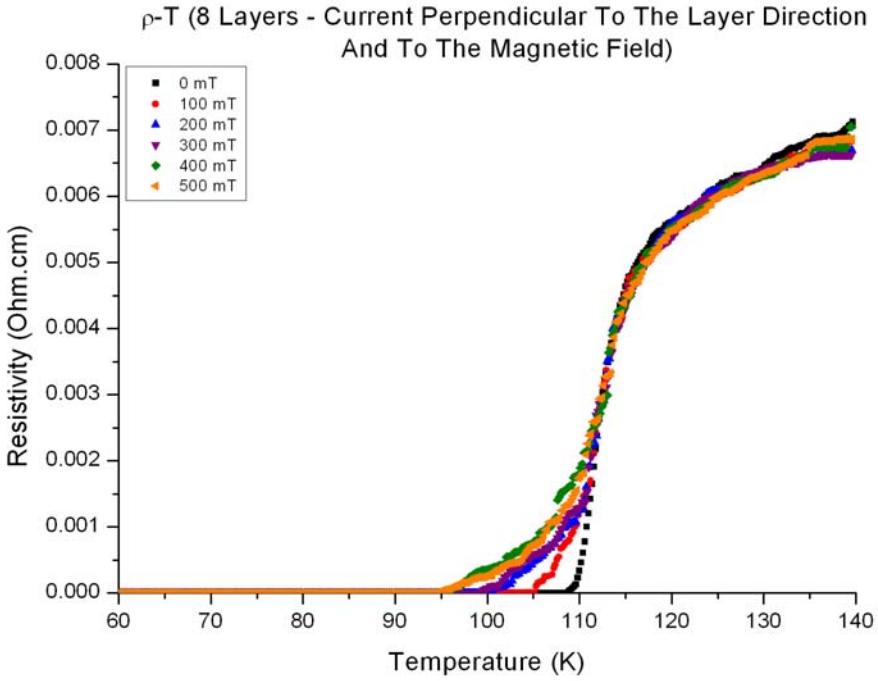

(c)

Figure 4-22: Magnetoresistivity measurements at 0, 100, 200, 300, 400 and 500 mT for a) 2-layered, b) 4-layered and c) 8-layered samples using the configuration C4 (Figure 4-19d).

As a conclusion, transition temperature increases with increasing the number of Ag layers and magnetoresistivity versus temperature measurements in all configurations for all samples showed the same behavior such as the transition temperature decreases and the broadening of the resistivity transition width increases with increasing external dc magnetic field. We have found that the broadening is different for each of the samples at every configuration investigated in the present work. The highest T_c values under dc magnetic field were obtained in the configuration C4 for all the samples. This finding can be interpreted as a result of Ag doping in the intergrain boundaries which cause an increase of intergrain contact surface or decreasing the intergrain resistivity.

Critical current density measurements for all the samples in the external magnetic fields from zero to 0.5 T with 100 mT increment at 77K were performed in

configurations C1 and C3. In Figure 4-23, the J_c versus B curve of the Bi-oxide (B840), two-, four-, and eight-layered samples in the configurations C1 and C3 are shown. For all the samples and the configurations, the J_c increases with increasing number of layers and reaches a maximum value of 600 A/cm^2 for eight layers, which corresponds to an I_c of 126 A while the J_c decreases with increasing dc magnetic field and reaches a minimum value of 54 A/cm^2 at 0.5 T. The J_c value of Bi-oxide bulk without Ag layer is 124 A/cm^2. The J_c at 77 K under magnetic field of 500 mT perpendicular and parallel to the layered sample surface were measured as 16 and 43 A/cm^2 for the two-layered sample, 19 and 54 A/cm^2 for the four-layered sample, and 21 and 79 A/cm^2 for the eight-layered sample, respectively. J_c of Bi-2223 bulk and 4 Ag-layered samples were reported as less than 50 A/cm^2 and around 300 A/cm^2 respectively [61]. In our investigation, J_c value of Bi(Pb)-2223 is found to be around 124 A/cm^2 and that of four Ag layer is 380 A/cm^2. As can be clearly seen from the figure 4.23, J_c value of the eight-layered sample was more than two times higher than J_c value of two-layered sample. Transport J_c value is linearly increased with increasing the number of Ag layers (Figure 4-24) [61]. These results are related to the high c-axis alignment and dense structure of Bi-2223 phase that was formed at the both surface sides of the inserted Ag layer. Figure 4.24 shows the relationship between transport J_c value at 77 K under zero field and number of Ag layers. J_c property of Bi-2223 /Ag multilayered bulk sample seems to be improved with increasing number of Ag layers. The mechanism of the J_c improvement may be related to the improvements in the properties at the grain boundaries which is due to increasing layers. It is well known that the value of the critical current density J_c of Bi-2223/Ag is dominated by two factors. One is the volume fraction of Bi-2223 phase in the superconducting core, the other is the degree of the grain alignment [82].

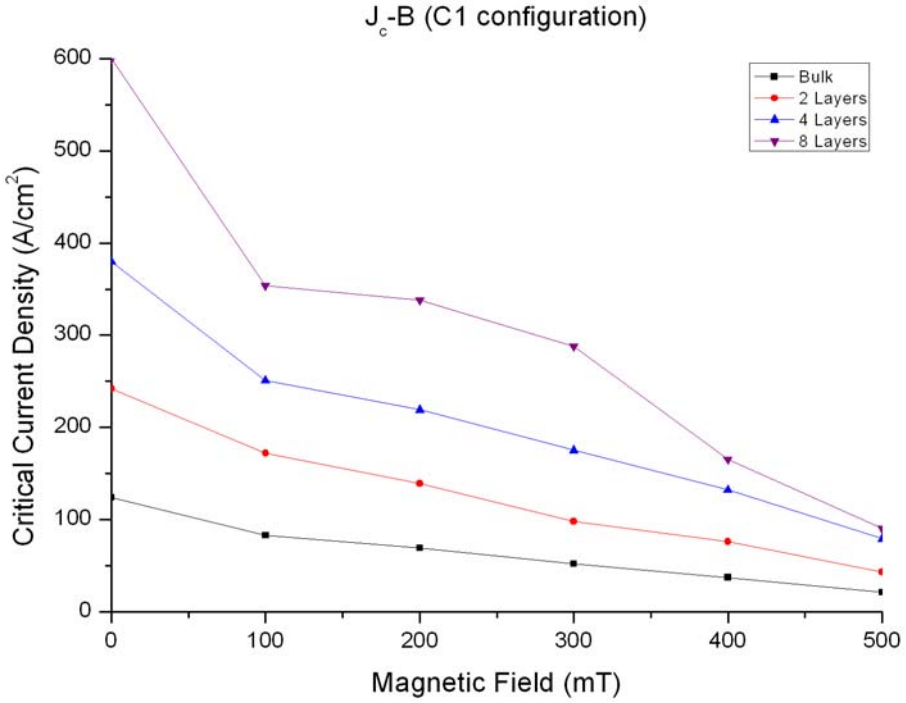

(a)

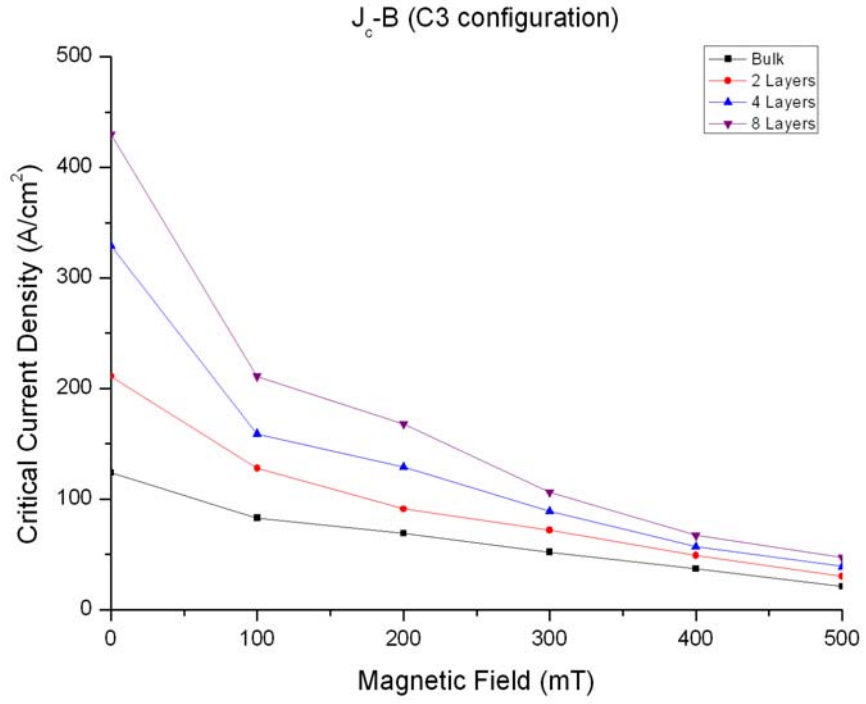

(b)

Figure 4-23: J_c versus B curve of Bi-oxide (B840), two-, four- and eight-layered samples in the configurations of a) C1 and b) C3.

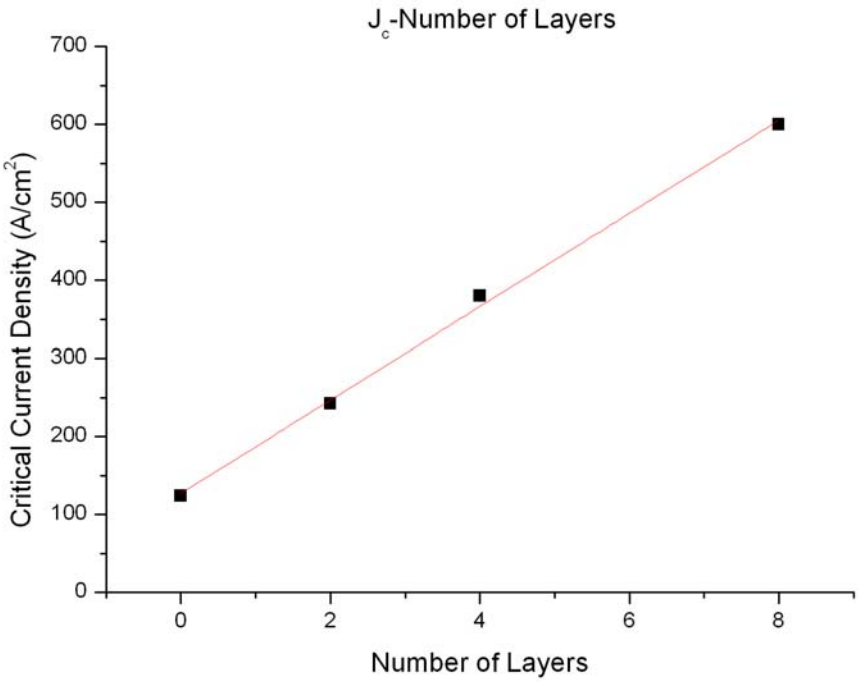

Figure 4-24: Dependence of critical current densities on the number of layers at 77 K.

CHAPTER 5 – CONCLUSION

The main objective of this thesis was the preparation of $Bi_{1.8}Pb_{0.4}Ca_{2.2}Sr_2Cu_3O_x$/Ag multilayered samples (2, 4 and 8 layers) and to investigation of the effect of multilayering with Ag on the superconducting and the microstructural properties of $Bi_{1.8}Pb_{0.4}Ca_{2.2}Sr_2Cu_3O_x$. Towards that end, I have done a three main investigations: 1) Studied the optimal annealing temperature for bettering superconducting properties, 2) Investigated the effect of diffusion doped Ag on the microstructure and superconducting properties of $Bi_{1.8}Pb_{0.4}Ca_{2.2}Sr_2Cu_3O_x$ and 3) Studied the effect of Ag layering on the superconducting and microstructural properties of $Bi_{1.8}Pb_{0.4}Ca_{2.2}Sr_2Cu_3O_x$.

As first step, we prepared $Bi_{1.8}Pb_{0.4}Ca_{2.2}Sr_2Cu_3O_x$ by using the solid state reaction method to investigate the optimum annealing temperature. The investigations consist of XRD, SEM, dc resistivity and transport critical current density measurements. The highest T_c and J_c values were observed for the sample annealed at 840 °C for 48 hours. Large grain size, denser surface and high volume fraction of the high-T_c phase were obtained for the sample B840. From these results, 840 °C for 48 hours was decided as the optimum annealing temperature and duration.

Then, we investigated the effect of Ag diffusion doping. The effect of Ag doping was studied by XRD, SEM, dc resistivity and transport critical current

measurements. *Ag*-doping is found to affect $Bi_{1.8}Pb_{0.4}Ca_{2.2}Sr_2Cu_3O_x$ samples in two main ways: 1) The *c* lattice constant is increased by 0.15% compared to the undoped case. 2) The surface morphology changes to a smother and denser structure with much larger and well-oriented grains. Ag is found to reside also in the intergrain boundaries and acts as a short-circuit. These structural changes lead to better superconducting properties as indicated by a 3 K increase in T_c and 500% increase in J_c. The short-circuit property is found to cause a decrease of 300% in room temperature resistivity. In addition, Ag doping increased the lattice parameter *c* and the amount of high-T_c phase and improved the surface morphology.

We have also determined the Ag diffusion coefficient in $Bi_{1.8}Pb_{0.4}Ca_{2.2}Sr_2Cu_3O_x$ as function of temperature and found it to be 2.11×10^{-10} and 1.15×10^{-8} cm^2/s for samples annealed at 500 and 800°C, respectively. The corresponding activation energy is determined to be 1.05 eV which higher than the ones reported in the literature. The low value of activation energy shows that the silver diffusion proceeds through defects in the ceramic samples.

Finally, $Bi_{1.8}Pb_{0.4}Ca_{2.2}Sr_2Cu_3O_x$/Ag multilayered samples were fabricated by powder in tube method, packing the precursor Bi-oxide powder inside silver tube of 6.30 mm outer diameter. The density of powder increases during the drawing procedure and inside the composite wires and the final diameter is 3.54 mm. By an intermediate rolling, pressing and annealing procedure, the wires were rolled to obtain tapes. The rolling process was not effective in obtaining substantially higher powder density, but greatly improved the orientation of ceramic grains inside the silver sheath. The sample is composed of a highly oriented Bi-2223 phase in the region near the Ag layer. The eight-layered sample exhibits a rather high I_c value of 125 A. T_c and J_c are enhanced by increasing the number of Ag layers. The

incorporation of Ag within the grain boundaries is thought to be a positive influence on the superconducting and microstructural properties. This conclusion is based on SEM micrographs which show larger grains as the amount of Ag increases, as well as J_c measurements which indicate linear increase with number of Ag layers.

REFERENCES

[1] H. K. Onnes, The superconductivity of mercury, Communications Physics Laboratory University Of Leiden (1911) 122–124.

[2] J. G. Bednorz, K. A. Müller, Possible high T_c superconductivity in the Ba-La-Cu-O system, Zeitschrift für Physik B 64 (1986) 189.

[3] H. Takagi, S. Uchida, K. Kitazawa, S. Tanaka, High-T_c superconductivity of La-Ba-Cu oxides. II.-specification of the superconducting phase, Japanese Journal of Applied Physics 23 (1987) L123.

[4] K. Wu, J. R. Ashburn, C. Torng, P. H. Hor, R. L. Meng, L. Gao, Z. L. Huang, Y. Q. Want, C. W. Chu, Superconductivity at 93 K in a new mixed-phase Y-Ba-Cu-O compound system at ambient pressure, Physical Review Letters 58 (1987) 908.

[5] H. Maeda, Y. Tanaka, M. Fukutomi, T. Asano, A new high-T_c oxide superconductor without a rare earth element, Japanese Journal of Applied Physics 27 (1988) L209–L210.

[6] C. Michel, M. Hervieu, M. M. Borel, A. Grandin, F. Deslandes, J. Provost, B. Raveau, Superconductivity in the Bi-Sr-Cu-O system, Zeitschrift für Physik B 68 (1987) 421–423.

[7] J. W. Ko, J. M. Yoo, Y. K. Kim, K. H. Oh, S. J. Choe, H. Chung, Effect of starting precursor powders on microstructural development and critical current density properties of BSCCO 2223 tapes, Cryogenics 43 (2003) 549–553.

[8] B. Zhao, X. Wan, W. Song, Y. Sun, J. Du, Nano-MgO particle addition in silver-sheathed $(Bi,Pb)_2Sr_2Ca_2Cu_3O_x$ tapes, Physica C: Superconductivity 337 (2000) 138–144.

[9] C. Thomsen, M. Cardona, B. Gegenheimer, R. Liu, A. Simon, Untwinned single crystals of $YBa_2Cu_2O_{7-\delta}$, Physical Review B 37 (1988) 9860.

[10] H. Takagi, T. Ido, S. Ishibashi, M. Uota, S. Uchida, Y. Tokura, Superconductor-to-nonsuperconductor transition in $(La_{1-x}Sr_x)_2CuO_4$ as investigated by transport and magnetic measurements, Physical Review B 40 (1989) 2254.

[11] J. D. Hettinger, K. E. Gray, D. J. Miller, D. H. Kim, D. G. Steel, B. R. Washburn, J. Sharping, C. Moreau, M. Eddy, J. E. Tkaczyk, J. DeLuca, J. H. Kang, J. Talvacchio, Identification of grain boundary effects in current-voltage curves of polycrystalline high-T_c superconductors, Physica C: Superconductivity 273 (1997) 275–280.

[12] B. Hensel, C. J. Grivel, A. Jeremie, A. Perin, A. Pollini, R. Flukiger, A model for the critical current in $(Bi,Pb)_2Sr_2Ca_2Cu_3O_x$ silver-sheathed tapes: The role of small-angle c-axis grain boundaries and of the texture, Physica C 205 (1993) 329–337.

[13] J. Mannhart, C. C. Tsuei, Limits of the critical current density of polycrystalline high-temperature superconductors based on the current transport properties of single grain boundaries, Zeitschrift für Physik B 77 (1989) 53–59.

[14] H. Hilgenkamp, J. Mannhart, Grain boundaries in high-T_c superconductors, Reviews of Modern Physics 74 (2002) 485–549.

[15] D. Dimos, P. Chaudhari, J. Mannhart, F. K. LeGoues, Orientation dependence of grain-boundary critical currents in $YBa_2Cu_3O_{7-\delta}$ bicrystals, Physical Review Letters 61 (1988) 219–224.

[16] D. Dimos, P. Chaudhari, J. Mannhart, Superconducting transport properties of grain boundaries in $YBa_2Cu_3O_7$ bicrystals, Physical Review B 41 (1990) 4038.

[17] A. Schemehl, B. Goetz, R. R. Schulz, C. W. Schneider, H. Bielefeldt, H. Hilgenkamp, J. Mannhart, Doping-induced enhancement of the critical currents of grain boundaries in $YBa_2Cu_3O_{7-\delta}$, Europhysics Letters 47 (1999) 110–115.

[18] S. E. Babcock, Roles for electron microscopy in establishing structure-property relationships for high T_c superconductors, Physica C: Superconductivity 30 (1999) 449–461.

[19] J. Mannhart, H. Bielefeldt, B. Goetz, H. Hilgenkamp, A. Schmehl, C. W. Schneider, R. R. Schulz, Doping induced enhancement of the critical currents of grain boundaries in high-T_c superconductors, Physica C: Superconductivity 341-348 (2000) 1393–1396.

[20] P. Diko, G. Krabbes, Formation of c-macrocracks during oxygenation of TSMG $YBa_2Cu_3O_7/Y_2BaCuO_5$ single-grain superconductors, Physica C: Superconductivity 399 (2003) 151–157.

[21] H. Kumakura, K. Togano, H. Maeda, Bi(Pb)-Sr-Ca-Cu-O superconducting composite tapes prepared by the powder method using an Ag sheath, Journal Of Applied Physics 67 (1990) 3443.

[22] M. Wilhelm, H. W. Neumüller, G. Ries, Fabrication and critical current densities of 2223-BiPbSrCaCuO silver sheathed tapes, Physica C: Superconductivity 185-189 (1991) 2399–2400.

[23] L. Martini, J. Bechtold, M. Majoros, V. Ottoboni, J.-C. Vallier, S. Zannella, Superconducting properties of multilayered *Bi*(*Pb*)-2223/*Ag tapes*, Superconductor Science and Technology 7 (1994) 24–29.

[24] M. T. Malachevsky, D. A. Esparza, Metal-ceramic interfaces in Ag-BSCCO composites, Physica B 284-288 (2000) 2085–2086.

[25] S. V. Sudareva, E. P. Romanov, Y. V. Rats, D. V. Surnin, T. P. Krinitsina, A. N. Maratkanova, M. V. Kuznetsov, A. K. Shikov, I. I. Akimov, Y. N. Belotelova, Mechanisms of Ag penetration into the ceramics of *Ag*/*Bi*-2223 ribbon composites, Physica C: Superconductivity 371 (2002) 243–257.

[26] C. B. Eom, A. F. Marshall, Y. Suzuki, T. H. Geballe, B. Boyer, R. F. W. Pease, R. B. van Dover, J. M. Philips, Growth mechanisms and properties of 90 grain boundaries in $YBa_2Cu_3O_7$ thin films, Physical Review B 46 (1992) 11902–11913.

[27] R. D. Doherty, D. A. Hughes, F. J. Humphreys, J. J. Jonas, D. J. Jensen, M. E. Kassner, W. E. King, T. R. McNelley, H. J. McQueen, A. D. Rollett, Current issues in recrystallization: a review, Material Science and Engineering A 238 (1997) 219–274.

[28] S. E. Babcock, J. L. Vargas, The nature of grain boundaries in the high-T_c superconductors, Annual Review of Materials Science 25 (1995) 193–222.

[29] J. W. Ekin, T. M. Larson, A. M. Hermann, Z. Z. Sheng, K. Togano, H. Kumakura, Double-step behavior of critical current vs. magnetic field in Y-, Bi- and Tl-based bulk high-T_c superconductors, Physica C 160 (1988) 489–496.

[30] J. Horvat, W. G. Wang, R. Bhasale, Y. C. Guo, H. K. Liu, S. X. Dou, Critical currents in Ag/Bi-2223 superconducting tapes: grain connectivity and flux pinning, Physica C 275 (1997) 327–332.

[31] A. Umezawa, Y. Feng, H. S. Edelman, T. C. Willis, J. A. Parrell, D. C. Larbalestier, G. N. R. Jr., W. L. Carter, Further evidence that the critical current density of $(Bi,Pb)_2Sr_2Ca_2Cu_3O_x$ silver-sheathed tapes is controlled by resudial layers of $(Bi,Pb)_2Sr_2CaCu_2O_y$ at (001) twist boundaries, Physica C 219 (1994) 378–388.

[32] B. Zeimetz, H. K. Liu, S. X. Dou, Microstructural study of Bi2223/Ag tapes made using a two-stage sintering procedure, Superconductor Science and Technology 11 (1998) 505–508.

[33] J. W. Anderson, J. A. Parrell, P. V. P. S. S. Sastry, D. C. Larbalestier, The effect of wire drawing cold rolling on the precursor 2212 phase texture and its subsequent influence on the $(Bi,Pb)_2Sr_2Ca_2Cu_3O_x$ texture in Ag-clad tapes, IEEE Transactions on Applied Superconductivity 7 (1997) 1422–1425.

[34] Q. Y. Hu, H. W. Weber, H. K. Liu, S. X. Dou, H. W. Neumüller, Angular dependence of critical currents and grain misalignment in Ag clad $(Bi,Pb)_2Sr_2Ca_2Cu_3O_{10}$) tapes, Physica C 252 (1995) 211–220.

[35] B. Zeimetz, S. X. Dou, H. K. Liu, Recrystallization effects and grain size in Bi-2223 tapes, Superconductor Science and Technology 11 (1998) 1082–1086.

[36] L. N. Bulaevskii, J. R. Clem, L. I. Glazman, A. P. Malozemoff, Model for the low-temperature transport of Bi-based high temperature superconducting tapes, Physical Review B 45 (1992) 2545–2548.

[37] X. Yang, T. K. Chaki, Alignment of grains in $Bi_{1.6}Pb_{0.4}Sr_2Ca_2Cu_3O_x$ by hot deformation, Superconductor Science and Technology 6 (1993) 269–275.

[38] K. Sato, T. Hikata, H. Mukai, M. Ueyama, N. Shibuta, T. Kato, High-J_c silver-sheathed Bi-based superconducting wires, IEEE Transactions on Magnetics 27 (1991) 1231–1238.

[39] S. X. Dou, H. K. Liu, J. Wang, M. H. Apperley, C. C. Sorrell, S. J. Guo, B. Loberg, K. E. Easterling, Microstructure and flux pinning in superconducting Bi-Pb-Sr-Ca-Cu-O wires, Physica C: Superconductivity 172 (1990) 63–70.

[40] S. Jin, J. E. Graebner, Processing and fubrications techniques for bulk high-T_c superconductors: a critical review, Materials Science and Engineering: B 7 (1991) 243–260.

[41] X. Y. Lu, A. Nagata, K. Sugawara, S. Kamada, Grain alignment and critical current densities of (Bi,Pb)-2223 phase in the partial-melting and sintering process, Superconductor Science and Technology 12 (1999) 1098–1101.

[42] U. Syamaprasad, M. S. Sarma, P. Guruswamy, V. P. Kumar, R. Ragini, K. G. K. Warrier, A. D. Damodaran, Effect of precursor phase assemblage on 2223 phase formation and J_c in Ag/(Bi,Pb)-2223 tapes, Physica C 297 (1998) 85–90.

[43] C. Terzioglu, M. Yilmazlar, O. Ozturk, E. Yanmaz, Structural and physical properties of Sm-doped $Bi_{1.6}Pb_{0.4}Sr_2Ca_{2-x}Sm_xCu_3O_y$, Physica C 423 (2005) 119.

[44] T. D. Dzhafarov, M. Yilmazlar, The effect of Ag electromigration on the properties of BiPbSrCaCuO superconductors, Physica C 292 (1997) 140–146.

[45] V. G. Prabitha, A. Biju, R. G. A. Kumar, P. M. Sarun, R. P. Aloysius, U. Syamaprasad, Effect of Sm addition on (Bi,Pb)-2212 superconductor, Physica C 433 (2005) 28.

[46] T. D. Dzhafarov, H. Cömert, M. Altunbas, . Alver, T. Küçükömeroğlu, A. . Kopya, Diffusion of Ag in Bi(Pb)-Sr-Ca-Cu-O superconductors, Journal of Alloys and Compounds 221 (1995) 264–266.

[47] K. N. Kishore, M. Muralidhar, V. H. Babu, O. Pena, M. Sergent, F. Beniere, Effect of rare-earth Sm3+ substitution on the superconducting properties of the $Bi_{1.7}Pb_{0.3}Sr_2Ca_{2-x}Sm_xCu_3O_y$ system, Physica C 204 (1993) 299.

[48] A. Y. Ilyusechkin, T. Yamashita, L. Boskovic, I. D. R. Mackinnon, The effect of Yb addition in $Bi_2Sr_2Ca_{1-x}Yb_xU_2O_y$ partial melted thick films, Superconductor Science and Technology 17 (2004) 1201.

[49] A. Biju, R. P. Aloysius, U. Syamaprasad, Enhanced critical current density in Gd-added (Bi,Pb)-2212 bulk superconductor, Superconductor Science and Technology 18 (2005) 1454.

[50] Y. Li, S. Kaviraj, A. Berenov, G. K. Perkins, J. Driscoll, A. D. Caplin, G. H. Cao, Q. Z. Ma, B. Wang, L. Wei, Z. X. Zhao, Enhancement of critical current density of (Pb,Sn)-doped Bi-2212 superconductors at high temperature, Physica C 355 (2001) 51.

[51] B. J. Kim, H. T. Kim, Y. Matsui, D. Y. Jeong, C. Deinhofer, G. Gritzner, Microstructure of screen-printed $(Tl_{0.5},Pb_{0.5})(Sr_{0.8},Ba_{0.2})_2Ca_2Cu_3O_y$ superconducting films on untextured silver substrate, Physica C 460-462 (2007) 736–737.

[52] A. Kumar, P. Singh, D. Kaur, Low cost synthesis of high-T_c superconducting films on metallic substrates via ultrasonic spray pyrolysis, Cryogenics 46 (2006) 749–758.

[53] K. Sato, T. Hikata, M. Ueyama, H. Mukai, N. Shibuta, T. Kato, T. Masuda, Transport current properties of silver-sheathed BiPbSrCaCuO wire and coil, Cryogenics 31 (1991) 687–689.

[54] R. Wesche, A. M. Fuchs, B. Jakob, G. Pasztor, Diameter-dependent critical current densities for superconducting Bi-2212/Ag wires, Cryogenics 34 (1994) 805–811.

[55] K. Sato, N. Shibuta, H. Mukai, T. Hikata, M. Ueyama, T. Kato, Silver-sheathed Bi (2223) wire and application, Physica C: Superconductivity 190 (1991) 50–52.

[56] S. Patel, T. Haugan, F. Wong, S. Chen, S. S. Li, J. Ye, D. T. Shaw, Effect of non-uniform core thickness on critical current density of silver-sheathed oxide superconducting tapes, Cryogenics 35 (1995) 249–256.

[57] J. K. F. Yau, N. Savvides, C. C. Sorrell, Influence of mechanical strain on critical current density and microstructure of silver-sheathed Bi(Pb)2223 superconducting tapes, Physica C: Superconductivity 266 (1996) 223–229.

[58] J. Herrmann, N. Savvides, K. H. Müller, R. Zhao, G. McCaughey, F. Darmann, M. Apperley, Current distribution and critical state in superconducting silver-sheathed (Bi,Pb)-2223 tapes, Physica C: Superconductivity 305 (1998) 114–124.

[59] T. Sakai, H. Utsunomiya, Y. Saito, T. Hanamachi, M. Shinkawa, Effect of intermediate rolling condition on the critical current density of silver-sheathed Bi(2223) superconducting tapes, Physica C: Superconductivity 277 (1997) 189–195.

[60] L. Hua, Q. Z. Yao, M. Jiang, Y. Z. Wang, H. T. Z. R. Li, G. W. Qiao, Study of Ag/Oxide interface of Bi-2223 silver-sheathed superconducting composite, Journal Of Applied Physics 78 (1995) 3274–3277.

[61] Y. Hishinuma, S. Nemoto, S. Yoshizawa, Microstructure and J(c) property on the Bi-2223 bulk prepared by inserting Ag layers, Physica C: Superconductivity and Its Applications 351 (2001) 409–414.

[62] H. Satoh, T. Tanabe, H. Hakane, S. Yoshizawa, M. Nori, Fluctuation conductivity in $(Bi,Pb)_2Sr_2Ca_2Cu_3O_y/Ag$ multi-layered bulk system, Physica C 412-414 (2004) 307–311.

[63] T. D. Dzhafarov, A. Varilci, M. Sadygov, M. Altunbas, The effect of Ag diffusion on properties of BiPbSrCaCuO thin films, Physica C 268 (1996) 143–149.

[64] H. Cömert, M. Altunbaş, T. D. Dzhafarov, T. Küçükömeroğlu, Y. G. Asadov, H. Karal, The effect of Ag diffusion on the crystal structure and electrical properties of Bi(Pb)SrCaCuO superconductors, Superconductor Science and Technology 7 (1994) 824.

[65] C. W. Chu, L. Gao, F. Chen, Z. J. Huang, R. L. Meng, Y. Y. Xue, Superconductivity above 150 K in $HgBa_2Ca_2Cu_3O_{8+\delta}$ at high pressures, Nature 365 (1993) 323–325.

[66] S. A. Halim, S. A. Khawaldeh, S. B. Mohamed, H. Azhan, Superconducting properties of $Bi_{2-x}Pb_xSr_2Ca_2Cu_3O_y$ system derived via sol-gel and solid state routes, Materials Chemistry and Physics 61 (1999) 251–259.

[67] C. Terzioglu, O. Ozturk, I. Belenli, The effect of Au diffusion on some physical properties of $Bi_{1.8}Pb_{0.35}Sr_{1.9}Ca2.1Cu_3O_y$ superconductors, Journal of Alloys and Compounds 471 (2009) 142–146.

[68] H. Ma, S. Liang, Q. Feng, Y. Sun, S. Yan, H. Zhang, The effect of interstitial Ag-doping on Flux Pinning in the $YBa_2Cu_3O_7$ superconductor, Europhysics Letters 10 (1989) 375.

[69] J. H. M. Jr., S. L. Holder, J. D. Hunn, G. N. Holder, Improvement of $YBa_2Cu_3O_{7-x}$ thick films by doping with silver, Applied Physics Letters 54 (1989) 2256.

[70] S. Baliga, A. L. Jain, Enhanced grain growth in $YBa_2Cu_3O_{7-\delta}$, Applied Physics A 49 (1989) 139.

[71] J. W. Ekin, A. I. Braginski, A. J. Panson, M. A. Janocko, D. W. C. II, N. J. Zaluzec, B. Flandermeyer, O. F. de Lima, M. Hong, J. Kwo, S. H. Liou, Evidence for weak link and anisotrophy limitations on the transport critical current in bulk polycrystalline $Y_1Ba_2Cu_3O_x$, Journal of Applied Physics 62 (1987) 4821.

[72] G. B. Abdullaev, T. D. Dzhafarov, Atomic diffusion in semiconductor structures, Harwood, Newyork.

[73] S. X. Dou, K. H. Song, H. K. Liu, C. C. Sorrell, M. H. Apperley, A. J. Gouch, N. Savvides, D. W. Hensley, The interaction of Ag with Bi-Pb-Sr-Ca-Cu-O superconductor, Physica C 160 (1989) 533–540.

[74] S. F. Gafarov, T. D. Dzhafarov, G. S. Kulikov, R. S. Malkovich, E. A. Skoryatina, V. P. Usacheva, Diffusion of silver and copper in Y-Ba-Cu-O superconducting oxide ceramics, Pisma V Zhurnal Tekhnicheskoi Fiziki 15 (1989) 66–69.

[75] S. F. Gafarov, T. D. Dzhafarov, G. S. Kulikov, R. S. Malkovich, E. A. Skoryatina, V. P. Usacheva, Silver diffusion under the room-temperature in superconducting ceramics of the Y-Ba-Cu-O system, Pizma V Zhurnal Tekhnicheskoi Fiziki 16 (1990) 59–61.

[76] W. Gao, J. Chen, C. O. Yang, D. Mcnabb, J. Vandersande, The stability of high-T(c) BSCCO/Ag superconducting microcomposites in water, some inorganic solutions and organic-solvents, Physica C 193 (1992) 455–462.

[77] O. Satoru, O. Hideo, H. Kazuhiro, O. Masaya, Effects of Ag-doping on the formation of superconductive phase in Bi-Sr-Ca-Cu-O ceramics, Journal of the Japan Society of Powder and Powder Metallurgy 38 (1991) 1035.

[78] S. Kao, A. Elhamalawy, K. S. Y. NG, Effects of silver on the phase formation of the Bi-Pb-Sr-Ca-Cu-O superconductors, Journal Of Superconductivity 5 (1992) 301–311.

[79] N. Khare, D. K. Walia, G. S. N. Reddy, V. N. Ojha, N. D. Kataria, V. S. Tomar, A. K. Gupta, Low-resistance silver contact on Bi-Sr-Ca-Cu-O film, Journal Of Physics D-Applied Physics 22 (1989) 1237–1239.

[80] S. Yoshizawa, Y. Hishinuma, S. Nemoto, I. Tezuka, S. Haseyama, S. Yamazaki, H. Nakane, Applied Superconductivity 1999, Institute of Physics Publications (2000) 255.

[81] Y. Hishinuma, S. Nemoto, T. Shimada, I. Tezuka, S. Yoshizawa, S. Haseyama, S. Yamazaki, H. Nakane, Advances in Superconductivity, Springer, Berlin (2000) 548.

[82] J. Sha, X. J. Chen, Z. B. Wang, X. S. Ye, Z. K. Jiao, A new method for joining of Bi(2223) / Ag tapes, Physica C 297 (1998) 91–94.

APPENDIX A - LABVIEW PROGRAMMINGS

A.1 Susceptibility Measurement Programming Diagrams

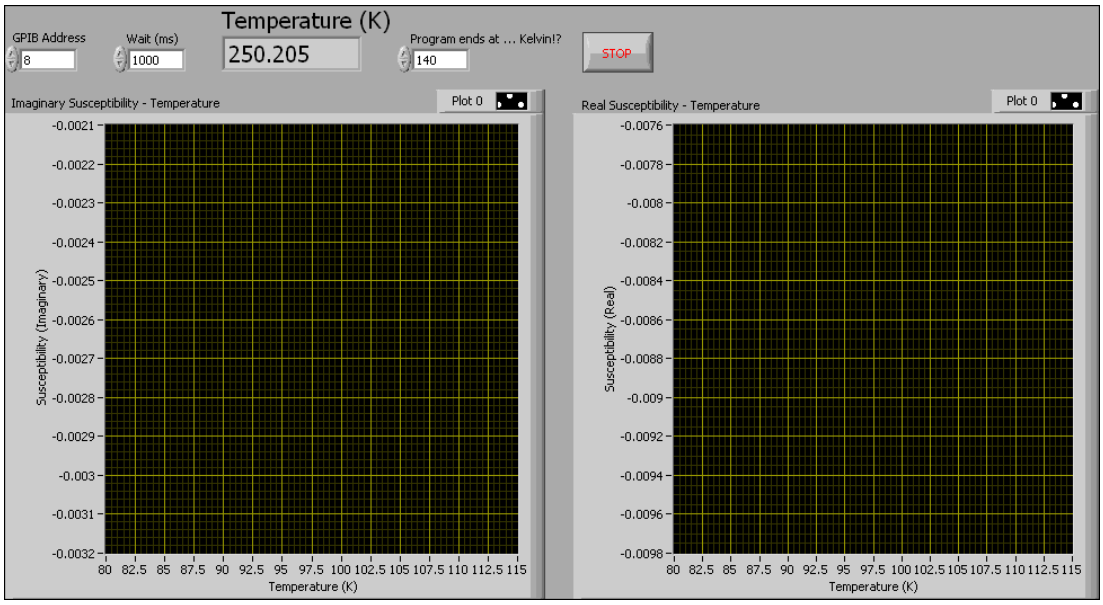

Figure_Apx A.1-1: Labview front panel of the AC susceptibility measurement programming.

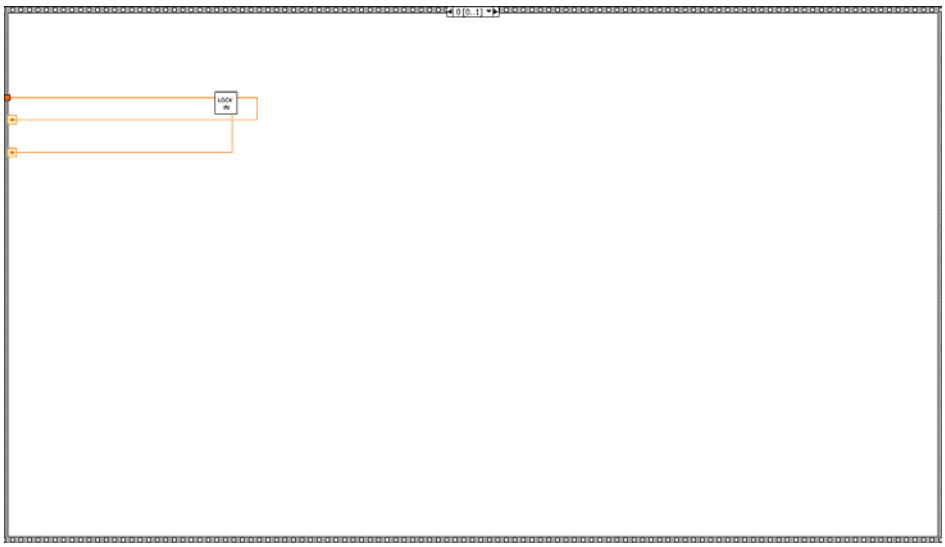

Figure_Apx A.1-2: Labview block diagram's first part of the AC susceptibility measurement programming.

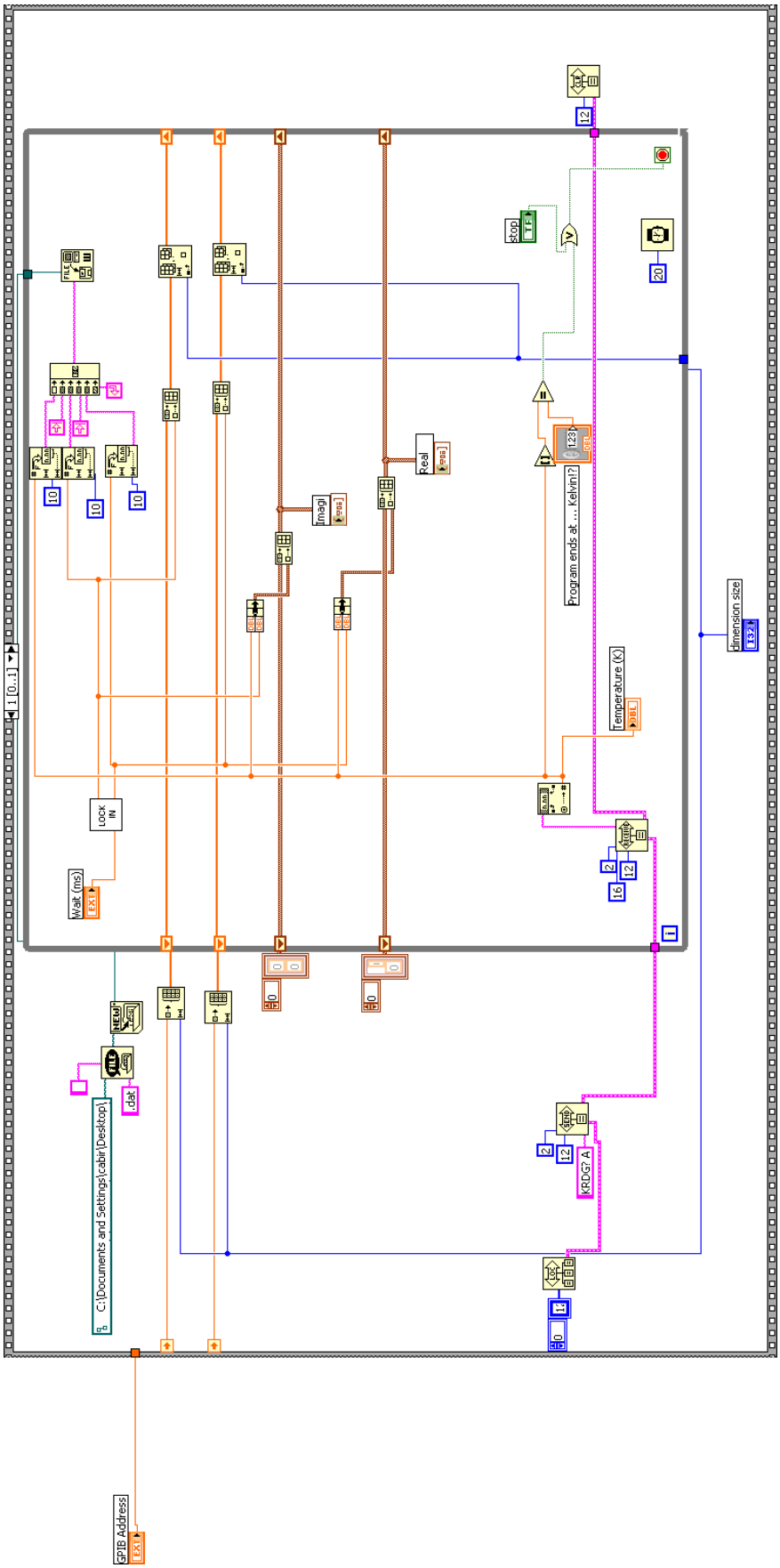

Figure_Apx A.1-3: Labview block diagram's second part of the AC susceptibility measurement programming.

Figure_Apx A.1-4: Lock-in vi icon of the Labview software.

Figure_Apx A.1-5: Labview software front panel of the Lock-in icon.

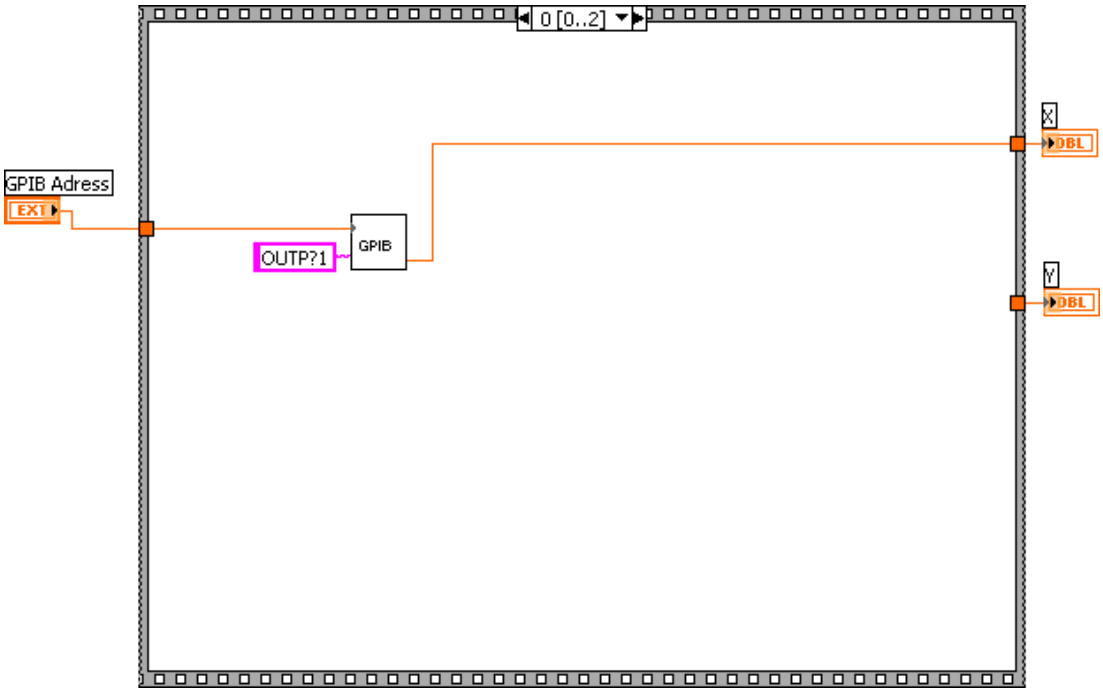

Figure_Apx A.1-6: Labview software block diagram's first part of the Lock-in icon.

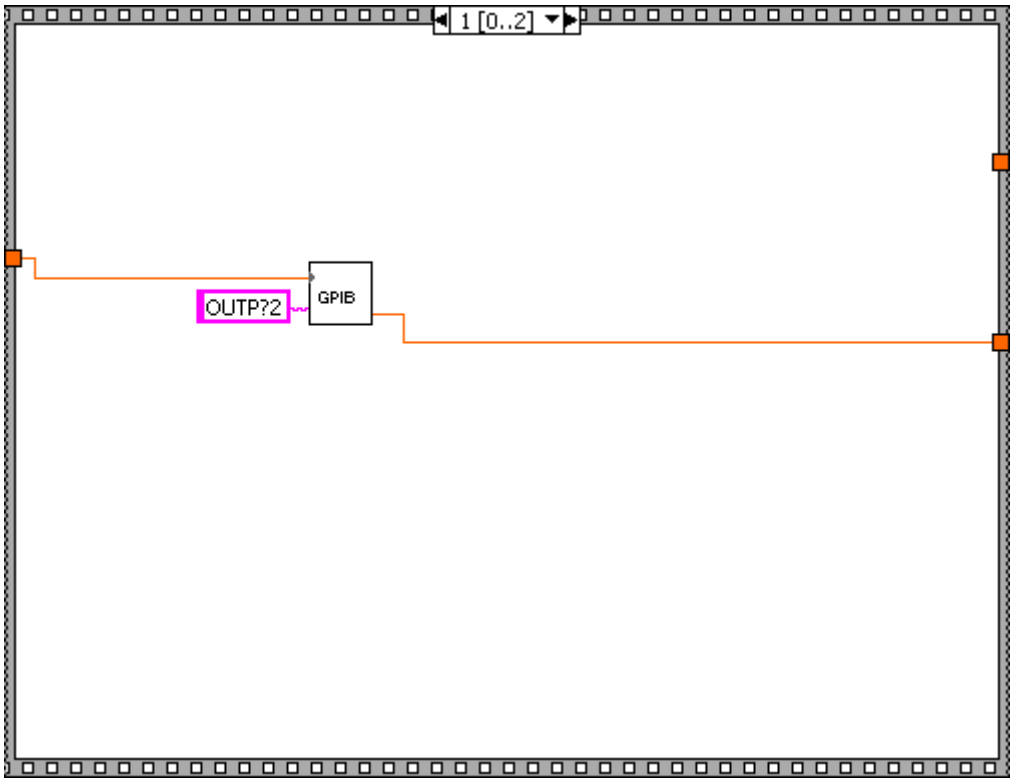

Figure_Apx A.1-7: Labview software block diagram's second part of the Lock-in icon.

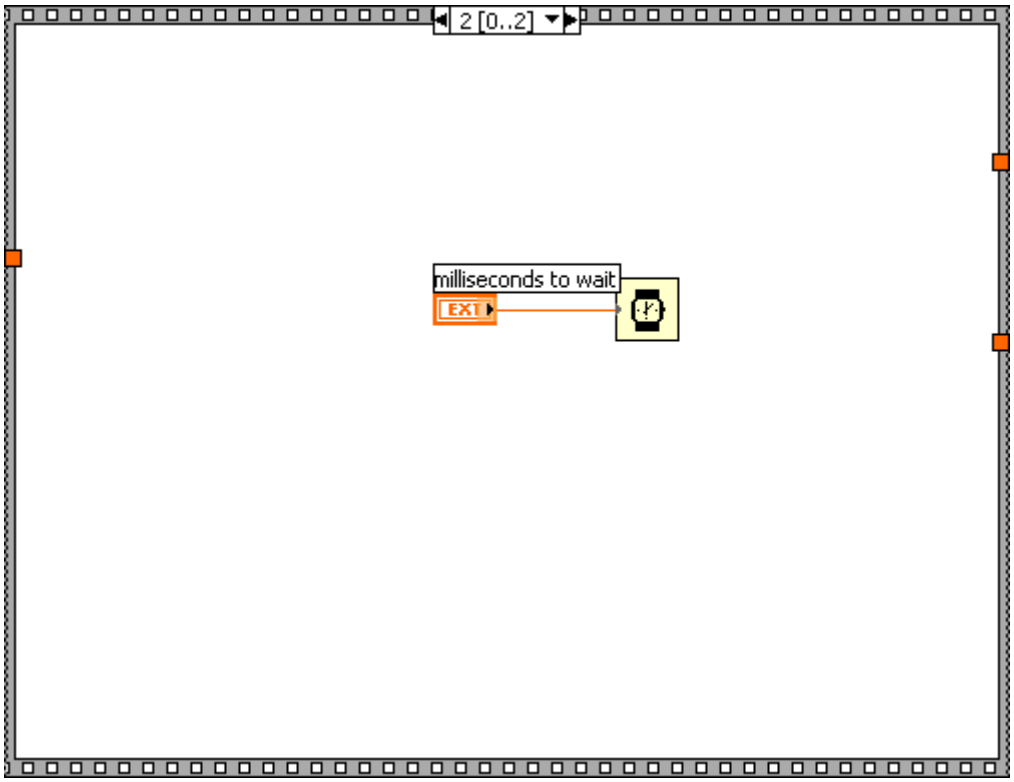

Figure_Apx A.1-8: Labview software block diagram's third part of the Lock-in icon.

Figure_Apx A.1-9: GPIB vi icon of the Labview software.

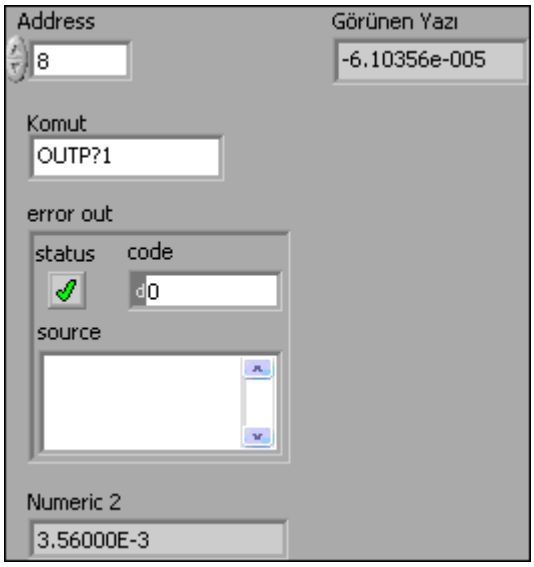

Figure_Apx A.1-10: Labview software's front panel of the GPIB vi icon.

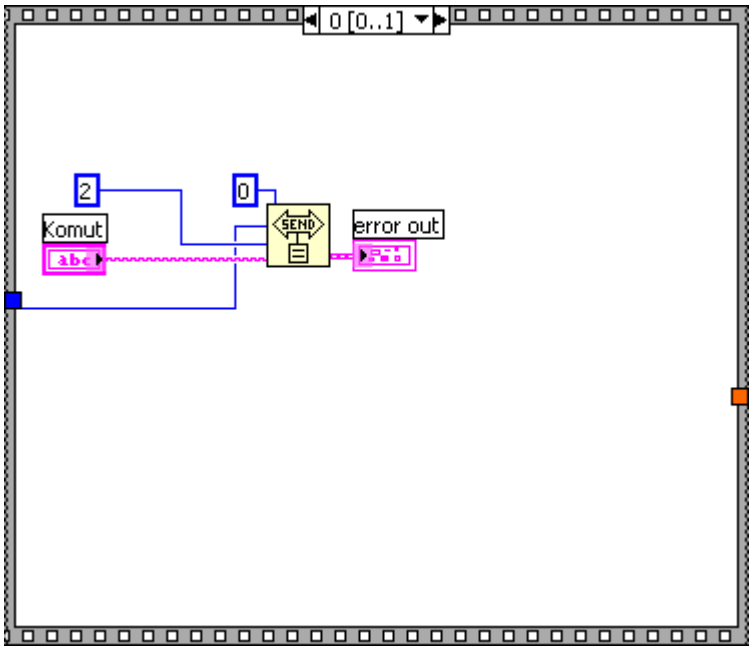

Figure_Apx A.1-11: Labview software block diagram's first part of the GPIB vi icon.

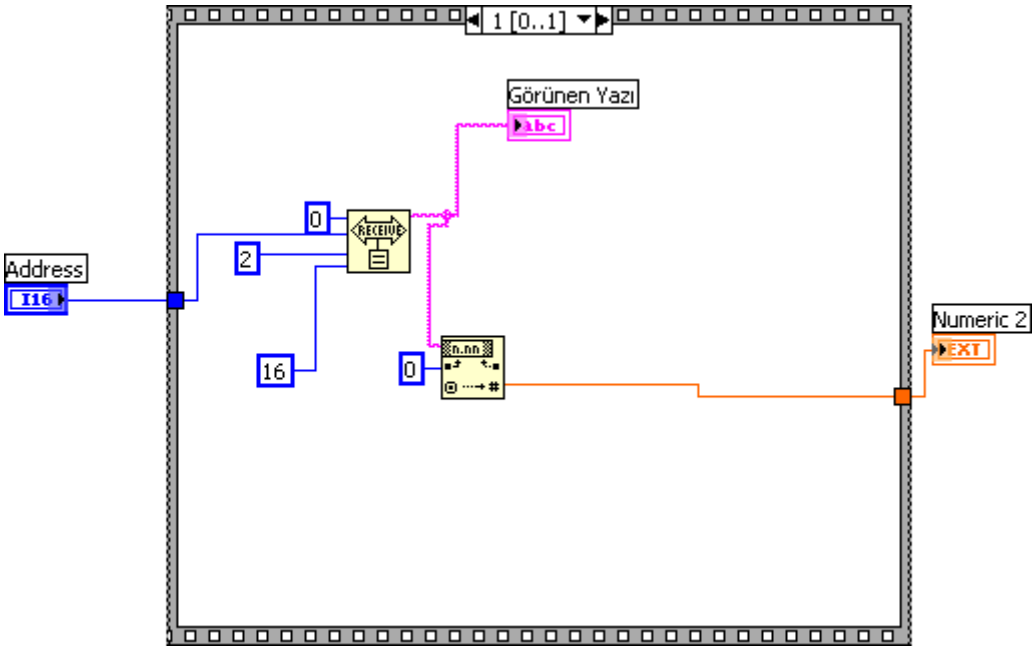

Figure_Apx A.1-12: Labview software block diagram's second part of the GPIB vi icon.

A.2 Resistance vs Temperature Measurement Programming Diagrams

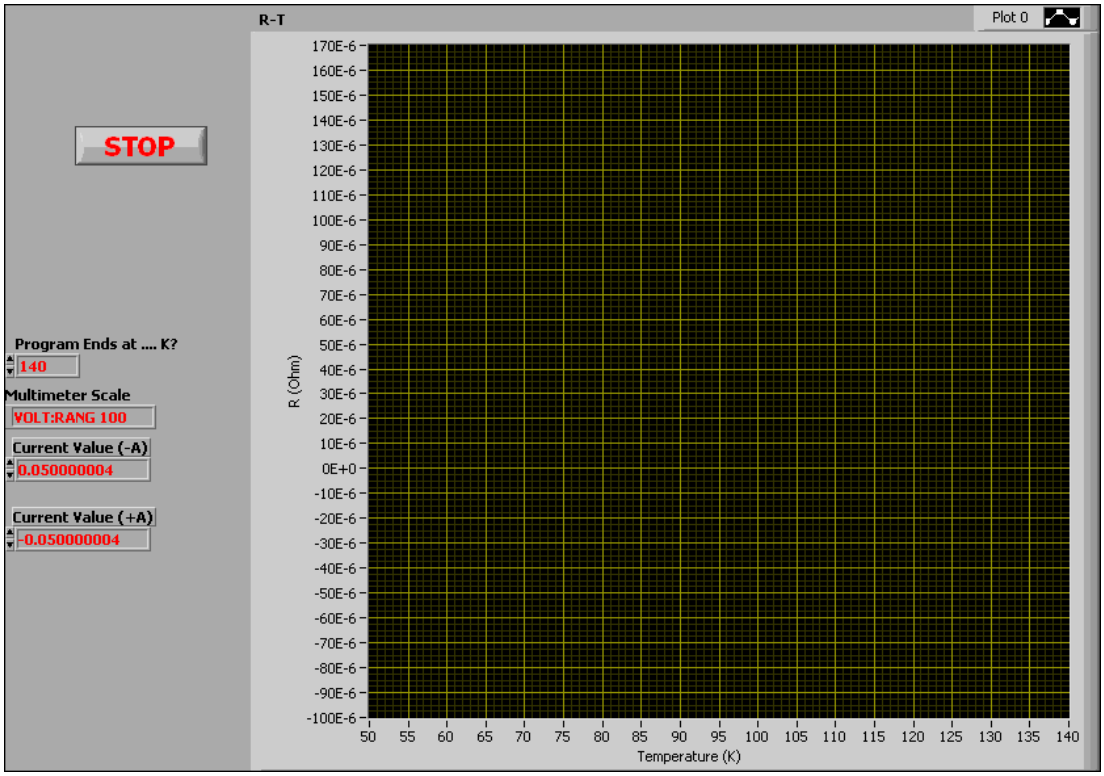

Figure_Apx A.2-1: Labview software front panel of the R-T measurement programming.

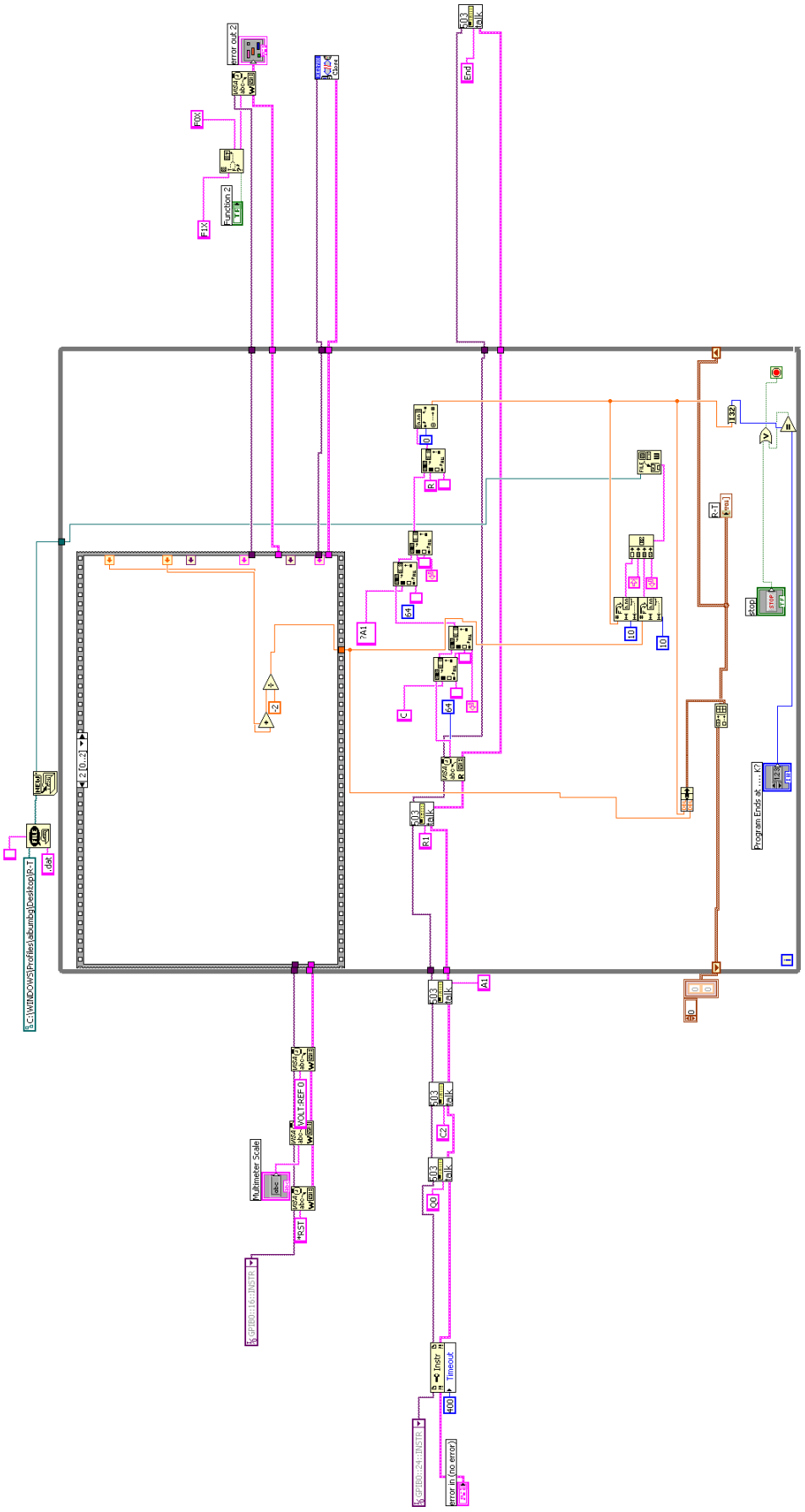

Figure_Apx A.2-2: Labview software block diagram of the R-T measurement programming.

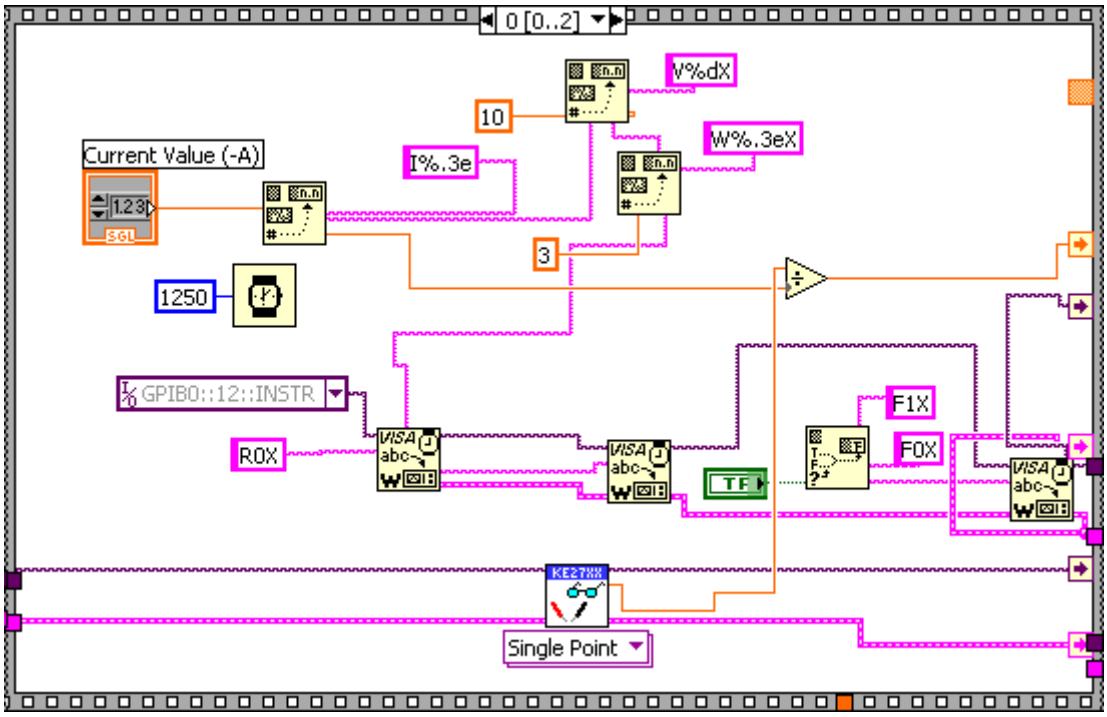

Figure_Apx A.2-3: First part of the while loop of the R-T measurement programming.

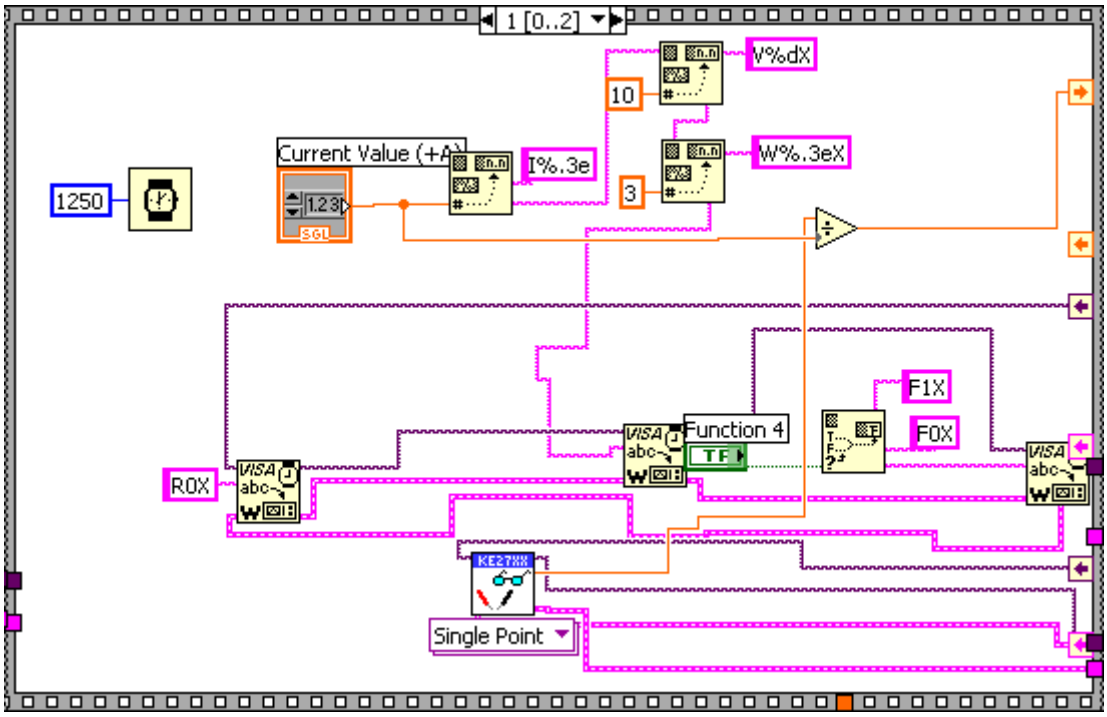

Figure_Apx A.2-4: Second part of the while loop of the R-T measurement programming.

Figure_Apx A.2-5: Labview software 503 talk vi icon.

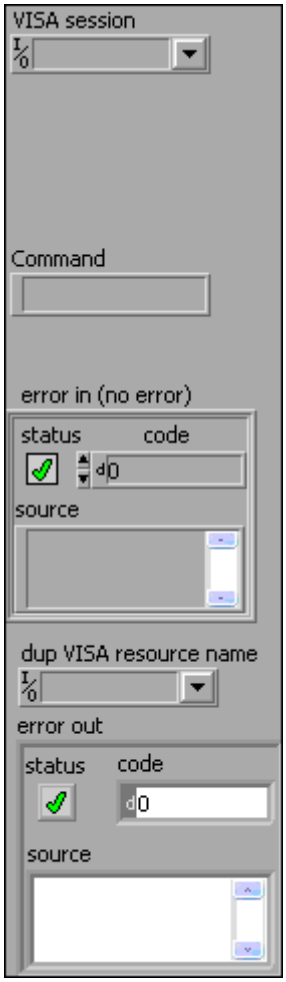

Figure_Apx A.2-6: Labview software front panel of the 503 talk vi icon.

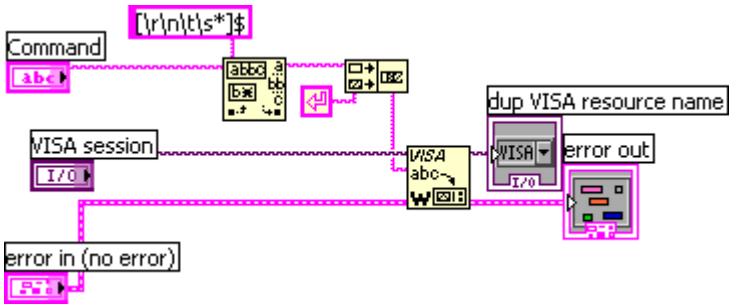

Figure_Apx A.2-7: Labview software block diagram of the 503 talk vi icon.

A.3 Current vs Voltage Measurement Programming Diagrams

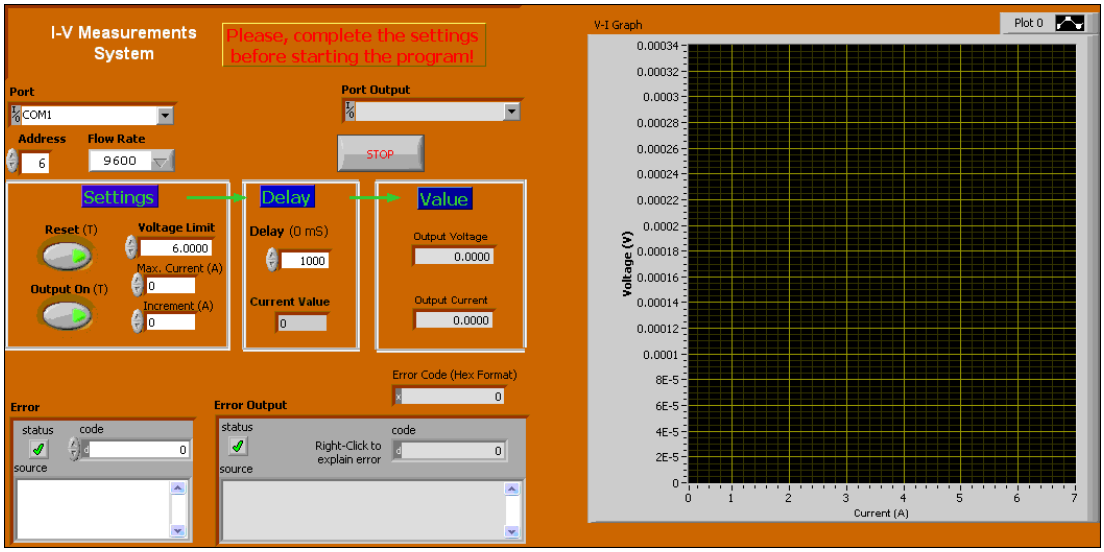

Figure_Apx A.3-1: Labview software front panel of the I-V measurement programming.

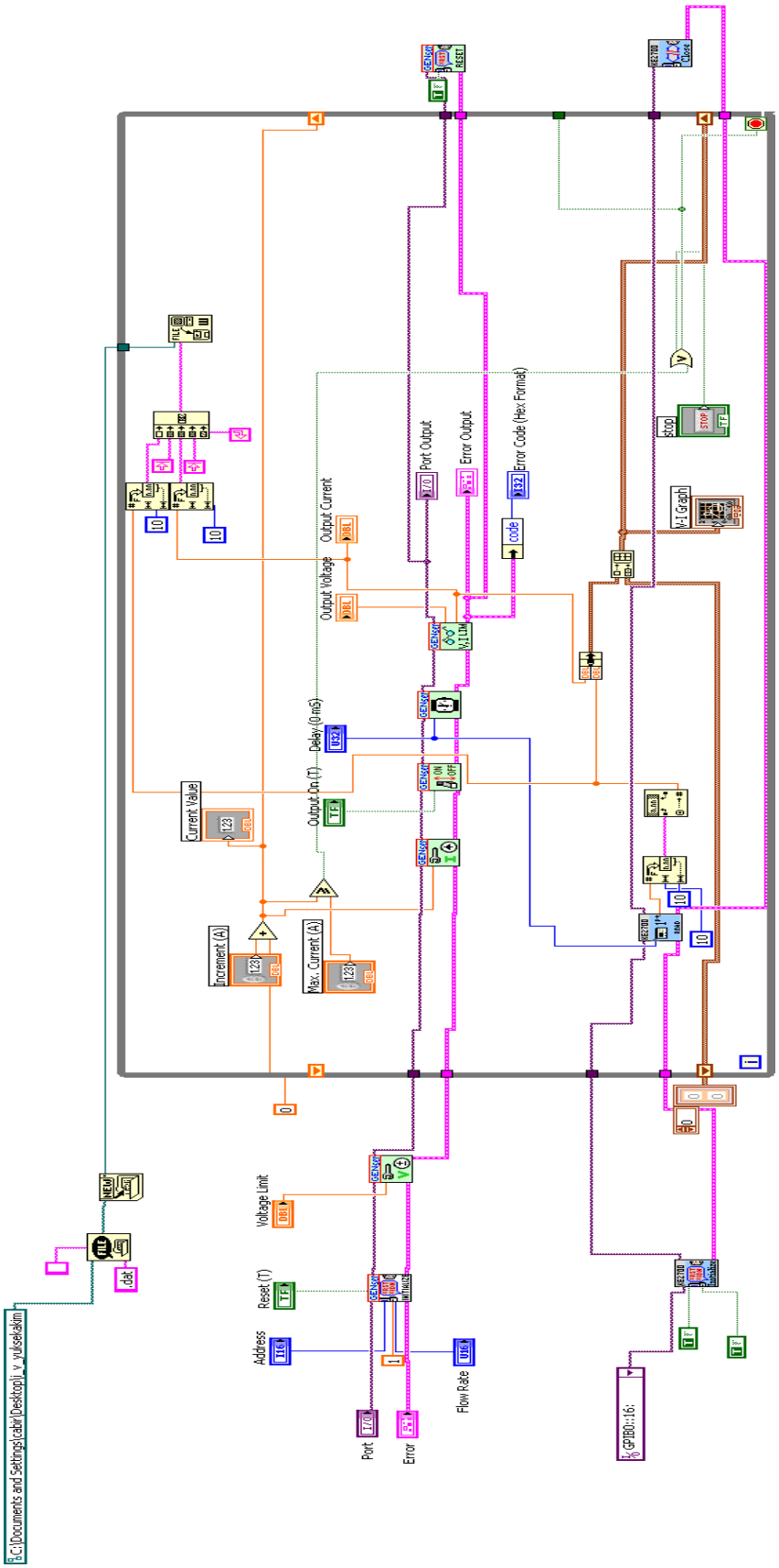

Figure_Apx A.3-2: Labview software block diagram of the I-V measurement programming.

CIRRICULUM VITAE

Mustafa Akdoğan

Address:

Abant İzzet Baysal University
Department of Physics,
Golkoy-Bolu, Turkey
Phone: +90 374 2541000 – 1274
Fax: +90 374 2534642
e-mail: akdogan_m@ibu.edu.tr – m_akdogan@hotmail.com

Personal Details:

Gender: Male
Date of birth: 17th of July, 1977
Place of birth: Istanbul, Turkey

Education:

1995-1999 Undergraduate Studies in Physics at the Abant İzzet Baysal University

2000-2002 MSc in Physics at the Abant İzzet Baysal University
Thesis: Ab initio Calculations of Lattice Dynamics of Ternary Semiconductors.

2003-2009 PhD in Physics at the Abant İzzet Baysal University
Thesis: Properties of Grain Boundaries and Ag-Ceramic Interface In Bismuth Based Superconductors.

Specialization: Superconductivity, BPSCCO.

Publications:

1. M. Akdogan, C. Terzioglu, I. Belenli, "Calculation of the diffusion coefficient, activation energy of silver in $Bi_{1.8}Pb_{0.4}Ca_{2.2}Sr_2Cu_3O_x$ and the effect of Ag-doping on some physical properties" Journal of Alloys and Compounds (Submitted) (2009).

2. O. Ozturk, M. Akdogan, C. Terzioglu and A. Gencer, "Influence of gold diffusion-doped on phase formation, superconducting and microstructure properties of $Bi_{1.8}Pb_{0.35}Sr_{1.9}Ca_{2.1}Cu_3O_y$ superconductors", Journal of Physics Conference Series, 153, 012024, (2009).

3. Terzioglu C., Yegen D., Yilmazlar M., Gorur O., Akdogan M., Varilci A. "Investigation of Sm → Ca substitution in Bi(Pb)SrCaCuO high temperature superconductor by low field AC magnetic susceptibility" Journal of Material Science 42, 4636-4641 (2007).

4. Ozturk O., Akdogan M., Aydin H., Yilmazlar M., Terzioglu C., Belenli I. "Substitution of Sm at Ca site in $Bi_{1.6}Pb_{0.4}Sr_2Ca_{2-x}Sm_xCu_3O_y$" Physica B 399, 94-100 (2007).

5. Yilmazlar M., Ozturk O., Aydin H., Akdogan M., and Terzioglu C. "The Effect of Sm → Ca Substitution on Mechanical Properties of BSCCO Superconductors" Chinese Journal of Physics, 45, 128-134 (2007).

6. Akdoğan M., Eryiğit R. "First-principles calculations on vibrational and dielectric properties of chalcopyrite $CuGaS_2$" Journal of Physics: Condensed Matter 14, 7493-7502 (2002).

Presentations:

1. M. Akdoğan, C. Terzioğlu, A. Varilci, R. Eryiğit, And İ. Belenli, "Diffusion coefficient, activation energy and the effect of Ag-doping on some physical properties of silver doped $Bi_{1.8}Pb_{0.4}Ca_{2.2}Sr_2Cu_3O_x$", International Student Workshop on Condensed Matter and Material Physics, Porto Bello Hotel – Antalya, 27-31 Aralık 2009.

2. M. Akdoğan, G. Yıldırım, Ö. Öztürk, M. Erdem, A. Varilci, C. Terzioğlu, And İ. Belenli, "The effect of annealing temperature and annealing time on thin film Bi-2223 samples preparation", 4. Ulusal Süperiletkenler Sempozyumu, Karadeniz Teknik Üniversitesi, Trabzon (2009).

3. O. Ozturk, E. Asıkuzun, M. Akdogan, D. Yegen, M. Erdem, I. Belenli, C. Terzioglu, "Investigation of mechanical properties of iron diffusion-doped Bi-2223 superconductors", 4. Ulusal Süperiletkenler Sempozyumu, Karadeniz Teknik Üniversitesi, Trabzon (2009).

4. M. Erdem, Ö. Öztürk, M. Akdoğan, H. Aydın, C. Terzioğlu, İ. Belenli, H. Topa, "Effect of Gd Addition on the Activation Energies of Bi-2223 Superconductor", 4. Ulusal Süperiletkenler Sempozyumu, Karadeniz Teknik Üniversitesi, Trabzon (2009).

5. Mustafa Akdogan, Ozgur Ozturk, Ugur Cevik, Ahmet Varilci, and Cabir Terzioglu, "Calculation of diffusion coefficient in Au diffusion-doped

$Bi_{1.8}Pb_{0.35}Sr_{1.9}Ca_{2.1}Cu_3O_y$ by EDXRF measurements" American Physical Society March Meeting, Pittsburgh-Pennsylvania, USA (2009).

6. Mustafa Akdogan, Ozgur Ozturk, Ersin Yucel, Erdal Bekiroglu, Mustafa Yilmazlar, and Cabir Terzioglu, "Influence of diffusion-annealing time on the mechanical properties of bulk $Bi_{1.8}Pb_{0.35}Sr_{1.9}Ca_{2.1}Cu_3O_y$ superconductors diffusion-doped with Fe" American Physical Society March Meeting, Pittsburgh-Pennsylvania, USA (2009).

7. M. Akdoğan and İ. Belenli, "Minute hBN addition to bulk Bi-2223 superconductor", International Conference on Superconductivity and Magnetism (ICSM2008), 25-29 August 2008, Side-Antalya, Turkey.

8. Mustafa Akdogan, Ozgur Ozturk, Huseyin Aydin, Murat Erdem, and Cabir Terzioglu "Mechanical and Superconducting Properties of $Bi_{1.8}Pb_{0.35}Sr_{1.9}Ca_{2.1}Cu_3Gd_xO_y$ System", American Physical Society March Meeting, New Orleans-Louisiana, USA (2008).

9. Murat Erdem, Ozgur Ozturk, Huseyin Aydin, Mustafa Akdogan, Cabir Terzioglu, Ahmet Varilci, Ibrahim Belenli "Investigation Of Some Physical Properties Of Gd Added Bi-2223 Superconductors" American Physical Society March Meeting, New Orleans-Louisiana, USA (2008).

10. Mustafa Akdogan, Erhan Budak, Ozgur Ozturk, Cabir Terzioglu, and Ibrahim Belenli, "The Effect Of hBN Addition On Properties Of Bi-2223 Superconductors" American Physical Society March Meeting, Denver-Colorado, USA (2007).

11. H. Aydın, M. Yılmazlar, Ö. Öztürk, M. Akdoğan, S. Nezir, C. Terzioğlu, "Sm Katkılanmış BiPbSrCaCuO Süperiletkenlerin Transport Ölçümleri" III. Ulusal Yüksek Sıcaklık Süperiletkenler Sempozyumu, Bolu-Turkey (2005).

12. M. Akdoğan, D. Yeğen, C. Terzioğlu, O. Görür, İ. Belenli and A. Varilci, "Investigation of Cooling Rate in Bi(Pb)SrCaCuO High Temperature Superconductor by Low Field AC Magnetic Susceptibility" III. Ulusal Yüksek Sıcaklık Süperiletkenler Sempozyumu, Bolu-Turkey (2005).

13. Ö. Öztürk, M. Yılmazlar, C. Terzioğlu, M. Akdoğan, E. Yanmaz, İ. Belenli, "Sm Katkılı $Bi_{1.6}Pb_{0.4}Sr_2Ca_{2-x}Sm_xCu_3O_y$ Bileşiğinin Elektriksel ve Yapısal Özelliklerinin İncelenmesi" III. Ulusal Yüksek Sıcaklık Süperiletkenler Sempozyumu, Bolu-Turkey (2005).

14. C. Terzioglu, D. Yegen, M. Yılmazlar, E. Kucuk, M. Akdogan and A. Varilci, "Investigation of Sm→Ca Substitution in Bi(Pb)SrCaCuO High Temperature Superconductor by Low Field AC Magnetic Susceptibility" III. Ulusal Yüksek Sıcaklık Süperiletkenler Sempozyumu, Bolu-Turkey (2005).

Workshops and Schools:

1. International Student Workshop on Condensed Matter and Materials Physics, Porto Bello Hotel-Antalya, 27 – 31 Aralık 2009.

2. Süperiletkenliğin Temel Prensipleri, Teorileri ve Teknolojik Uygulama Alanları Kış Okulu, Side-Antalya, 24 Ocak – 1 Şubat 2009.

3. Endüstriyel Kalkınma Açısından Türkiye'de Süperiletkenlik ve Manyetizma için Güçlü Ar-Ge Gerekçeleri, Belek-Antalya, 25 Nisan 2008.

4. National Student Workshop on Superconductivity and Magnetism, Ankara University, Örsem, Çolaklı, Side-Antalya, 28th September – 5th October, 2008.

Projects:

1. "Lantanidlerle Katkılanmış $(Bi,Pb)_2Sr_2Ca_2Cu_3O_{10+x}$ Fazından Üretilen Filmlerin Süperiletkenlik Özelliklerinin Farklı Dalga Boyundaki Işınımlar Altındaki Davranışının Kritik Sıcaklık Civarında İncelenmesi" AIBU Research Fund, Grant No. BAP-2003.03.02.194, 2003-2005 (Researcher).

2. "Bizmut temelli yüksek sıcaklık üstüniletkenlerde mikroyapı-özellik ilişkilerinin üretim parametrelerine bağlı olarak incelenmesi" T.C. Başbakanlık Devlet Planlama Teşkilatı Müsteşarlığı, Grant No. 2004K120200, 2004-2006 (Researcher).

3. "Bizmut temelli süperiletkenlerde tanecik sınırlarının ve Ag-seramik arayüzün özellikleri" Tübitak, Grant No. TBAG (104T323), 2005-2007 (Researcher).

4. "Lazer Girişimi ve Elektron Demeti Litografisi Yöntemi Kullanılarak, Nano Ölçekte Üretilen Delik ve Nokta Biçimli Manyetik ve Süperiletken Malzemelerin Örgü-Düzen Etkilerinin İncelenmesi ve Nanoteknolojide Uygulamaya Konulması" T.C. Başbakanlık Devlet Planlama Teşkilatı Müsteşarlığı, Grant No. 2004K120200, 2005-2008 (Researcher).

5. "Sürekli boru yapma ve doldurma yöntemi ile B(P)SCCO-2223 üstüniletken şerit üretimi ve bu şeritlerden üstüniletken trafo yapımı" Tübitak, Grant No. MAG(108M201), 2009-2010 (Scholar).

Work Experience:

From 1999 to 2009 I have worked at the Abant İzzet Baysal University, Physics Department as a Research Assistant and I am still working at the same place.